Novel NIR Endoscopic Techniques for Medical Imaging – An Investigation Considering both LED and LASER Excitation Sources

PhD Thesis

Angharad Curtis

A submission presented in partial fulfilment of the requirement of the University of South Wales / Prifysgol De Cymru for the degree of Doctor of Philosophy

November 2021

Mae'r Ysgoloriaeth Sgiliau Economi Gwybodaeth (KESS 2) yn fenter sgiliau lefel uwch Cymru gyfan a arweinir gan Brifysgol Bangor ar ran y sector AU yng Nghymru. Fe'i cyllidir yn rhannol gan raglen cydgyfeirio Cronfa Gymdeithasol Ewropeaidd (ESF) ar gyfer Gorllewin Cymru a'r Cymoedd.

Knowledge Economy Skills Scholarships (KESS 2) is a pan-Wales higher level skills initiative led by Bangor University on behalf of the HE sector in Wales. It is part funded by the Welsh Government's European Social Fund (ESF) convergence programme for West Wales and the Valleys.

University of South Wales
Prifysgol De Cymru

kess 2
Ysgoloriaethau Sgiliau Economi Gwybodaeth
Knowledge Economy Skills Scholarships

UNDEB EWROPEAIDD
EUROPEAN UNION
Llywodraeth Cymru
Welsh Government
Cronfa Gymdeithasol Ewrop
European Social Fund

For Mum and Dad,

Thank you for your unlimited love and support, I could not have done this without you both. I credit my determination and dedication to being raised by two of the hardest workers I know.

-Mum, my rock and cheerleader, thank you for always being there for me and for believing in me. Thank you for your understanding and for always knowing the right thing to say. Your faith in me gives me the confidence to always have a go and give my best effort.

-Dad, thank you for always being so proud of me and for telling everyone we meet that I got it all from you. Thank you for reading to me growing up and for encouraging me to challenge myself always. Thank you for staying up late to help me with calculations and for always drawing me a diagram – even if it's on the freshly painted walls!

Acknowledgements

Thank you to KESS for the opportunity to study towards this award. KESS funding has allowed me to commit full time to my research and the programme has encouraged continuous professional development throughout my studies. KESS also offered me a network of support from the administrative team to fellow KESS students which has had a real positive impact on my journey to PhD.

A huge thank you to my team, Dr Kang Li, Director of Studies and Dr Ali Roula, Second Supervisor for all of your contributions and efforts throughout my studies. I really appreciate the time committed to supporting me through this project.

Thank you to Professor Nigel Copner, Director of Research and Chair or Optoelectronics for all of your support and encouragement throughout this research. When the company partner went into administration, thank you for all of your assistance in keeping the project motivation high.

Thank you to Dr Jungang Huang, my original Director of Studies who sadly left during this project.

Thank you to Cymtec Ltd, the original company partner for this project who allowed me unlimited access to the site and material, Ron, Chris, Dan, Judith, Yang and Simon I really appreciate your support and encouragement.

Dr Amandeep Kaur, thank you for taking the time to look through my written work and to meet with me for support. Your feedback was fantastic and I am so grateful that I got to meet you and read through your research.

Dr Gareth Owen, thank you for allowing me access to the chemistry facilities and introducing me to the PhD students within the Chemistry department. Without this access I would not have been able to complete this research and I am so grateful for your support.

Thank you to the Photonics Group, for giving opportunities to present and discuss my research. Group meetings offered me the opportunity to share my results and to discuss any problems encountered amongst friends. It was valuable for me to learn what colleagues within the group were working on in order to identify opportunities to learn from one another. Dr Peter Rees, Dr Hatef Dinparasti Saleh and Dr Yuanlong Fan, thank you for your support through these group interactions.

Thank you to my research colleagues and friends, Chris, Enrica, Mahmod, Boris, Yang, Adam, Bethan, Tom, Richard, Miriam, Chika, Yusuf, Matthew, Xinyu, Dun, Wayne and Amrarul for your support and encouragement.

Thank you to the KESS administrative team, Alison, Clare and Chloe. Thank you for all of the support provided from day one and for all of the efforts made to keep me motivated and positive. I am so grateful for your wisdom and for allowing me to connect with fellow KESS students on campus. The accessibility to the KESS team has had a real impact on my motivation, thank you for your encouragement and positivity.

Thank you to the staff at the Graduate Research Office, particularly Llinos who's kindness and support was so valuable. Llinos is responsible for inspiring me to complete this work and she was such a reliable source of knowledge and positivity throughout this journey. For Paul, Elaine and the rest of the GRO team, thank you for all of the hard work that you do, it does not go unnoticed. The content, quality and frequency of training organised by the GRO was excellent and has made an impact on my professional and personal development.

To the staff at Imperial College London Surgical Department, thank you for welcoming me to your team and for taking the time to present your research to me and allow me to further my knowledge.

Thank you to the support staff on campus. Carys, Wendy and Helen in the office thank you for welcoming me and for providing such a friendly environment. To the IT support, lab technicians and support staff on campus, thank you for being so helpful and friendly.

To my family and friends outside of academia, I will not name you all but I want to thank you for being there throughout this journey. I have often neglected relationships due to my work ethics and thank you for your understanding, patience and love.

For my fiancé and best friend Christopher, thank you for believing in me and always encouraging me. Thank you for your patience, understanding and unconditional love. I am so lucky to have had you by my side throughout this process.

Abstract

The aim of this project is to build and test an illumination and detection system for fluorescence endoscopy in order to image the fluorophore Indocyanine Green. The project was developed through collaboration with clinicians at Imperial College London, the company partner Cymtec Ltd and the University of South Wales for imaging cancerous tissue in the breast via minimally invasive surgical procedures. The use of Indocyanine Green as a fluorescent marker at Near Infrared excitation wavelengths is well established in clinical imaging. Typical systems comprise multiple LED sources, or even Xenon bulbs, for optimal imaging which can result in unnecessary energy transfer to patients and contribute to tissue damage. The use of LASER as an illumination source is not well established nor is the possibility of using a single camera for the simultaneous imaging of fluorescence and bright-field components. Furthermore, there are gaps in knowledge regarding the optical properties of Indocyanine Green for endoscopic applications.

An experimental setup comprising a 780nm excitation channel generating up to 10mW of optical power is used so as to determine if there is potential to exploit the optical properties of ICG, in order to reduce the total excitation power through pulsing. We demonstrate in this work that a single 1.6 Megapixel CMOS camera, with quantum efficiency less than 30%, is appropriate to capture both fluorescent and non-fluorescent landmarks at Near Infrared wavelengths. Aqueous solutions containing Indocyanine Green in varying concentrations are imaged under three illumination conditions.

Experimental results verify that all solutions tested, yielded detectable fluorescence and that degradation of fluorescence intensity over time is complex. The intensity of fluorescence and image quality is analysed to confirm the viability of a single camera system with LED or LASER as the preferred illumination source. With a single detector, the presence of ICG within a sample can be verified without the need for filtering, this has the potential to impact on the commercial market for these systems. Results suggest that there is no profound difference between illumination source which is valuable for

future system design and manufacture. This study signifies that current technologies are not well adapted to focus on patient outcomes, complex filtered systems require image merging which reduces the overall image quality.

This research contributes to knowledge with regards to the optical properties of Indocyanine Green while proposing significant changes to system design which would maintain image quality while enhancing patient safety.

Table of Contents

Table of Figures

List of Tables

List of Abbreviations

Abbreviation	Description
AW	Actual Weight
BMLA	British Medical LASER Association
BOM	Bill of Materials
cCCD	Cooled Charge Coupled Device
CCD	Charge Coupled Device
CMOS	Complementary Metal-Oxide Semiconductor
CT	Computerised Tomography
DW	Desired Weight
FBS	Fetal-Bovine Serum
FDA	Food and Drug Administration
FDA	Food and Drug Administration
FOV	Field of View
GSU	Grayscale Unnit
HSA	Human Serum Albumin
ICG	Indocyanine Green
ICG:HSA	A complex formed when Indocyanine Green and Human Serum Albumin are mixed
ICNIRP	International Commission on Non-Ionizing Radiation
IPL	Intense Pulsed Light
IR	Infrared
LASER	Light Amplification by Stimulated Emission of Radiation
LED	Light Emitting Diode
LLG	Liquid Light Guide
MB	Methylene Blue
MRI	Magnetic Resonance Imaging

NA	Numerical Aperture
NIR	Near-Infrared
OCT	Optical Coherence Tomography
PBS	Phosphate-Buffered Solution
QE	Quantum Efficiency
RGB	Red, Green & Blue
ROI	Region of Interest
sCMOS	Scientific Complementary Metal-Oxide Semiconductor
SLN	Sentinel Lymph Node
SNR	Signal to Noise Ratio
TEC	Thermoelectric Cooler
UV	Ultra Violet
WHO	World Health Organisation

1 Introduction

Phototherapy and Diagnostics are the two applications best associated with medical excitation sources, whereby light of varying wavelength and power is used as a tool for the treatment and identification of conditions respectively. The regions of the electromagnetic spectrum which extend past visible light Ultraviolet (UV) and Infrared (IR) interact with biological tissue in very different ways, the longer the wavelength, the deeper the waves penetrate the skin. The relationship between the light power and the maximum penetration depth is disproportional, doubling the power input for example, will not double the penetration depth but instead may damage tissue (Envemeka, 2001).

This project focuses specifically on the NIR wavelength range for a diagnostic application. NIR light is typically within the wavelength range of 700nm to 1100nm, this is the window in which the chemical marker Indocyanine Green (ICG) excites and emits. ICG is a well-established fluorescent marker which can assist in the detection and surgical removal of cancerous tissue in the breast. Breast cancer affects both men and women and sadly, it is the most common cancer in women both in the developed and less developed world according to the World Health Organisation (WHO, 2017). The focus of this project is to contribute to the understanding of fluorescence imaging in general and enhance the research in this area.

One study (Frangioni, 2008) gives a good insight into the problems faced in clinical imaging, re-defining the signal-to-background ratio as the tumour-to-background ratio. The benefits of targeted fluorescent contrast agents at the NIR portion of the spectrum are discussed focusing on the importance of critical structure avoidance during diseased tissue resection via direct visualisation. The current approximate detection threshold is defined for solid tumours as 10^9 cells growing as a single mass. A search through literature indicates that a mammalian cell has an approximate volume of between 100 to 10000μm^3 (Andersen, Gundersen and Pakkenberg, 2003, Bohil, Robertson and Cheney, 2006, Frank, Chuong and Johnson, 1997, Krombach et al., 1997) which would result in

a solid tumour size of between 100mm^3 and 1cm^3, no more than the volume of half of a glass marble.

"*A meaningful impact in cancer screening, staging and treatment is unlikely to occur until the tumor-to-background ratio improves by three to four orders of magnitude which in turn will require proportional improvements in sensitivity and contrast agent targeting*" (Frangioni, 2008)

1.1 Project Context and Motivation

The company partner Cymtec Ltd, which unfortunately entered into administration during mid-2018, designed and developed photonics systems for a variety of industries including medical, automotive and manufacturing. During time spent there researching and testing, I assisted in the design and build of a prototype multichannel endoscopic light source featuring red, green, blue and NIR LED channels which could be controlled independently. This light source is discussed further in the literature review and was delivered to Imperial College London (ICL) for human clinical trials in early 2017. Throughout the prototype stage, with the support of the clinical team at ICL, one of my responsibilities was to communicate with the Medicines and Health Regulatory Authority (MHRA) to provide all relevant test results and documentation in order to approve the human clinical trial. If the human clinical trials proved successful, this would lead to commercialisation of this light source for fluorescence endoscopy in collaboration with market leader, KARL STORZ Ltd.

The motivation for this project developed during testing of both this light source and a similar product that was prototyped for a fluorescence microscopy application. A liquid light guide (LLG) is attached to the "light box" and measurements are recorded at the distal end and monitored for continuity. The LLG is a flexible tube which fundamentally carries light from the source to the patient/sample. A standard LLG was used with a 3mm core diameter for the bench testing at the company partner facility. During the testing period, the effect of keeping all LED channels on at maximum power had a noticeable

thermal effect. While the LLG focuses light, it also acts as an output for the heat which too becomes concentrated due to the efficiency of the light collection.

When writing the supporting documentation for the fluorescence microscopy product, where it is important to note that the optical power is significantly higher than the medical device, the output very quickly melted a 3mm hole into a nearby black plastic item during the start-up routine.

This experience interested me and I wanted to investigate the thermal issues surrounding diagnostic devices using light. Specifically, to answer questions such as; how much thermal damage is caused with current equipment, is this damage recorded and is it possible to minimise the risk of thermal damage in a simple way? Essentially, is thermal damage a concern and could this equipment be made safer for use with something as simple as pulsing the light source.

1.2 Project Objectives

- To design and manufacture a prototype test unit comprising an NIR LED and NIR LASER channel.
- To collect fluorescence and white light data from an ICG stained sample under test conditions using a single detector without filters.
- To contribute to the gap in research concerning filtering. Filters significantly contribute to the cost and complexity of the design, there is no existing literature to suggest that this signal can be captured with a single detector and/or without the use of dichroic filters.
- To determine a suitable channel pump rate, specifically in regards to the NIR channel. Existing literature is conflicting when determining a suitable pulsing frequency for the excitation source for this application. Pulsing the excitation source effectively reduces the time that tissue is exposed to energy which is significant with this application.

- To contribute to existing knowledge in regards to the photobleaching properties of the chemical marker.
- To analyse data collected for image quality using a suitable programme, with the aim of presenting the findings as a comparison to accepted methods. The aim here is to verify the possibility that a pulsed system can offer a significant reduction in build cost and patient safety without compromising on image quality.
- To confirm and present a preferred NIR excitation source, LED or LASER based on experimental testing.
- To confirm that a simplified setup is sufficient and that a single detector is a possibility for the future of this imaging. To confirm if the imaging can be carried out without the use of filters. This could lead to cheaper endoscopic light sources being available commercially which in turn, may improve access to endoscopic procedures in developing countries.

1.3 Project Relevance

This project aims to design and investigate endoscopic light sources for fluorescence endoscopy, specifically to assist in the detection and removal of cancerous tissue in the breast. There are currently no endoscopy products utilising LASER as the excitation source for imaging available on the market however, there are many commercially available medical devices comprising LASER source of varying wavelengths and power.

General background research into available LASER devices has shown that there are plenty of clinically approved products however, there is a real lack of diversity amongst applications. Many devices using the traditional bulb technology have migrated, or are beginning to migrate over to LED technology. LEDs are cheaper and better suited to medical applications whereby energy is required locally over a large area. LASERs provide a monochromatic, coherent and collimated beam with much faster on/off switching. Depending on the pulse frequency required for the pump, LASERs are much

easier to pulse which is why this project has suggested that fluorescence endoscopy is an ideal application for LASER technology.

From experience, there are other parameters to consider which will contribute to the success of a medical device including but not limited to; eye safety, ease of use and public perception. The proposed experiments will excite a fluorescent marker using either an NIR LED or LASER as well as imaging the field of view (FOV) in order to complete a comparative analysis. Due to the closure of the company partner, there was a requirement to shift the focus of the research. Specifically, with the company partner's support withdrawn, it was no longer feasible to move forward with the original design and research plan as the expertise required to design and build was not available.

Experiments are now setup under lab conditions at the university LASER laboratory, for simplicity smaller experiments have been designed so that time in the lab is used efficiently. Setting up and designing experiments is challenging without the company support, separating the project into smaller experiments helps in keeping project context and the characteristics of the original scope.

The aim remains to design and test a system which would allow a surgeon to visualise fluorescent material under bright field conditions in real-time, using off-the-shelf components without including filters into the design.

Fluorescence and white light data will be captured and processed to assess image quality. Following procurement, prototyping and testing, a final design will be presented for the future work component of the research without a commercialisation plan.

1.4 Thesis Structure

A literature review will discuss current techniques and technologies, commenting on existing methodologies and commercially available systems. A broad introduction to components and any equations used is also included where necessary as this is a multidisciplinary project.

The materials and methodology chapter will then describe details of the setup used for each experiment including any techniques and calculations used. Photographs and schematics are used for reference where possible. The methodology chapter includes subheadings related to each experiment respectively.

The results are presented and discussed before the thesis is concluded. Appendices containing raw data, material safety information and other relevant information are found towards the end of the document.

2 Literature Review

This chapter will deliver a brief introduction to topics and themes relevant to this multidisciplinary project in order to assist in providing a sufficient background knowledge for all readers. A general understanding of the selected subjects is important to appreciate the importance of this application and the relevance of this work. A review of existing technologies and techniques is included as this will be used as a point of reference to measure the success of this project's findings. The literature review aims to be both informative and guide the reader through to the intended line of thought via the inclusion of opinion and commentary.

A collection of essays from Professor Martin Klein (Klein,1964) based on Einstein's theory that light behaves as both a wave and a particle (photons), also known as wave-particle duality, have been an important reference source reviewed during background reading on the topic. For continuity, throughout this thesis unless otherwise stated, light and its properties will be referred to as waves propagating through material. In the early 90's, Sir William Henry Bragg famously said "*On Mondays, Wednesdays and Fridays we use the wave theory; on Tuesdays, Thursdays and Saturdays we think in streams of flying energy quanta or corpuscles*" (Bragg, 1921)

2.1 The Medical Importance of Near-Infrared Light

Near-Infrared covers the 700nm to 1100nm range of the spectrum which is where light has longer wavelengths, lower frequency and less energy than light at wavelengths in the visible range. At this wavelength range, light is able to travel through the surface of the skin and into the subcutaneous tissue. Biological tissues have maximum light transparency at this wavelength range (Ai et al., 2016). Penetration depths of up to 40mm have been recorded on cadaver studies (Tedford et al., 2015) however, typical penetration depths are recorded as being between 2mm and 15mm in living subjects (Rosenthal et al., 2015, Ai et al., 2015). One study confirms that NIR imaging can provide contrast at tissue depths of 1cm (Gioux et al., 2010). In addition to the above, NIR light is much less sensitive to tissue scattering and haemoglobin absorption which enhances

the penetration depth through the tissue (Wang and Van Dam, 2004). With regards to DNA safety, unlike UV, IR rays have no effect on DNA (Ito et al., 2006). There are also no known natural substances in vivo which emit IR radiation (Ito et al., 2006) which is beneficial to applications such as fluorescence endoscopy as there is no chance of background signal during imaging. With an understanding of the properties of light at this wavelength and its interaction with tissue, it is evident that there is a real advantage for NIR imaging for this application amongst others.

Infrared (IR) light, as a general region of the wavelength spectrum, is best associated with its thermal properties and its use in night vision technology. A review of patient forums would suggest that during minimally invasive, or keyhole surgery using an IR excitation source, thermal effects can sometimes be felt causing discomfort. This internal heating phenomenon is unsupported in literature and the NIR wavelength range encompasses a relatively small range of values extending from the longest wavelength values for red light. NIR light is generally considered as a precursor to IR as the properties of light at NIR wavelengths are not in-line with the Mid-Infrared or Far-Infrared. Beyond 1100nm, the upper limit of NIR, is typically where thermal radiation occurs which is, what most would consider to be the most familiar property found commonly in thermal imaging cameras which are a part of everyday life.

The thermal effect of prolonged exposure to an NIR LASER excitation source has not been recorded for this application and there is no comparable literature using similar values for optical power. A study exploring the thermal effects of endoscopy using an NIR LED source however documents and verifies a rapid increase in local temperature (Kozin et al., 2014). This would indicate that thermal effects are a possibility when using NIR light in medicine.

Thermal damage is often considered collateral and not significant enough to cause harm in human trials however, a study reviewing state of the art Laparoscopic Gastrointestinal surgery highlights the dangers and severity of thermal injury during procedures. This

study (Modlin et al., 2010) states that not only is thermal injury difficult to identify during the procedure but, it often leads to complications following surgery that can result in fatalities. This highlights a real danger when using light at NIR wavelengths under minimally invasive conditions and a thorough investigation considering this risk is required.

After reviewing several guidelines on the safety of NIR exposure to biological material, there is a worrying theme. The International Commission on Non-Ionizing Radiation Protection (ICNIRP) provide guidelines to limitations of exposure to protect the skin from thermal injury however, they also state that there is no defined limit for longer exposure durations. The reason for this is due to thermal pain felt when the skin is exposed to temperatures greater than 45°C, subsequently the pain would limit the exposure so that thermal injury is prevented by avoidance reactions (ICNIRP, 2013). This is also stated in the US department of Health and Human Service guidance, "*the degree of damage (direct and/or indirect) can be significantly influenced by the absence or effectiveness of physiological reflexes and responses*" (NIOSH, 1982).

For this endoscopic application, the patient is typically administered a general or local anaesthetic depending on procedure and so live feedback is not always an option. One health and safety study (Bozkurt and Onaral, 2004) suggests pulsing the NIR light and controlling the frequency of pulses can significantly reduce thermal effects, this supports the proposed work plan.

2.2 Endoscopy and Fluorescence Endoscopy

Minimally invasive surgery or keyhole surgery has many benefits when compared to traditional open surgery. Endoscopy is one type of minimally invasive procedure whereby an endoscope is used to image the tissue. The endoscope comprises a light source and camera at one end and can be rigid or flexible depending on its intended usage. According to a market analysis, the global endoscopy market is worth an estimated

$25.59 billion in 2019 (MarketsandMarkets, Aug 2019), with the NIR imaging market worth an estimated $416 million in 2018 (MarketsandMarkets, Feb 2019).

Ellison's review of endoscopy describes the transition from Bozzini's original candle-lit endoscopic procedure to current cold-light technology. The review is concluded with the following statement which I found to be fitting with the themes in this project "*endoscopy's extensive history teaches us to remain ever the vigilant student, seeking ways to continually better this branch of the medical field*" (Ellison, 2015).

Fluorescence endoscopy utilises a fluorophore which essentially fluoresces when excited with light at the correct wavelength. This offers a visual aid to surgeons during diagnostics and treatment. For this application, a fluorophore is used to mark cancerous cells within breast tissue. The diseased cells absorb and retain a fluorescent marker which when illuminated with a suitable wavelength causes fluorescence of the tumour area. Statistics documented in one study highlight one of the biggest risks following surgical resection of diseased tissue is that 20-25% of breast cancers are resected incompletely (Gioux et al., 2010). One would determine that an incomplete resection would ultimately result in the need for further treatment which presents further risk and distress for patients.

Fluorescence endoscopy offers many benefits to patient outcomes, one lesser-known advantage of using NIR fluorescence imaging is that a significantly lower dose of fluorophore is injected (~10mg) compared to Magnetic Resonance Imaging (MRI) at 700-times this dosage and Computerised Tomography (CT) contrast agents at 5600-times this dosage (Gioux et al., 2010). This has a significant impact on cost of procedure and patient safety, fluorophores used in fluorescence endoscopy are administered during the procedure for immediate usage and so this will also contribute to a reduction in waste of time, money and contrast agent. Certain MRI and CT contrast agents are required to disperse through the body via the cardiovascular system and require administration several hours prior to imaging.

A fluorescence endoscopy light source typically contains multiple excitation sources in order to best illuminate the working area. This is evident in the review of technology within this chapter. The surgeon should be able to view all structures within the field of view, such as blood vessels, as well as fluorescing regions. One study estimates that loss of function through surgical nerve damage occurs in 20,000 to 600,000 patients per year in the US (Gioux et al., 2010). This is an incredibly large population and highlights the need for surgical tools to show as much of the surgical field as possible including non-fluorescent structures when conducting fluorescence-image-guided surgery.

2.3 Chemical Markers and ICG

Chemical markers containing fluorophores are commonly used in modern medicine however, due to expensive and lengthy clinical testing only a limited number have been granted approval for use and of these, even fewer are eventually used due to their expensive price-tag. Use of fluorophores is crucial in surgeries for the removal of cancerous tissue, as when marked cells are excited with the correct wavelength, they fluoresce thus indicating the exact regions of tissue affected by a disease. This in turn means a complete removal of diseased tissue and a reduction in the removal of healthy tissue. A basic image search can quickly reveal the difficulty in differentiating the healthy tissue from the diseased under broadband-light illuminated surgical conditions. It is reasonable to assume that for a trained professional with the option of manual palpation and years of experience, that this would remain problematic and always present a risk of incomplete removal.

The surgical team at Imperial College London use the fluorescent chemical marker Indocyanine Green (ICG). ICG was approved for clinical use in 1956 (Alander et al., 2012) and is currently one of two Food and Drug Administration (FDA) approved dyes at this wavelength range (Gibbs, 2012). Figure 2.1 shows the absorption and emission spectra for ICG diluted in whole blood (Akorn Inc., 2009). The Cymtec light source comprises a 780nm LED channel which is used exclusively to excite the ICG. From meetings with the clinicians, an 810nm light source could also be an option for future

work. ICG has an absorption peak of around 807nm and an emission peak around 822nm when analysed in a plasma solution (Schaafsma et al., 2011). As the emission and absorption peaks are relatively close together and there is significant spectral overlap, filtering is required to establish the highest signal to noise ratio should the excitation remain constant. A narrow band pass filter would be required however, this project aims to present a design without the use of expensive filters through exploiting the properties of the fluorescent marker.

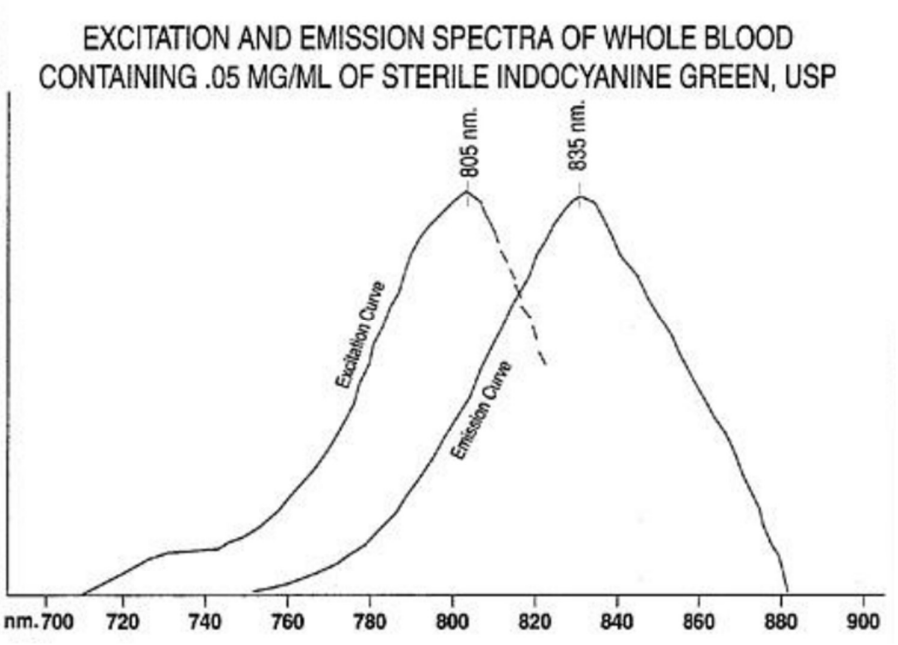

Figure 2.1: Absorption and emission spectra for ICG (Akorn Inc., 2009)

ICG Photobleaching and Signal Degradation

ICG fluoresces when illuminated with light at specific wavelengths, the intensity of the fluorescence is expected to degrade over time also known as photobleaching. Photodegradation negatively impacts quantum yield and is one disadvantage of using ICG (Boddington et al., 2008).

This degradation rate will depend on the concentration of ICG in solution, the solvent and the output power of the excitation source. An understanding of the optical properties of ICG would indicate the optimal operating conditions of the light source at any given concentration of ICG. For clarity, photobleaching or fluorescence intensity degradation

relates to the effect of prolonged or “over” excitation whereby the fluorescent marker suffers irreversible photo-damage leaving the fluorescent signal faded or undetectable.

When a fluorophore is excited with light at the correct wavelength, it moves from a ground state to an excited singlet or triplet state. When transitioning from a ground state to an excited state, a photon is released which causes fluorescence. When in an excited state, the fluorophore may interact with other molecules and form covalent bonds which can change its structure resulting in photobleaching. The structure and local environment of the fluorophore are two factors in determining how many successful cycles of excitation and emission are possible before photobleaching occurs. Unfortunately, the excited triplet stage is prolonged compared to the excited singlet stage therefore increasing the risk of interactions with other molecules. (Surat, 2021)

It is easy to imagine the frustrations in completing a life-changing procedure using equipment which has safety parameters related to exposure time. Liken this situation to using a rechargeable vacuum cleaner with a charge hold equivalent to 15 minutes of constant usage, on the basis that you need to vacuum your home which may or may not take longer than 15 minutes. A reasonable amount of time would be required by the surgical team to complete their investigations and to carry out any additional exploratory work to achieve the best patient outcome. The issues regarding photobleaching are clear, exposure time needs to be long enough to excite the ICG without degrading the compound. The solution is not to simply re-administer the ICG locally for it to be degraded in a matter of seconds as this is wasteful and not economically viable. The ICG exposure parameters for excitation need to be defined and understood so that a suitable light source can be designed allowing clinicians to spend less time administering additional doses and potentially searching for a signal with lower intensity as a result of degradation. This could impact on the success rate of tissue removal as diseased cells may be present, but marked with fluorophore that has become photobleached and can no longer provide sufficient contrast for identification.

If a reduction in the output power of the light source better preserves the ICG signal and reduces the rate of photobleaching, then this may prove a worthwhile opportunity for optimal usage. A secondary benefit to reducing the optical power would assist in addressing the primary concern of minimising the risk of thermal damage to tissue thus stretching the limit on safe time of use.

Literature suggests that photodegradation of ICG is reduced once it is bound to albumin (Prahl, 2019) this is discussed further under the ICG:HSA heading found within this chapter. With regards to documented photobleaching, there are many resources available however each uses a unique combination of excitation power, concentration and solvent. One study generalises that irreversible photobleaching of small molecule organic fluorophores, such as ICG, typically occurs with excitation fluence is greater than 50mW/cm^2. Any fluence rate above this increases the risk of thermal damage to surrounding tissue (Gioux et al., 2010).

The photobleaching threshold of indocyanines on test in another study was approximately 50 mW/cm^2 (Ohnishi et al., 2005), this strongly agrees with the previous research.

One study (Jonak et al., 2011) suggests that ICG's photobleaching rate is significantly lower than its competitors, with fluorescence still detectable up to 48 hours after injection, the excitation source used here was a 785nm LASER but the exposure time is unknown. A second study explores the photobleaching mechanism of ICG (Yaqoob et al., 2006) and concludes that 7kW/cm^2 irradiance would completely photobleach 200μM and 400μM samples of ICG in water in just one second. Another study indicates that fluorescence of ICG at its optimal concentration reached its half-life time within 10 minutes which is more than sufficient for surgery (Haj-Hosseini et al., 2014). The optical properties of ICG are not well documented in literature and while photobleaching is recorded, it is not done so in a standardised way making it difficult to comment on. From the literature reviewed thus far, there are many conflicting statements which suggests

that signal degradation and photobleaching of ICG are not of critical concern and, that there are no standardised instructions for use in research environments.

Fluorescent decay or fluorescence lifetime, which is another parameter under investigation, refers to the residual fluorescence observed following a burst of excitation. An example is the glow of a newly charged glow-in-the-dark sticker once the lights have been switched off. The intensity of the glow is strongest in the immediate aftermath of darkness, this then fades to zero until the object is next charged.

According to literature, ICG fluorescence lifetime appears to vary with solvent and a wide range of values are presented. One study calculates ICG lifetime at around 1ms in its cis photo-isomer and triplet state which accumulate and are observed when the excitation pulse repetition rate is at 1KHz. (Nairat et al., 2014). It is evident that a variety of biochemical mechanisms are involved following excitation of ICG however, this research project will not comment on these in depth. Another study generalises that fluorescence lifetime of indocyanines, such as ICG, in serum ranges from 0.5-1.1nm (Gioux et al., 2010).

Studies investigating the decay of the fluorophore ICG have determined that this is within the femtosecond (Gerega et al., 2011) and picosecond range (Homulle et al., 2016) however, these studies do not specify that ICG is bound to HSA in a 1:1 molar ratio, both used milk as a solvent but only the picosecond study utilised blood. Literature has indicated that ICG bound to HSA enhances fluorescence and improves stability and generally disagrees with the relevance and findings from these two studies. When bonded to a platinum electrode, the lifetime of ICG was found to be between 36 and 55ps (Geddes et al., 2003), this agrees with the previous comment however is not relevant to the application under investigation. The Geddes study also confirms that decreased lifetimes can result in an increased photostability and so there is a relationship between these two parameters.

For this project, decay rates at this speed would not be beneficial to the application as the system is limited by the response of the human eye. The minimum viewing time required for visual comprehension is slightly quicker than 50 milliseconds (Potter et al., 2014) however this would depend on the age and health of the subject. Average eye response is approximately 250 milliseconds according to a study whereby the study population comprises medical students (Jain et al., 2015), assuming that the medical students are young and in good health, it is reasonable to assume that this response time will increase with age and various health factors.

Unfortunately, the excitation and emission peaks of ICG are very close together and the decay rate for ICG is not well documented for this application but is expected to be very fast (microsecond to picosecond range). The experimental setup aims to verify a decay rate for ICG. Images will be analysed in LabVIEW on a frame-by-frame basis, this should contribute to existing knowledge on this topic and ensure that data relevant to fluorescence endoscopy using ICG as the selected fluorophore is available.

Two papers investigating the fluorescence properties of ICG do not comment on the fluorophore decay rate but instead, discuss the differences in fluorescence spectrum depending on the solute and concentration of ICG at determined wavelengths which is useful to understand (Philip et al., 1995, Benson and Kues, 1979)

ICG:HSA

Literature has identified the importance that solvent has on the properties of ICG for example, ICG absorbance peaks at 780nm with emission at 830nm, when combined with HSA, this absorbance peak shifts to 805nm (Boddington et al., 2008).

The Prahl study confirms that the molar extinction coefficient for ICG changes both with its concentration and in the presence of certain protein such as albumin. (Prahl, 2019) The molar extinction coefficient represents a measure of how strongly a chemical species absorbs light at a particular wavelength.

Human Serum Albumin (HSA) constitutes around 50% of human blood protein and is the most abundant protein in plasma. The Nairat study (Nairat et al., 2014) confirms that when ICG is mixed with HSA, both the photostability and fluorescence quantum yield increase. HSA has been selected for use in this research in order to keep the project relevant to the application and to best mimic the behaviour of ICG under real-world conditions where blood would be present in the immediate fluorophore environment.

The following tables have been extracted from the Ohnishi (Ohnishi et al., 2005) study, whereby the physical and optical properties of ICG, ICG:HSA and the “best on test” quantum dot (QD) marker are displayed to compare. Clearly the QD marker is not ideal due to its toxic makeup and the little-known long-term safety of QD usage. This displays the immediate benefits in using ICG:HSA over quantum dot markers or ICG alone.

Table 2.1: Physical Properties of ICG, ICG:HSA and Quantum Dot Molecules

Physical Properties		
	Molecular Weight (Da)	Hydrodynamic Diameter (nm)
ICG	776	1.2
ICG:HSA	67K	7.3
QD	400-800K	15-20

Table 2.2: Optical Properties of ICG, ICG:HSA and QD in solution

Optical Properties PBS Phosphate-buffered Saline (FBS Fetal-bovine Serum)				
	Extinction Coefficient ($M^{-1}cm^{-1}$)	Excitation Wavelength (nm)	Emission Wavelength (nm)	Per-fluorophore QY
ICG	110000 (166000)	779 (800)	806 (811)	1% (9%)
ICG:HSA	121000 (169000)	792 (800)	811 (814)	3% (9%)
QD	559000 (581000)	n/a	808 (814)	8% (9%)

The Ohnishi study (Ohnishi et al., 2005) describes ICG alone as “difficult to detect” due to its poor quantum yield however, ICG bound to HSA or ICG:HSA was found to improve ICG fluorescence and SLN retention however, the fluorescence yield remains significantly lower than other inorganic products on test. This is reflected in the Hutteman study (Hutteman et al., 2011) whereby ICG was mixed with HSA to form a complex (ICG:HSA) which provided many benefits including increased retention within the SLN and improved detection, this research eventually concluded that there was no real advantage in using ICG:HSA over ICG for the SLN procedures completed. Improved retention was also witnessed when 25mg ICG was diluted to 2.5mg/mL with either 25% HSA or sterile water, albumin has been proven to significantly increase the hydrodynamic diameter of ICG resulting in an increase in lymphatic retention. (Hachey et al., 2016)

The Geddes research (Geddes et al., 2003) tested ICG:HSA and defined the concentrations of ICG and HSA using the extinction coefficients Ɛ(780nm) = 130,000cm^{-1} and Ɛ(278nm) = 37,000cm^{-1} respectively.

The Gioux research (Gioux et al., 2010) is the only research identified documenting the peaks for absorption and emission of ICG in serum. The peak absorption is presented as 807nm while the peak emission value is presented as 822nm. Following this literature review, it is evident that the camera selected for experiments should comprise a sensor with a relatively high quantum efficiency value across the 800 to 820nm wavelength range in order to capture the fluorescence.

The image seen in Figure 2.2 taken from the Prahl study (Prahl, 2019) shows the absorbance of ICG in plasma which is essentially what one should expect when using ICG:HSA, it shows that there is a relationship between the concentration of ICG in solution and the absorbance.

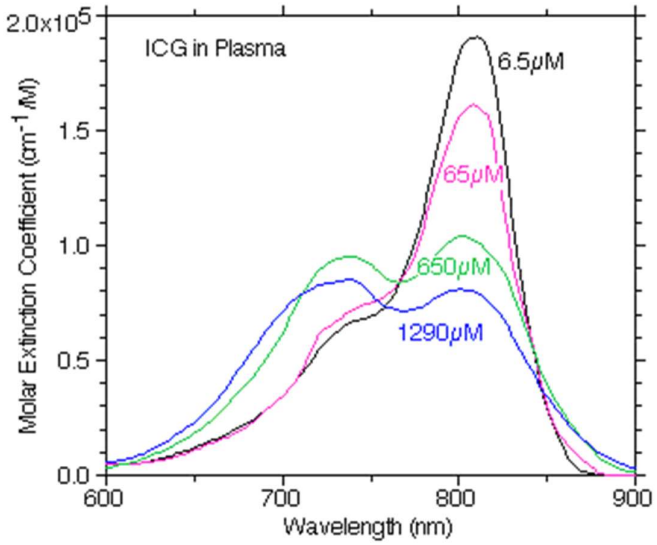

Figure 2.2: A Plot to show the absorption of ICG in plasma at different concentrations. (Prahl, 2019)

2.4 Detecting Cancerous Tissue

Lymph nodes are the initial site for metastases for most cancers. The sentinel lymph node (SLN) receives the first lymph flow from a malignant tumour and is the first location where a malignant disease can be identified (Mellor et al., 2000). If no malignant cells are discovered in the SLN then there will be no requirement for further investigation and the patient will not be subject to any additional invasive procedures (Ohnishi et al., 2015).

The SLN is located around 1cm beneath tissue, as discussed previously, it is known that tissue is highly scattering due to its high water content (Ohnishi et al., 2005). ICG is injected under the skin where it travels via the lymphatic system to the lymph nodes (Fujiwara et al., 2009). The Hachey study (Hachey et al., 2016) on esophogeal cancer patients, concluded that NIR lymphatic mapping is both feasible and safe when used to identify regional lymph nodes when ICG:HSA is used. In fact, ICG was found to be the superior lymphatic imaging agent during this study, with positive identification of 100% of regional lymph nodes. When removing cancerous tissue from the breast without use of fluorescence endoscopy, also known as lumpectomy, it is common practice to insert a guide wire into the tumour site with the assistance of x-ray or ultrasound. A reasonable portion of tissue surrounding this wire is then removed. Following excision, the tissue is then lab tested to check the margin around the cancerous tissue. A positive margin indicates that the cancer removal was incomplete and further surgery may be required. It is clear that use of fluorescence endoscopy is suitable for breast cancer removal and offers a significant improvement to patient outcomes and surgical success rates.

2.5 Optical Modelling and Design Considerations

The company partner Cymtec Ltd have designed and manufactured an LED excitation source comprising red, green, blue and NIR LEDs. This light source has guaranteed that it is possible for surgeons to select any combination of LEDs and obtain a fully homogenised output at the distal end of the liquid light guide (LLG). Should the red, green and blue LEDs all be switched on for white light, colour temperature may be adjusted by fine-tuning the power selection of individual colour channels via a LabVIEW interface. The LabVIEW programme was designed by the staff at Imperial College London for exclusive use with this device. The optics in this design are custom and are coated with dichroic and anti-reflective coatings to reduce the number of components. Desired specifications are communicated by the surgical team at ICL during the design process.

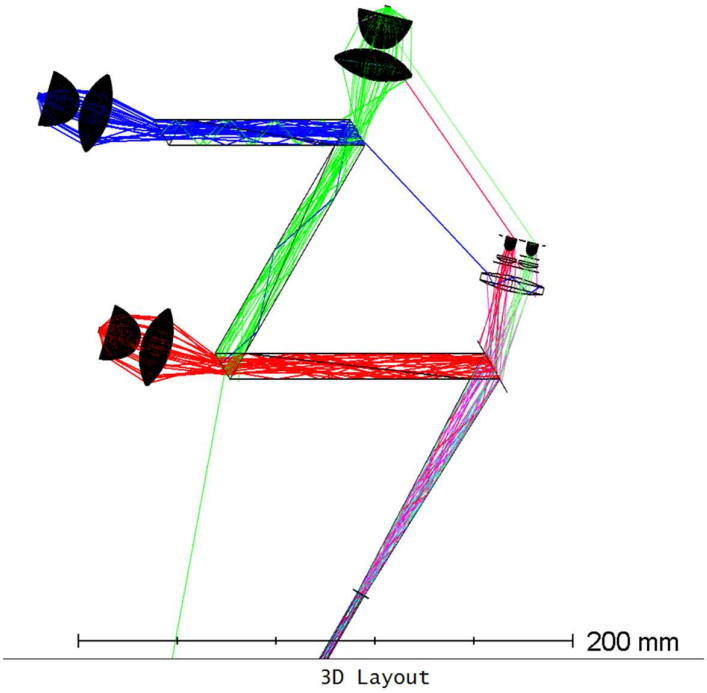

Figure 2.3: Zemax model of the Cymtec RGB and IR endoscopic light source

Figure 2.3 shows the optical model for this design in Zemax, light is combined and homogenised via three, tapered light pipes. This light pipe design was patented by Cymtec Ltd. In 2013. Each corner of the light pipe is finished with a dichroic coating so that light of the desired wavelength cannot leave the system; this improves efficiency and reduces losses. The Red, Green and Blue LEDs are mounted behind one of three custom lenses. The NIR LEDs are in a 2x2 array and are mounted behind another custom lens. Not seen in the Zemax model is the extensive thermal management system, mounts and electronics which are found within the housing of the delivered unit.

An intense white light is observed at the output of the finished system once all channels are powered up. Light is focused down to the LLG aperture which is 3mm in diameter for this design. Figure 2.4 presents the output at the distal end of the light pipe for each channel as per Zemax calculations, here the uniformity of light can be appreciated. The Zemax programme presents the optical output following ray tracing however, the measured output from the prototyped design is typically less than that calculated in

Zemax due to a multitude of reasons for example, dust or particles in the atmosphere landing on optical surfaces and the environmental conditions.

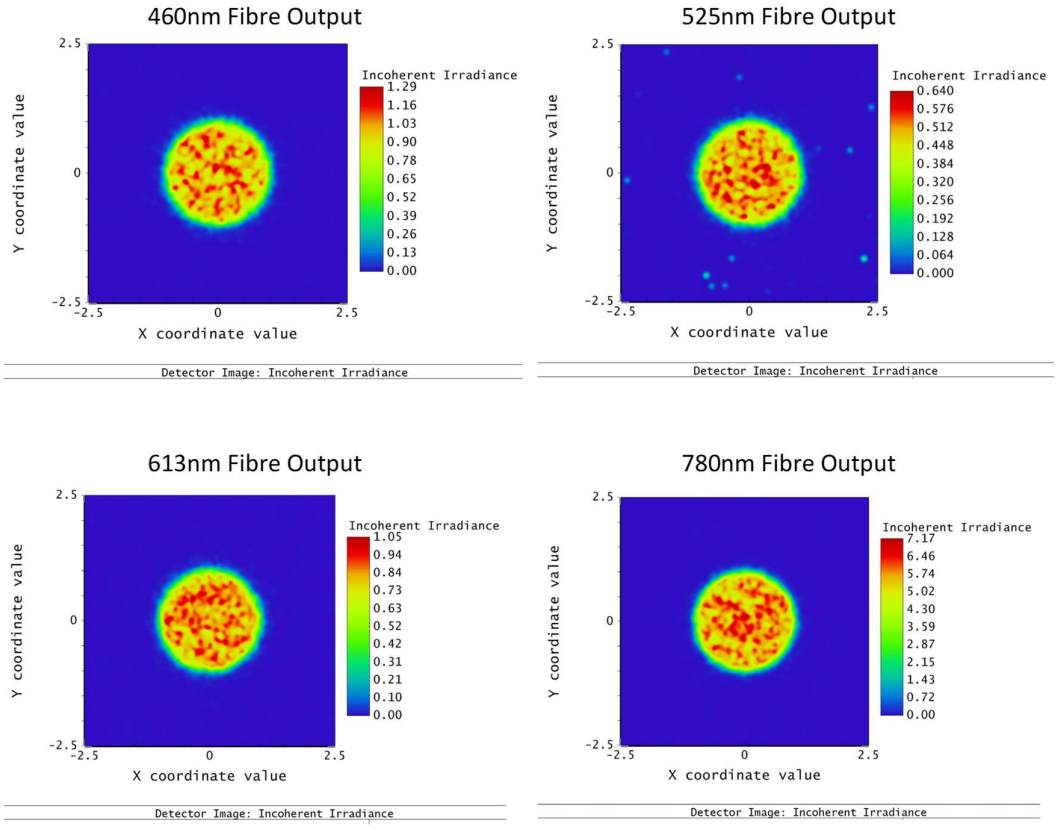

Figure 2.4: Output at the fibre for each channel in Zemax

Etendue

For the most effective light coupling, the etendue of the light at the distal end of the multiplexer should match the proximal end of the LLG to reduce light loss in the system. Etendue (G) is equal to the area of the light emitter (S) multiplied by the solid angle of the light (Ω). The component within the optical system with the lowest etendue sets the limit of the entire system (Zhu and Blackborrow, 2011). Etendue cannot decrease, it can remain constant or increase. Etendue must be considered at each coupling point throughout the system however, the aperture of the LLG is of a fixed dimension and is likely to present the biggest challenge during design. For the experimental setup, without

the assistance of the company partner, a simpler setup has been designed whereby light isn't focused down to match a specific component.

$$G \approx S\Omega \ [mm^2.sr] \qquad \textbf{2.1}$$

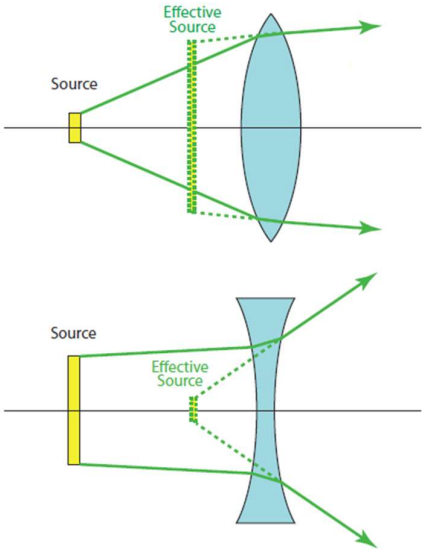

Figure 2.5: An illustration of Etendue conservation (Wood, 2012)

Figure 2.5 shows two systems comprising a simple source with a converging and diverging lens respectively (Wood, 2012), the illustrations show how the actual source together with the "effective" source differ – that is the source you might expect by tracing the resultant beam through the system in reverse.

Snell's Law

When light propagates from one medium into another, it is fundamental to understand Snell's Law especially when you are aiming to exploit the phenomenon of total internal reflection (TIR) to increase system efficiency. At the critical angle, 100% of light is reflected at the boundary (no light transmits through the boundary), the angle of refraction θ_r is equal to 90°. The critical angle θ_c is derived from Snell's law, see Figure 2.6.

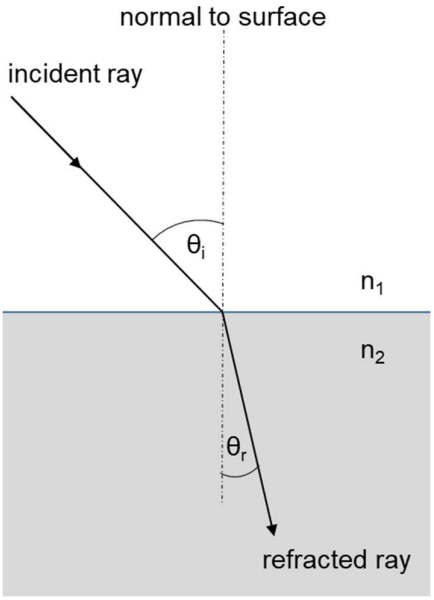

Figure 2.6: A schematic diagram to help describe Snell's Law

$$n_1 \mathrm{Sin}\theta_i = n_2 \mathrm{Sin}\theta_r \quad \textbf{2.2}$$

$$n_1 \mathrm{Sin}\theta_c = n_2 \mathrm{Sin}90° \quad \textbf{2.3}$$

$$\theta_c = \sin^{-1}\frac{n_2}{n_1} \quad \textbf{2.4}$$

2.6 Current Application-Specific Technology

Existing literature is rich with medical research utilising ICG as a fluorophore for imaging the hepatic, cardiovascular and ocular systems. Filtering this wide selection of reference material to endoscopy-based research allows for the existing and gold-standard examples of technology to become clear along with other prototyped systems undergoing pre-approved testing.

ICG has been used medically since the mid 60's, around 10 years after it had been clinically approved, an ICG review paper published in 2012 shows just how popular this

chemical marker is and its many applications, see Table 2.3 for the number of queries from four leading databases.

Table 2.3: The number of ICG-related publications (Alander et al., 2012)

Keyword	Total number of ICG-related publications– correct for 2011
“Indocyanine” (ICG)	11,586
ICG and “surgery”	3,248
ICG and “liver”	3,218
ICG and “retina”	1,600
ICG and “cancer”	1,251
ICG and “tomography”	1,381
ICG and “imaging”	1,698
ICG and “heart”	660
ICG and “wound”	268
ICG and “lymph”	255
ICG and “brain”	262
ICG and “breast”	339
ICG and “laparoscopy”	73

It is evident from the information above that ICG use is established in breast cancer research. To assist with component selection for this project, information with regards to experimental light source and camera setup has been documented in the review paper which Table 2.3 was extracted from, see Table 2.4 (Alander et al., 2012). Where λ_e represents the minimum emission wavelength in nm and λ_c represents the minimum camera wavelength, Table 2.4 shows that there was no study utilising LASER light source to excite at 810nm, the excitation wavelength proposed by the team at ICL. There is an instance of both LED and LASER with emission wavelength at 780nm within the data however, which is in line with the Cymtec design. What we cannot gather from this data is whether the ICG is in solution, this has a significant impact on the peak excitation and emission values. The data does indicate that a cooled charge coupled device (cCCD) or charge coupled device (CCD) camera type is typically used when imaging fluorescence at this wavelength range. The camera selected for use in this study is

important to the success of acquiring a quality image. The majority of studies reviewed over the course of this project utilise multiple cameras, this is both costly due to the high number of filters required and inefficient in terms of synchronisation. Experimental data acquired during this project should utilise a single camera only, more details of this can be found in later chapters.

Table 2.4: ICG Instrument Properties (Alander et al., 2012)

Device	Light	λ_e	Camera	λ_c
AA_1	LED	740	cCCD	820
FX	Halogen	755	cCCD	830
H_1	Xenon	Unspecified	CCD	810
IC-View	LED	780	CCD	835
Maestro	Unspecified	710	Unspecified	800
OMC_1	Halogen	760	KP-160	820
Pentero	LASER	780	Unspecified	835
PDE	LED	760	CCD	820
VasView	LED	760	CCD	830
UK_1	SLD	793	Unspecified	807

There are a wide variety of published studies relevant to the imaging of ICG stained tissue and only a fraction are related to the detection of cancerous tissue in the breast. Regardless of application, these studies are helpful in understanding a good working practice when using ICG, the most common detection methods and suitable sources of excitation. Figure 2.7 shows ICG stained breast tissue under bright-field (labelled Colour) and dark-field (labelled NIR) conditions. The reference does not indicate the imaging technique utilised or if the combined image was available to the surgeon in real-time (Schaafsma et al., 2011). It is useful to see the colour and NIR images side by side as they both show such different structures, ideally the surgical team will have access to

both images on a single screen to allow them the best of both views. The colour-NIR merge image offers a quality image with good synchronisation of image overlay, structures lying beneath the skin can easily be viewed, this quality should be matched or improved on during the experimental portion of this project. It is clear that the colour and NIR images alone are not helpful to the surgeon and it can be dangerous to use just one, we can see that any unstained tissue appears as background under NIR conditions – including the fingers of medical staff holding the swab or the surgical tools used to retract the skin. Detail from both images must be available to enhance surgical success.

To assess the quality of the synchronisation, the corner of the swab from Figure 2.7 was analysed as this is a landmark that can be seen in both the colour and NIR frame. The location on this point in both frames matches thus the image synchronisation here is excellent.

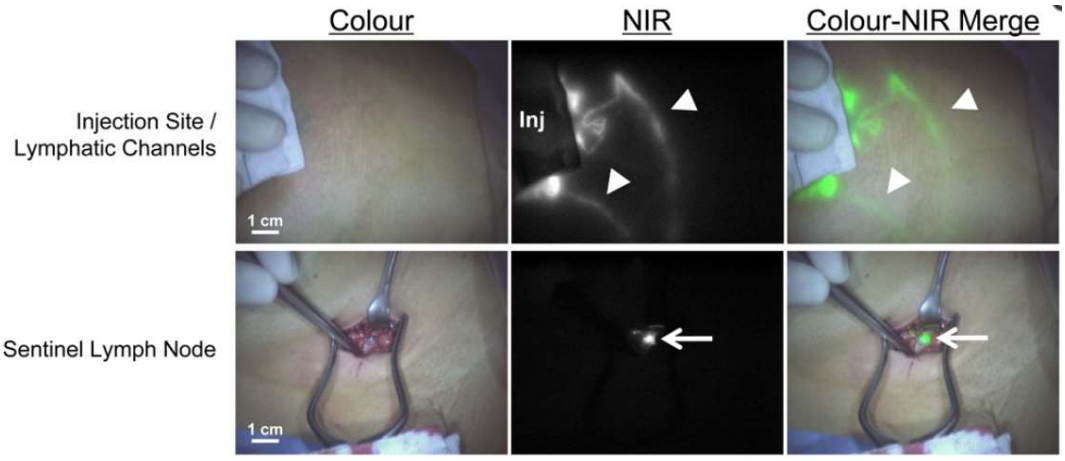

Figure 2.7: ICG stained tissue under bright-field and dark-field conditions (Schaafsma et al., 2011)

The following Figure 2.8 shows an ICG stained lymph node, in full colour, fluorescence only and combined overlay (Crane et al., 2011). The study looks at real time NIR fluorescence imaging of sentinel lymph nodes in cervical cancer surgery. The study does not indicate specific details of the excitation source utilised other than that there is a white light source and NIR LASER diode, details of the camera system are unclear. Overall, the study presents a successful detection method however, the overlay image

suggests that the combination approach used here cannot retain the fine detail of the fluorescence signal. There is a risk that internal/underlying structures will be missed and potential for unnecessary removal of healthy tissue. Ideally, the overlay of the pseudocolour should be identical to the fluorescence signal, in this case the saturation of the pseudocolour is too high and so the complexity of the fluorescing tissue is lost. The equipment seen in the frame has also received the pseudocolour which implies some inaccuracies with the method of combining the two data streams.

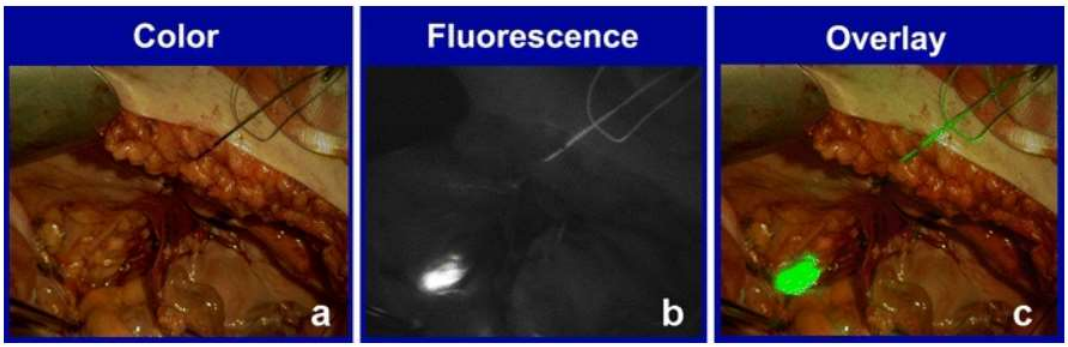

Figure 2.8: ICG stained lymph node under bright-field and dark-field conditions (Crane et al., 2011)

Taking the crossover of instruments as a reference point in Figure 2.8 shows that the combined image is a good example of image synchronisation however the application of the pseudocolour is not specific enough and should not include the obvious reflection from the metal clamp.

Another study focuses only on detecting the ICG signal, the camera system named “HyperEye” is used during surgery to assess the success of graft placements (Handa et al., 2010). The study documents the numerous filtering steps required in order to simultaneously detect the bright field and fluorescence signal. Results show success in designing and manufacturing an instrument capable of detecting both signals while maintaining image quality however, there is no comment on is the cost involved with using custom filters or specifics of the excitation source used during surgery.

A publication documenting the findings of a first-in-human clinical trial of an ICG and Methylene Blue (MB) detection system is very relevant to this work. The FLARE^{TM},

Fluorescence-Assisted Resection and Exploration system (Troyan et al., 2009) has progressed one stage further than the Cymtec light source as the human clinical trials are complete and commercialisation has begun. The design utilised in this study combines the NIR fluorescence signal from two chemical markers so as to show additional structures. In brief, the MB shows all lymph nodes whiles the ICG shows only the sentinel lymph node whereby the sentinel lymph node represents the presence of disease. The excitation source in this system is high power LED however the specifics are not provided. From the images provided in Figure 2.9 it is clear that the colour temperature of the white light has been adjusted as the tissue appears very grey (cold), it is unclear whether the surgeon is able to colour balance during usage. The schematic of the instrumentation is presented in Figure 2.10, dichroics are used to split the output signal into three wavelength bands for detection by one of the three cameras. Again, the pseudocolour applied to the merge image is not a perfect match, this becomes a problem when the fluorescing area is very small in comparison with the FOV and internal structures become lost due to reduced contrast. The pseudocolour appears as a homogenous region which is not a true reflection of the fluorescent data. One study utilising this system verifies that the grayscale NIR image is simply converted to pseudocolour and overlaid on top of the colour video image (Lee et al., 2010).

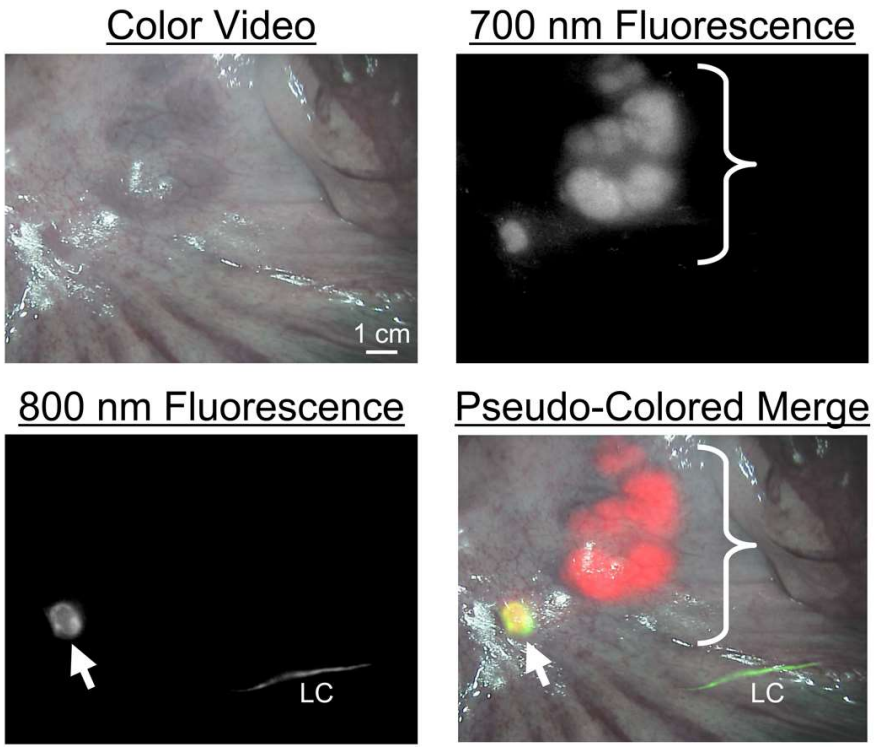

Figure 2.9: ICG and MB stained tissue imaged using the FLARE(TM) system (Troyan et al., 2009)

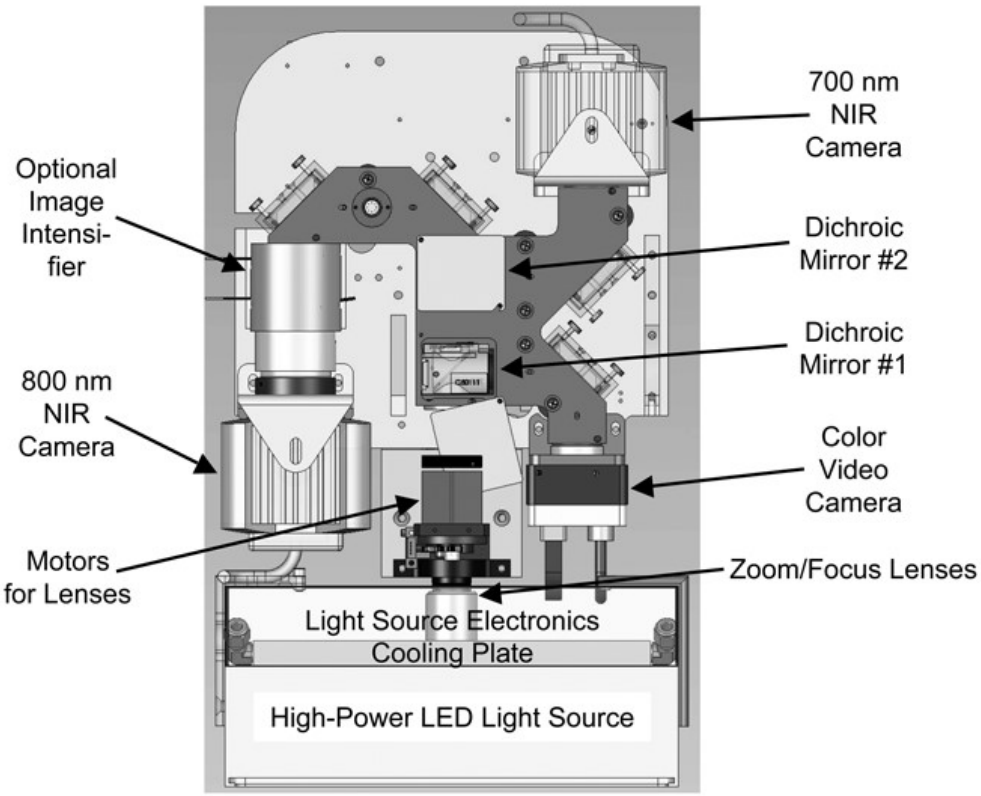

Figure 2.10: Schematic of the FLARE^{TM} system (Troyan et al., 2009)

The three cameras in the above system would significantly contribute to cost, the reported cost of the FLARE™ system is $150-120K (Binns, 2009, Nagaya et al., 2017). A miniFLARE™ system has been designed and selected for use in a human clinical trial (Mieog et al., 2011) whereby ICG and MB are administered to patients for SLN mapping in breast cancer. The system is described as offering the two semi-independent NIR channels. In general, this allows for a smaller, cheaper system however, when compared with the original product the specifications suggest a lower sensitivity, rigidity and fluence. Reported cost of the miniFLARE™ system is $40K (Nagaya et al., 2017) which is a significant difference. An F-FLARE system is proposed to combine the advantages of the two previous models and offer a level of sensitivity somewhere between the original and mini designs. The F-FLARE system is a proposed addition to the FLARE family. Dr. John Frangioni is the inventor of the FLARE™ system and CEO of the company Curadel which exclusively develops, manufactures and markets the product range. From the literature reviewed, this appears to be the most popular system relevant to this project and has received huge success in its field.

A handheld two channel (NIR and White LED) system manufactured by Hamamatsu Photonics K.K. known as the Photodynamic Eye or “pde-neo” is commercially available and research has been published using this system to excite and image ICG in vivo (Furukawa et al., 2010, Hirano et al., 2012, Abo et al., 2015). The NIR LED channel is documented at 760nm with unknown power and no possibility of merging colour and grayscale images. Cost of this handheld system is £40K excluding accessories and installation. Unfortunately, it is difficult to obtain the detailed technical specifications for this product direct from the manufacturer.

A more popular and well-established system is available from Stryker Endoscopy whereby a family of SPY products exists for NIR imaging. The systems are multichannel and include a combination of fluorescence and white light imaging. One study reported that images are combined post data acquisition and an exposure time of 67msec is used (Ohnishi et al., 2005). SPY Fluorescence Imaging was launched in 2005 and the design

incorporates LASER light sources for white light and NIR channels for ICG imaging applications (Stryker). Specifications are not published in the company sales literature other than the NIR light being of “low intensity”. The company lists over 230 publications whereby SPY products are used up to 2019 which is very impressive.

2.7 LED vs LASER for Medical Equipment

Traditionally, medical equipment comprising a light source would utilise broadband bulb technology. While this made the most of components available at the time of manufacture, this technology has become outdated and any existing bulb-based equipment leads to high operating and maintenance costs. The modernisation of medical equipment and the rise in cheap and affordable LED components has resulted in LEDs virtually replacing all bulb technology. In 2018, market leader KARL STORZ released its latest NIR/ICG imaging system for Neurosurgery (KARL STORZ Endoscopy-America Inc., 2018) which comprised a Xenon light source which implies that this remains a reliable technology, for reference this company uses either Xenon bulbs or LEDs within its illumination range. Another market leader, Olympus, also choose to exclusively use Xenon bulb technology within its medical illumination systems (Olympus, 2020).

There are a multitude of benefits with choosing LEDs when compared to traditional bulb technology however, the comparison between LED and LASER is not frequently discussed for medical applications.

In general, LEDs provide good compromise between efficiency, power, cost and spectral confinement. Unfortunately, the power of a single LED is typically insufficient for medical equipment and so multiple LEDs are required, typically packed into dense arrays. When in an array, as seen in the Cymtec light source, thermal management becomes an issue as does the number of collimators, filters and lenses required to provide the correct optical power within the FOV. On the other hand, LASER diodes are spatially and spectrally confined but can become expensive and difficult to integrate depending on their specifications. Safety concerns exist and there is typically a requirement for

personal protective equipment (PPE) in the form of protective glasses and shields. Integration of temperature control, which is fundamental when using LASERs, can add complexity and cost to design. Speckle can also cause problems and may need to be removed from the FOV via additional optics for certain applications (Gioux et al., 2010).

For endoscopic applications, the surgical field is illuminated remotely whereby light is delivered to the patient via a light guide. When using a light guide, the coupling efficiency needs to be excellent with a high fluence rate across the FOV. While LEDs are preferable for local applications (illumination directly above the patient), LASER is preferable for remote applications (Gioux et al., 2010).

It appears as though LASER is the superior choice for endoscopic applications however, an export of LASER medical devices on the FDA's website returns around 2500 products, none of which utilise LASER as an endoscopic light source or excitation source for chemical markers. These devices can be broken down into the following applications as listed in Table 2.5:

Table 2.5: A list of Medical LASER Applications and the Quantity of Associated Devices

Application	Number of Devices
Ophthalmology	539
Surgery – LASER Cutting	742
Dentistry	284
Dermatology	872
Cosmetic Surgery	10
Thermal Therapy	4
Other	86

A search for medical papers utilising LASER in either phototherapeutic or diagnostics offers similar results where other than the SPY products (Stryker) commented on earlier in the chapter, there are virtually no pure LASER endoscopic light sources. This project

will investigate the advantages and disadvantages of using LED and LASER when imaging solutions containing the fluorophore ICG to help understand the lack of commercially available LASER products for endoscopy.

One contribution to the lack of LASER products could be perceived safety, it is common to find surgeons choosing a LASER cutting tool in place of the traditional scalpel and sutures, perhaps the idea of LASER as an illumination source seems excessive and dangerous.

Selecting Ophthalmology from the above table, LASER eye-surgery is a good example whereby equipment has been designed around a LASER component for a specific application. A class 4 LASER, the highest class in regards to potential danger, is used to restore vision. A medically trained professional will administer the treatment following a previous patient consultation. It is estimated that around 600,000 procedures utilising the LASIK products are complete each year in the united states (Watson, 2019) This procedure has become very accessible, affordable and popular with the understanding that a LASER beam pointed directly into the eye is not strong enough to deter patients. This is interesting as the success of medical equipment, such as the LASIK devices, can heavily depend on perceived risk and whether the benefits outweigh this risk from a patient's perspective.

There is a wide range of IPL, intense pulsed light, LASER hair removal and LED and LASER based skin-care products available on the market for unsupervised home-use. It is understood that at home devices are not well regulated as products do not require FDA clearance however, the risk lies with the user. For safety and a guarantee of quality outcome, treatments should be administered by trained professionals using approved products. From brief research completed in the availability and safety of these types of product, there really does not appear to be any strong negative reviews or negative feedback from a safety perspective. There is a large market for these types of products, they are affordable and can be purchased at large supermarkets and pharmacies.

Although, prolonged and incorrect use of these products is more than likely going to result in damage, perhaps the target audience has more sense than to overlook instruction manuals and safe limitations, the only negative findings were related to disappointing results. From a health and safety perspective, there are dangerous hand-held LASER pointers available for purchase by the public however, there does not appear to be an equivalent problem with LED devices. Again, this may have to do with the age of the consumer and easy access to these types of product.

A visit to the BMLA annual conference, British Medical LASER Association, towards the early stages of this project highlighted the variety of procedures which rely on LASER-based techniques. The majority of applications were aesthetic/cosmetic surgical tools whereby the light (typically pulsed) is administered by a trained professional. The BMLA is one of many global organisations which campaign for LASER safety and education.

The argument that public perception of safety with regards to LASER products may be the reason behind the differences in number of medical light sources with LED and the number with a LASER component but the evidence is weak. With so much saturation in the endoscopy market for LED or LED/LASER combination systems there must be a reason why pure LASER is not considered equally.

2.8 Conclusion

Following a review of existing literature, several gaps in knowledge have been identified which will be addressed with this research, these are as follows:

- There is very little research available focusing on the optical properties of ICG, specifically its decay rate and lifetime.
- There are a very small number of papers which concentrate on the equipment itself and not the various procedures. Even so, these are not detailed and the technique in which images are captured and combined remains unclear. Multiple detectors and filters are commonplace amongst the equipment used in these

studies and it is not clear if there is a possibility to remove them or significantly reduce their number.

- There are conflicting reports with regards to pulsing the excitation of ICG
- There is no research to suggest that a single monochrome detector could replace the multi-detector type products which have been reviewed.
- There are many LASER-based medical devices however only one commercially available system related to endoscopic imaging where LASER is used as an excitation source. Several LED and LED/LASER combination products are commercially available for endoscopy which represents the majority of the market for endoscopy illumination systems.
- LED and LASER outputs have not been compared in-vivo for endoscopic applications in order to determine if the properties of the light impact on image quality.

In general, fluorescence imaging is a very popular and successful diagnostic tool and has existed for a number of years. The field in general generates a lot of sales and research interest with marketing literature predicting significant growth over the next five years.

In regards to minimally invasive cancer resection, fluorescence endoscopy is not yet an industry standard and as a procedure, is mainly performed at teaching hospitals such as ICL. Traditionally, teaching hospitals are the main facilities that can afford the chemical markers and expensive equipment which is the real issue for this application.

The Cymtec light source offers real advantages to existing methods and enhances the quality of excitation however, this is an expensive design with custom optics and coatings. This system was designed specifically for a customer according to their list of desired specifications. This customer is able to capture two channels of imaging, white light and fluorescence, leaving the surgeon to select which LED channels are configured

and what is displayed on screen in real-time. This data capture is not simultaneous and adopts a white-NIR-white-NIR-white-NIR synchronised collection technique.

It is clear that LEDs are beneficial to endoscopy and one can assume that this will become the standard technology to retrofit or upgrade current bulb-based models. For the merged white light and NIR images that have been reviewed, it is evident that applying a pseudocolor to merged images significantly alters the quality, resulting in a loss of complexity and depth of the fluorescence. There appears to be a gap in the market with regards to single camera systems which this research will contribute to. All work completed so far is original and all opinions presented in this chapter are personal.

3 Materials and Methods

This chapter will explain the experimental setup, data acquisition and data processing techniques used in this research. The selection process for specific components will be included along with any background theory. Where values have been taken directly from literature, these will be referenced accordingly.

For simplicity, this study is separated into three sections which are briefly described as follows:

Experiment 1 – Investigation of experimental parameters

This aims to confirm if fluorescence is detectable using the proposed techniques as well as the effect of changing illumination conditions and concentration of ICG in solution.

Experiment 2 – Identification of the presence of photobleaching of ICG in aqueous solution.

This includes determining if there is any detectable degradation of the intensity of fluorescence over time and if there is a specific parameter which governs the rate of this decay.

Experiment 3 – Trigger-controlled imaging of ICG fluorescence using a single camera.

This is to determine if there is any opportunity to detect residual fluorescence post-excitation.

3.1 Component Selection

3.1.1 Camera

Camera Technology

An initial review into cameras which would be suitable for this project, in regards to quality and cost, presented two choices as observed during the literature review Table 2.4, Charge Coupled Device (CCD) or Complimentary Metal-Oxide-Semiconductor (CMOS). While there are advantages and disadvantages with both, research indicated that a CMOS sensor would be suitable for this research. SONY, the largest camera sensor

manufacturer, have discontinued production of its CCD sensors (Asche, 2017). The team at ICL used a CCD camera however, the specifications of the CMOS camera selected were suitable and within budget, an increase in noise is expected when selecting CMOS over CCD. For future work, the option of using a scientific CMOS camera or sCMOS could also be an option. The sCMOS can fully replace CCD sensors with regards to efficiency and have been proven to improve key specifications such as dark noise, quantum efficiency and signal to noise ratio (SNR) (Asche, 2017). One comparison study, conducted by BASLER AG, indicates that a better image is produced with the CMOS sensor under low-light test conditions. Low-light conditions are significant for this research as exposure time is a parameter that will be under investigation, dark current typically increases under low-light conditions which impacts on image quality.

Essentially, the camera will detect the presence of fluorescence within the sample. The sample contains the fluorophore ICG which emits fluorescence when illuminated with the excitation wavelength. In order to create a digital image, photons (discrete packets of electromagnetic energy) incident on the sensor are converted into electrical energy. This energy is quantified and stored so as to reconstruct the visual characteristics of the field. Planck-Einstein relation allows calculation of the energy of a photon (in Joules),

$$E_p = \frac{h.c}{\lambda} \qquad \textbf{3.1}$$

The Planck-Einstein equation is presented in Equation 3.1 whereby h is Planck's constant, λ is the desired wavelength and c represents the speed of light. Joules can be converted into electron Volts (eV) by dividing by $1.6x10^{-19}$ using the relationship 1eV = $1.6x10^{-19}$Joules. At 780nm, the energy of a photon is calculated to be $2.547x10^{-19}$ Joules or 1.592eV.

The camera selected is 8-bit which provides 256 grayscale levels of luminance per pixel whereby 0 represents complete darkness and 256 is complete saturation which appears white.

Camera Specifications

The minimum intensity at the source should be larger than the dark noise in order to produce a readable and distinguishable signal. The camera noise related to the sensor is constant however we are using an external lens and so the total noise will increase slightly with an increase in light intensity.

Using the theoretical values from the camera technical specifications, temporal dark noise is 2.14e^- or 14.01DN (Data Numbers), saturation capacity or well depth is 11179e^-, absolute sensitivity threshold is 2.95e^-. Resolution is 1440 x 1080 pixels and images collected are 8-bit, pixel size is 3.45μM. The SNR is documented as 40.48dB which can be calculated using the equation below whereby FWC represents the full well capacity. The SNR is calculated using the following Equation 3.2.

$$\mathrm{SNR} = 20\log\sqrt{FWC} \qquad \textbf{3.2}$$

The dynamic range is an important camera parameter as this determines the number of distinguishable intensity levels, the equation for dynamic range is presented in Equation 3.3 whereby, FWC represents the full well capacity. For the selected camera, the dynamic range is 71.6dB.

$$\mathrm{Dymanic\ Range} = 20\log\frac{\mathrm{FWC}}{\mathrm{Dark\ Noise}} \qquad \textbf{3.3}$$

Figure 3.1 shows the quantum efficiency (QE) curve for the sensor within the selected camera. The Grey curve shows the data associated with the monochrome camera version chosen. At 800nm, the QE is estimated to be 27% therefore, for every 100 photons that arrive at the detector, only 27 will be converted into electrons. While this is significantly lower than the QE for the visible range, it should be sufficient to capture fluorescence and is similar to the QE curve of the camera used by ICL for their imaging study.

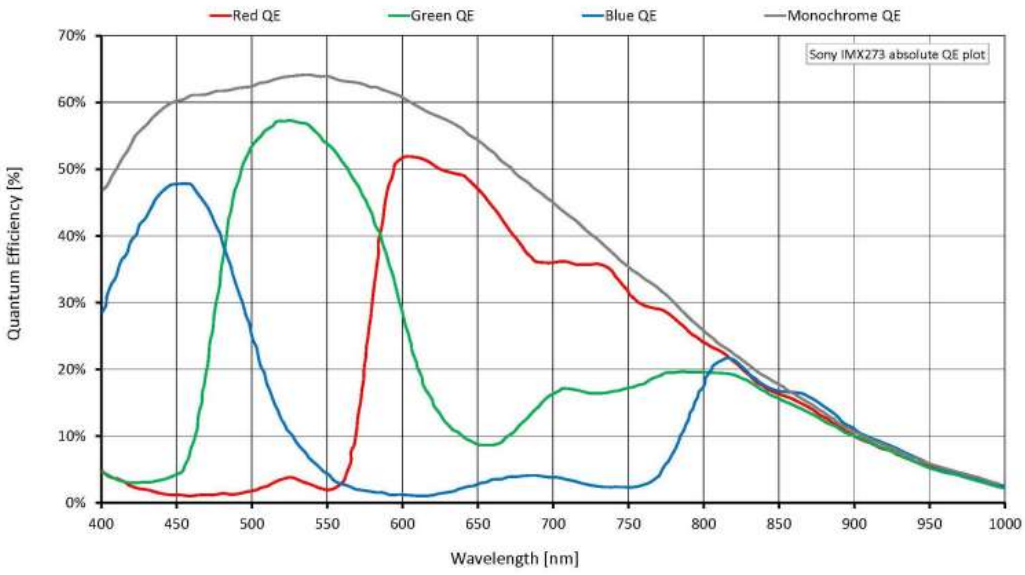

Figure 3.1: Quantum Efficiency Data for the Sony IMX273 (Allied Vision)

3.1.2 Excitation Source

The LED and LASER components are selected based on power, cost and availability. The excitation wavelength of 780nm is selected as this is in line with existing research. Fortunately, this wavelength is available for both the LASER diode and LED.

The power of the LED is not essential as there is flexibility within the circuit for an array should the power be insufficient. The power of both the LED and LASER is required to be similar in order to fairly evaluate the differences between both sources. The LEDs selected are described as “ultrabright” with 7.2mW of forward optical power. The spectral intensity distribution of the LED is seen in Figure 3.2 where we can see the central wavelength at 780nm.

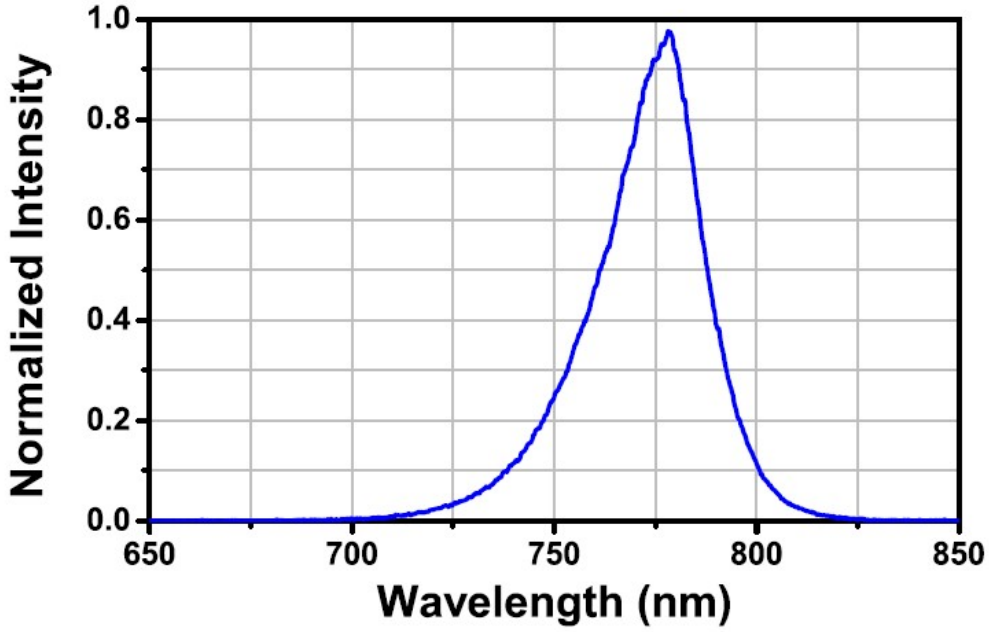

Figure 3.2: Spectral Intensity Distribution of LED780E (Thorlabs)

The LASER diode was selected from Thorlabs for easy integration into the existing Thorlabs mount for connection to both power and temperature control. The diode selected provides a maximum of 12mW of output power in an elliptical beam. Figure 3.3 shows the LASER diode mounted in the Thorlabs TCLDM9 mount which has a cover plate and large aperture. A lens adapter was used to secure the lens inside the aperture of the mount.

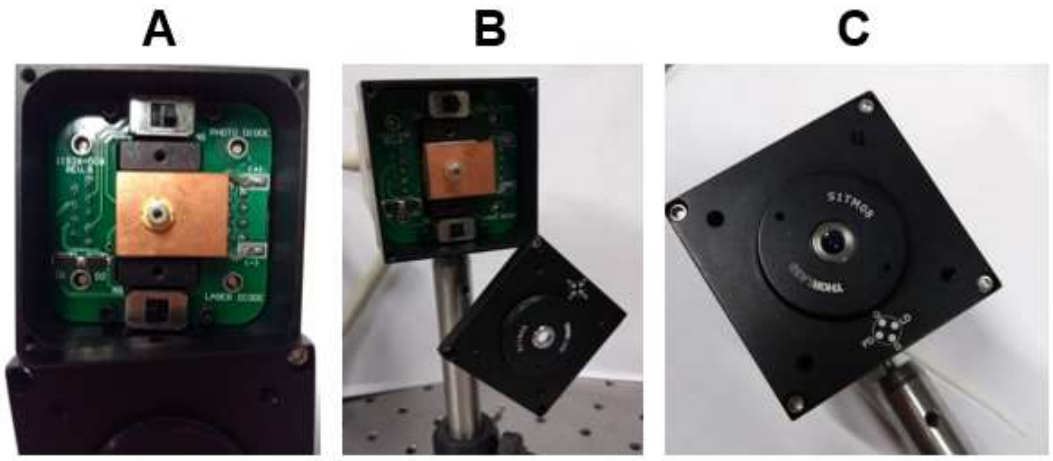

Figure 3.3: Photographs showing the mounted LASER diode (A), mounted diode with cover plate removed (B) and mount fitted with aspheric lens for beam collimation (C)

Beam Collimation

The LASER diode is pushed into the mount as per the mounting instructions so that good contact is made between the diode housing and the heat sink material as seen in Figure 3.3 insert A. An aspheric lens is mounted over the diode using an adapter in order to collimate the beam as seen in Figure 3.3 insert C, else the angle of divergence would result in poor control of sample illumination. For this diode, the perpendicular beam divergence is 30º and 8º for parallel. The collimating lens was selected as it has a numerical aperture (NA) of 0.3 which is larger than that of the diode (≈ 0.26) and a focal length of 6.2mm. The traditional numerical aperture calculation, as seen in Equation 3.4 is simply the refractive index (n) of the medium between the lens and sample multiplied by sine of half of the angular aperture (Θ).

Due to asymmetry in the axis, an elliptical beam forms as the light diverges, if this was a concern an amorphic prism pair would be required to magnify the minor axis and create a circular shaped beam. To calculate focal length, the lens makers equation in air is used as seen in Equation 3.5 whereby f represents the focal length, n is the refractive index of the lens material and R_1 and R_2 are the radii of curvature at each side of the lens.

$$NA = n\,(\sin\theta) \quad \textbf{3.4}$$

$$\frac{1}{f} = (n-1)\left(\frac{1}{R_1} - \frac{1}{R_2}\right) \quad \textbf{3.5}$$

Collimation is initially checked by eye using a beam viewing card and running this along the length of the optical bench to determine the change in beam spot size as shown in Figure 3.5. The beam is imaged using a beam profiler and accompanying software as seen in Figure 3.4. Uniformity along the optical bench was not essential for this experiment as the sample was secured as close to the light output as physically possible. An attempt to collimate was made however, an external mount was required to hold the lens which limited positioning of the sample stage and spectrometer thus proving counterproductive.

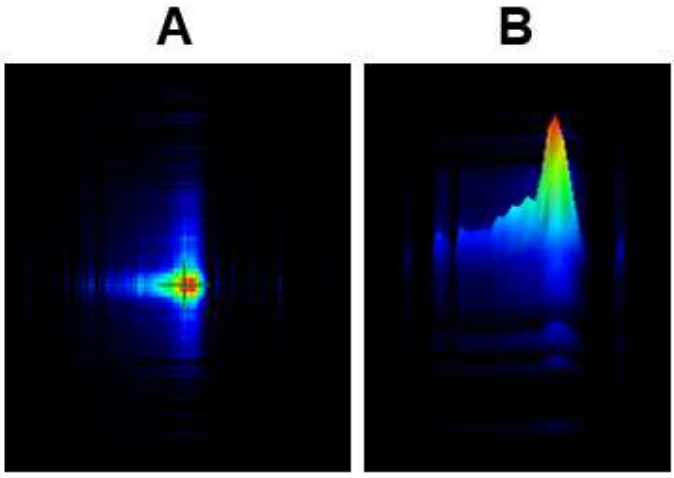

Figure 3.4: A screen grab from the Thorlabs Beam 7.0 showing the bream profile in 2D (A) and 3D (B)

Figure 3.5: A photograph showing the spot size (circled) visible on the beam viewing card

Optical Power

A Thorlabs digital power meter was used to record the optical power as the supply current was manually adjusted. Starting at 10.0mA the current was adjusted manually in 0.5mA increments to the maximum value of 40.0mA taken from the manufacturers data sheet. The Thermoelectric cooler (TEC) ensured that temperature remained constant at 25ºC throughout data collection. The results presented in Figure 3.6 show a linear relationship between output power and supply current, once the threshold current has been reached which is as expected. The instrument used for data acquisition required a 3 second period to obtain a true reading as per the technical specifications of the sensing head, three seconds was typically adequate for the value to remain constant however additional time was allowed for a constant readout if there were fluctuations on the display. Figure 3.7 shows the detector head of the power meter directly in front of the diode, the beam viewer card is used to ensure that the beam strikes the detector in the centre of the detection aperture.

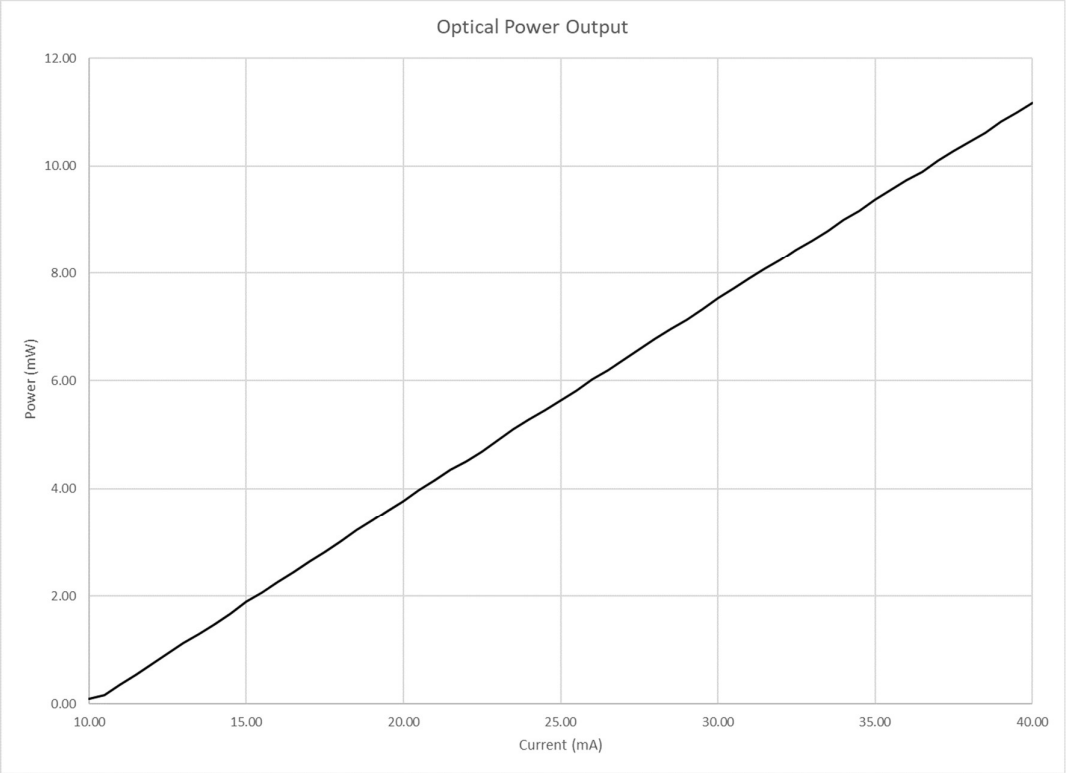

Figure 3.6: A graph to show the relationship between optical power (mW) and supply current (mA) at T=25.0ºC

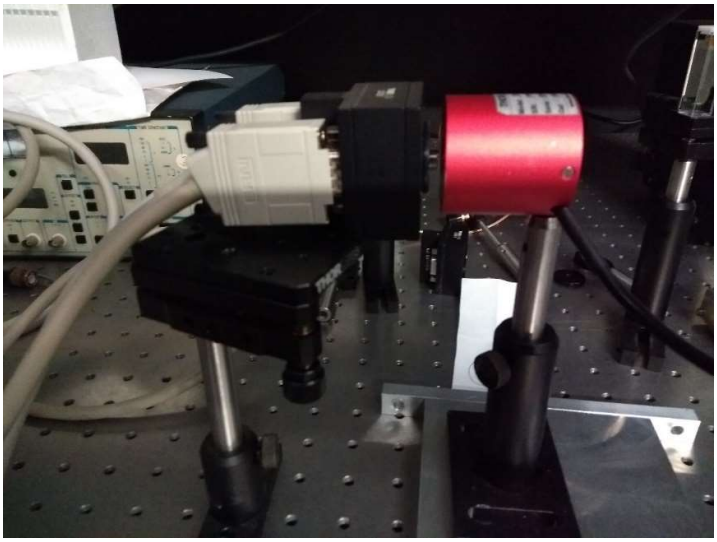

Figure 3.7: A photograph showing the power meter setup used to generate a calibration curve

Using the calibration curve seen in Figure 3.6, 5mW and 10mW LASER power is selected using 23.3mA and 36.8mA respectively. Figure 3.8 shows the controls and

display for each output condition whereby the temperature is maintained at 25ºC using the temperature controller, this ensures stability of LASER output.

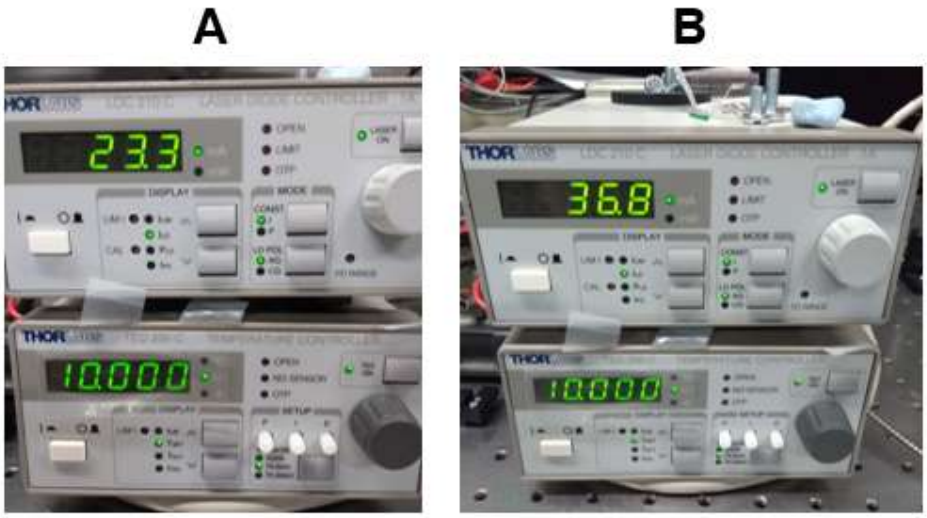

Figure 3.8: LASER Diode Controller and Temperature Controller for 5mW power at 25ºC (A) and 10mW power at 25ºC (B)

3.2 Materials

The materials used for the three experiments are listed below, any material safety data sheets are available in Appendix B where applicable.

- Gardasoft CC320 Multi-Trigger Module
- Thermometer fitted with external probe
- Power Meter (Thorlabs PM100A fitted with an S302C head)
- CMOS Camera with interface cable (BlackFly BFS-U3-16S2M-CS)
- GPIO connector for camera
- Camera Lens (KOWA LM35JC)
- Human Serum Albumin (PAN Biotech UK)
- Indocyanine Green (Tokyo Chemical Industry UK Ltd)
- Deionised Water

- NIR LED (Thorlabs LED780E)
- NIR Laser Diode (Thorlabs L780P010)
- Mount for LED
- Mount for Camera
- Mount for the LASER diode (Thorlabs LDM21)
- Calibrated Scale (Precisa XT220A)
- Cuvettes with lids (Kromatek 7.5mmD PL5 and 12.5mmD PL10)
- Glassware
- Pipettes (Gilson P1000 and P100)
- Pipette Tips (GilsonD1000 and D200)
- Excitation Filter (MIDOPT FIL LP800/30.5)
- Filter Holder
- Optical Bench
- Small Parts (Screws, Nuts)
- Various Tools (Wire Stripper, Wire Cutter, Screwdriver)
- Soldering Iron
- Solder
- Spectrometer (Ocean Optics USB4000)
- Mounted Collimating/Aspheric Lens (Thorlabs C171TMD-B)
- Lens Adapter (Thorlabs S1TM08)
- Beam Viewer Card (Thorlabs VRC5)

Materials and Methods

- Respective Software Applications
- Beam Profiler (Thorlabs BP109-IR)
- Laser Driver (Thorlabs LDC210C)
- Temperature Controller (Thorlabs TED200C)
- 15V Benchtop Power Supply
- Foam-Lined Enclosure
- Coloured Cable
- Cleaning Supplies for Glassware
- Permanent Markers for Glassware
- Refrigerated Storage

Software Tools

Zemax Software – This ray tracing software was used on-site at the partner company only. This is an optical modelling software which provides a calculated estimate of the output and efficiency of an optical system. The company partner used Zemax exclusively in custom optical designs including LED multiplexers and lightguides. Through very limited experience of using this software, the optical output simulated within Zemax is often higher than in reality due to a variety of conditions not included in the model – for example, condensation and air humidity, finger-marks on the surface of components and residual release agents or adhesives from the manufacturing process. Zemax provides a good indication of optical power and efficiency of a system, as well as opportunity to understand the impact of design modifications.

Gardasoft Maintenance Software – A network connection is made between the controller hardware and computer in order to establish communication via the maintenance software. The software is used to set the width of pulses and delays for each of the eight

channels independently. The Gardasoft software allows for changes to be uploaded to the hardware with immediate effect. If multiple channels are in use, there is a reported delay of up to 0.1ms possible which reduces to 1µs with single channel use. Channels can also be set high or low which was used for testing purposes during this work. Testing of the functionality of the Gardasoft hardware/software was completed prior to experiments using a simple breadboard circuit as well as initial investigations using an oscilloscope as seen in Figure 3.9.

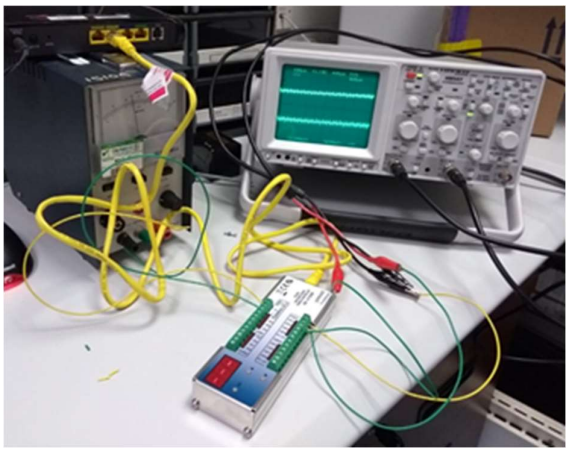

Figure 3.9: Testing the functions of the Gardasoft CC320 controller with an oscilloscope

Spinnaker Software – Supplied with the camera and developed by FLIR, the spinnaker software also known as SpinView is used to help setup the frame, the camera and length of recording. All camera settings can be adjusted with this software and frames are saved to a local file location with a selection of file-save formats available. The record functionality allowed for the success of the trigger-controlled experiments as each recording could be limited by a designated number of frames or number of microseconds available as video or a stack of frames. Although a minimum exposure time of 4µs was possible for this camera, under the current configuration this was significantly higher at just over 4000µs and is governed by the processing speed of the computer. A live view is visible on-screen which was essential for setting up the frame and for viewing fluorescence that proved invisible to the naked eye.

Thorlabs Beam 7.0 – This software is designed for use with the beam profiler and gives a real-time readout which can be saved to file in various formats including 2D and 3D plots. It is a very useful tool for beginners to use as it gives a statistical output on quality and precision of beam alignment and collimation. Screen grabs are collected and have been included in this work for reference, please see Figure 3.4.

Ocean Optics OceanView version 1.6.3 – This software is designed for use with the OceanOptics spectrometer. Dark and light references are taken with an empty cuvette in place prior to data collection, a suitable integration time and moving window are input manually. The software shows the spectra in real-time on screen with the opportunity to export data in text or as an image file. For this research, fluorescence data was exported in text format and processed post-data acquisition. After launching the software, several wizards are available to use, the Lite version used includes Fluorescence, Absorbance, Reflection and Transmission. More information including the equations used to calculate each option can be found in Appendix C.

LabView – LabVIEW software allows the user to design a custom programme using any combination of the tools and palettes available. An introduction to using the region of interest (ROI) and intensity counter tool was available as an online tutorial (credit to channel name “Intro to LabVIEW image processing” on YouTube) and this was followed and customised to suit the requirements of this project. An 8-bit image file is loaded and displayed; a region can then be manually drawn using any one of the shape-selection tools. As the region is established, the intensity values are presented in real-time next to the image where they can be copied and input into a spreadsheet. The region can be relocated in order to retain its size and shape. The region location and shape will be retained once a new image has been loaded to allow for continuity across a series of frames.

Screen grabs of the LabVIEW block diagram and front panel are presented in Figure 3.10 and Figure 3.11 respectively. The block diagram shows the background procedure

and analysis process while the front panel shows the user interface where the ROI is selected and the data analysis presented. Figure 3.12 shows an example of an image processed within the LabVIEW software, from the image we can see the cuvette containing ICG in solution as well as the single LED. A ROI has been drawn to cover the fluorescing contents of the cuvette; the LED can be seen on the right-hand side of the frame.

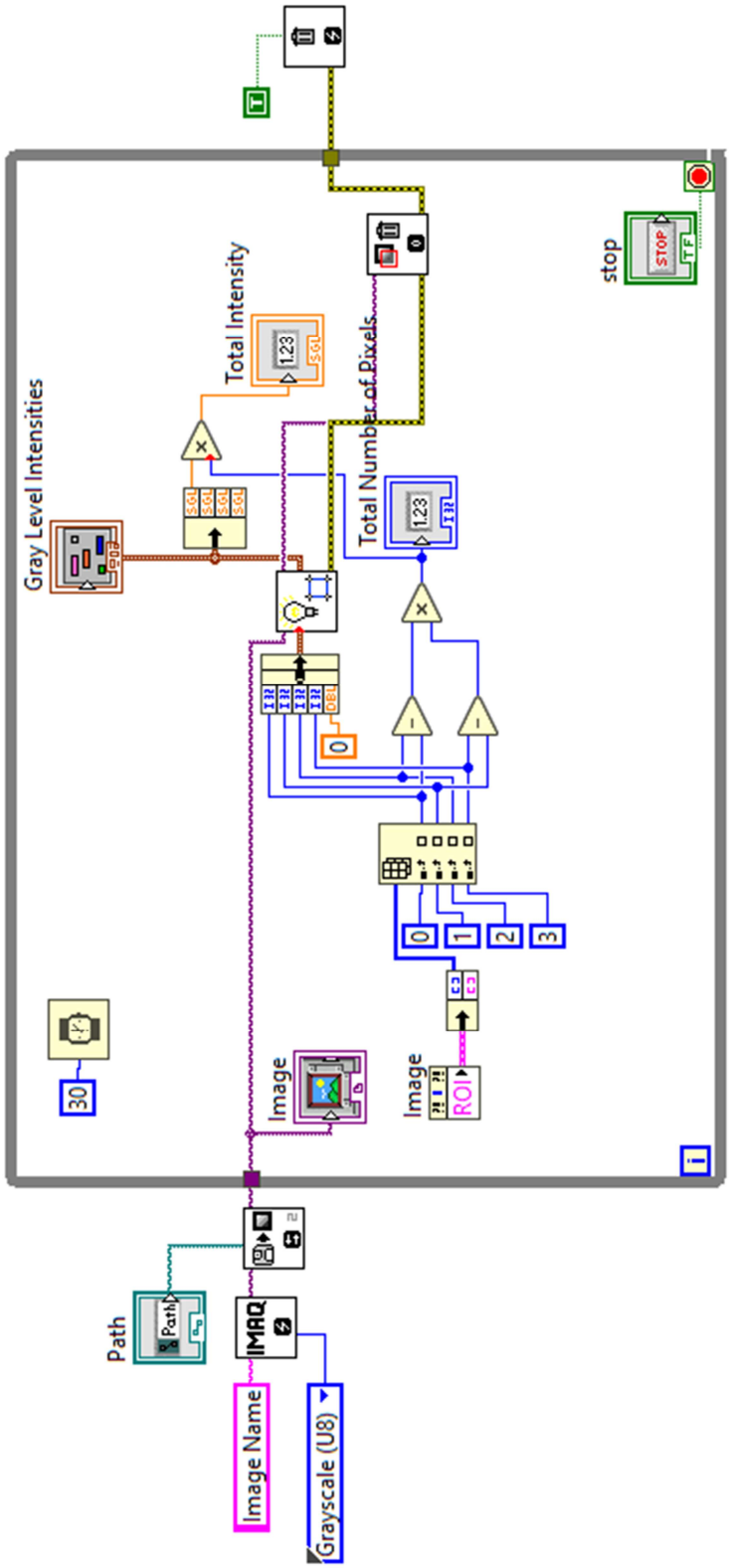

Figure 3.10: A screen grab of the LabVIEW Block Diagram

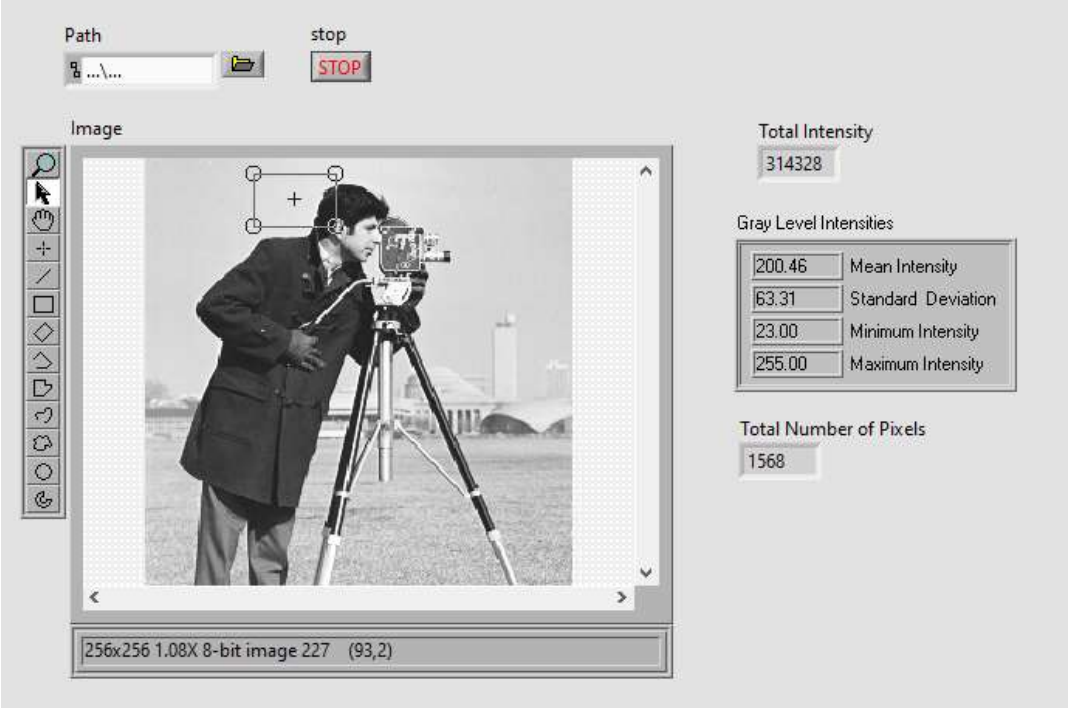

Figure 3.11: A Screen grab of the LabVIEW Front Panel with a test image loaded, the ROI is visible as a rectangular selection

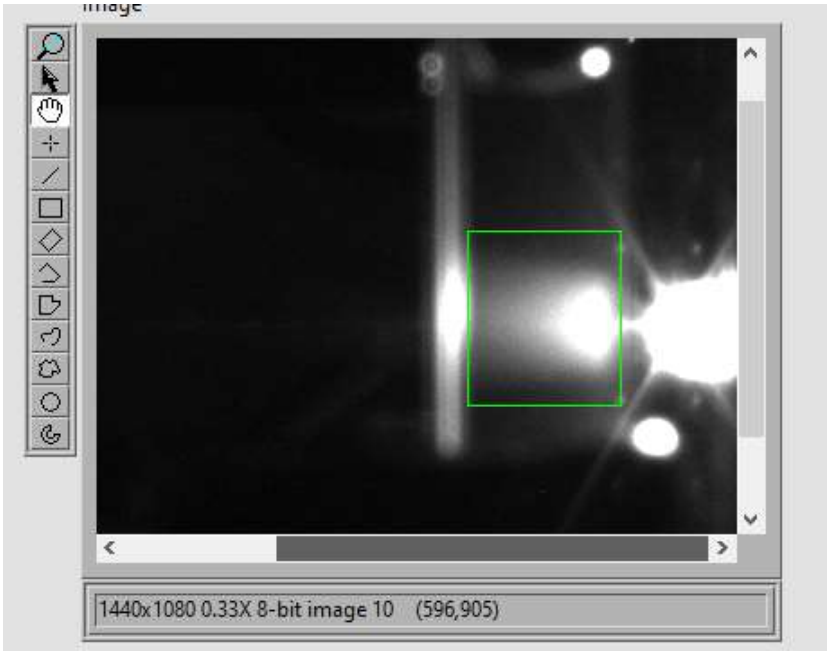

Figure 3.12: The Front Panel of LabVIEW showing ICG:HSA at 500μMol excited with a single LED, the Green boundary represents the region of interest for analysis, the LED is seen on the right hand side of the frame

3.3 Methodology

All experiments are conducted in the university LASER lab which provides a safe, dark and cold environment.

In order to enhance efficiency and productivity in the lab, literature has been reviewed so as to best understand the requirements surrounding usage of ICG in solution and set reasonable expectations. This reviewed research provides a solid foundation to assist in the selection and procurement of components and typical parameter limits for the proposed experimental setup as it reduces the time taken with trial decision making. It also keeps the research relevant by conforming with well-established methodologies and set procedures.

With regards to excitation, one study utilised a fluence rate of 5mW/cm^2 NIR light over a 15cm diameter FOV (Ohnishi et al., 2005). The results presented in this reviewed research showed that at this level of excitation ICG:HSA provided sufficient contrast to view subdermal lymphatics but not enough to view the SLN with certainty. Simultaneous photon collection was achieved with custom optics and the images collected were refreshed up to 15 times per second. This is a little short of the standard 24fps used in film and TV and may make the video appear choppy and less smooth than we are used to. Another study (Gioux et al., 2010) advises that the maximal frame rate of the detector should always be used with the lowest possible fluence rate to achieve fluorescence emission in the mid range of the camera.

Excitation power between 5mW and 10mW will be selected for these experiments to remain compliant with relevant literature where typical fluence rates for both LASER and LED excitation is between 1 and 10mW/cm^2 (Gioux et al., 2010) The NIR LED excitation source used in a separate study (Hutteman et al., 2011) provided 7.7mW/cm^2 of 760nm light which also supports this selected range.

One other study reviewed, (Nairat et al., 2014) used a significantly higher fluence rate comprising a pulsed laser source to excite the chemical marker, peak intensity at the

sample was $5x10^{9}Wcm^{-2}$ when transform limited. The laser pulses, centred around 800nm, were unfocused 90µJ with a repetition rate of 1KHz-200Hz however, this was a study focusing on the excited state dynamics of ICG and not the imaging of ICG stained tissue so will not be considered. A range of optical power will be used in this research between 5mW and 10mW so as to keep results relevant to the application.

Excitation wavelength for NIR will be as close to 800nm as possible, one study excited ICG compounds using an NIR endoscope with excitation (710-790nm) and filtering (810-920nm). (Ito et al., 2006) The Cymtec light source delivered to ICL comprised a 780nm NIR channel and for continuity, this will also be considered with regards to component selection as well as availability of components at this wavelength.

For detector methods, one study (Boddington et al., 2008) utilised a 0.5-inch CCD camera cooled to -70ºC, the FOV was fixed at 7cm with an exposure time of 2s, this study focused on analysing the effect of temperature on ICG. Fluorescence signal is measured by positioning ROIs (Region of Interest) over the light areas for analysis – this is the technique that will be used in this study to quantify the fluorescent signal. The Boddington study confirmed that increasing the temperature of the aqueous ICG solution accelerated the degradation of ICG. A typical FOV are maximum 10-20cm and minimum 1-2cm, the main trade-offs with FOV are the final resolution, collection optics and excitation fluence rate. (Gioux et al., 2010) The FOV in this research will be determined following setup however, the camera used is subject to change following testing. The camera used in the initial setup will be the FLIR BlackFly 16S2M. The intensity of the expected fluorescence is significantly lower than the excitation signal and so the detector will need to be sensitive enough to detect this signal with as high SNR as possible at this wavelength, when using small molecule NIR fluorophores, a quantum yield (QY) of around 10-20% is expected in serum. (Gioux et al., 2010)

Accuracy and repeatability are fundamental for the test procedure, unfortunately during the fluorescence testing, dark noise will be present at the detector. The experiment

should be repeated to verify the standard error and to confirm accuracy. The mean value +/- twice the standard deviation should account for at least 95% of the data collected assuming the data follows a normal distribution.

An electrical circuit is required for all experiments conducted in order to connect components to power as well as the trigger controller where needed. Power to the LED will come from an external 15V power supply which is also used to power the Gardasoft controller. The LASER is not connected to the trigger control unit but the diode is inserted into a mount which is connected to a power supply and thermoelectric cooling unit as seen in Figure 3.8.

Again, literature will be used to determine the procedure for preparation of stock solution of ICG:HSA as this will be the first time using this chemical marker in the department, the experience of other researchers provides a good understanding of best practice.

Literature suggests that the ICG and HSA should be mixed in a 1:1 molar ratio (Ohnishi et al., 2005, Nairat et al., 2014). The Crull (Crull and Schafer, 1996) mixing procedure will be followed therefore the molar ratio will be calculated to confirm that the stock solution conforms with this ratio. The Crull procedure (Crull and Schafer, 1996) has been selected as it provides the most detailed description of the mixing process and also involves diluting and dissolving dry materials instead of pre-mixed solutions. Both the ICG and HSA have been purchased as dry constituents so as to increase the shelf life of the product and to allow for a fresh stock solution to be prepared each day thus decreasing the risk of contamination and degradation.

Literature reviewed is unanimous in discussing ideal concentrations, at lower concentrations of ICG, the emission strength increases however, at higher concentrations the opposite is true and emission strength decreases with an increase in concentration (Yuan et al., 2004). The Hutteman study (Hutteman et al., 2011) comments on the quenching effect of increased concentration of ICG, this study reports that if

concentration of ICG (or ICG:HSA) is increased above 50μMol then a significant decrease in fluorescence intensity will result.

An optimal concentration for ICG:HSA is described as anywhere between 400μMol and 800μMol when used for SLN mapping in breast cancer patients (Hutteman et al., 2011, Mieog et al., 2011). The Yuan study (Yuan et al., 2004) utilised an ICG concentration of 0 to 20μMol as this is a typical selection with fluorescence imaging. At such a low concentration, the aggregation of ICG molecules is weak enough to significantly reduce the effect of molecule aggregation (Yuan et al., 2004). The Hutteman study (Hutteman et al., 2011) utilised ICG at a concentration of 500μM prepared as follows: A stock solution is prepared to yield a 2.5mg/mL (3.2mMol) concentration of ICG. To obtain the desired concentration (500μMol) 7.8mL of the stock solution is diluted into either 50cc of sterile water or 50cc of 20% HSA solution.

500μMol is the selected concentration as it lies between the pre-stated optimal concentration limits and requires very minimal manipulation to achieve (Hutteman et al., 2011) the concentration 500μMol is used in this research for its simplicity during initial testing however, the Crull method of preparation will be followed. Experiments 1 and 2 will involve changing the concentration of ICG:HSA and again, the Crull (Crull and Schafer, 1996) method of mixing will be applied. For this research, a solution of ICG:HSA will be prepared in a range of concentrations between 400μMol and 1000μMol.

The stock solution comprising dry and wet components will be prepared on the morning of testing, guidance has been consulted to ensure that sample preparation is repeatable and accurate.

The concentration of a solution can be expressed as either the molarity or concentration as a percentage of weight in volume.

$$\text{Molarity} = \frac{\text{Moles Solute}}{\text{Litres of Solution}} \qquad \textbf{3.6}$$

$$\text{Concentration in } \% \frac{\text{w}}{\text{v}} = 100 \text{ x } \frac{\text{Mass Solute (g)}}{\text{Volume Solution (mL)}} \quad \textbf{3.7}$$

To mix a 30mL, 1000μMol stock solution of ICG:HSA in a 1:1 molar ratio using a solid solute, the weight of solute must first be calculated using the following equation:

$$\text{Mass Solute (g)} = \text{Molarity } \left(\frac{moles}{litre}\right) \text{x Volume (L) x Molecular Weight } \left(\frac{grams}{mole}\right) \quad \textbf{3.8}$$

The molecular weight of ICG is 774.967g/mol (PubChem 2019) and so 0.23249mg of ICG should be used. Each 1mL volume of stock solution will then contain 0.00775mg ICG.

The molecular weight of HSA is 3722.136g/mol (PubChem 2019) and so 1.11664mg of HSA should be used to ensure a 1:1 molar ratio. Each 1mL volume of stock solution will contain 0.03722mg HSA.

Dilutions of the stock solution should be prepared for part 1 of testing by using the following equation:

$$C_s V_s = C_f V_f \quad \textbf{3.9}$$

Where C_s is the concentration of the stock solution, V_s is the volume of the stock solution, C_f is the concentration of the final solution and V_f is the volume of the final solution. For concentrations that are lower than the stock solution, deionised water should be added. For concentrations higher than the stock solution, solute should be added or, a high concentration stock solution should be prepared and diluted as necessary.

A reference cuvette should be used for each concentration change, the reference and test cuvettes should contain an equal quantity of HSA solution, this means that for each concentration analysed, a separate HSA solution should be prepared.

The concentrations under analysis will be as follows, a stock solution of 1000μMol is prepared so that adjustments for dilutions to lower concentrations are simple.

Unfortunately, due to a limitation with equipment available an initial stock solution of $1x10^{-4}$Mol is first mixed and then diluted to $1x10^{-6}$Mol. The weights used to create the initial stock solution are 23.249mg and 111.664mg of ICG and HSA respectively. The initial stock solution is pipetted, 200μL into a clean container and mixed with 19.8mL of deionised water to achieve the correct concentration of 1000μMol. All containers are labelled with permanent marker to reduce the risk of contamination, the initial stock solution is very dense and dark while the 1000μMol solution is transparent and a very subtle green colour, see Figure 3.13.

Table 3.1: Sample Preparation by Weight and Volume

ICG:HSA Sample				Reference	
ICG:HSA Concentration	Deionised Water	HSA	ICG	Deionised Water	HSA
800μMol	10mL	29.78mg	6.20mg	10mL	29.78mg
700μMol	10mL	26.05mg	5.42mg	10mL	26.05mg
600μMol	10mL	22.33mg	4.65mg	10mL	22.33mg
500μMol	10mL	18.61mg	3.88mg	10mL	18.61mg
400μMol	10mL	14.89mg	3.10mg	10mL	14.89mg

5mL dilutions from the 1000μM stock solutions are as follows, using the calculation from Equation 3.9.

Table 3.2: Sample Preparation in Volume

ICG:HSA Concentration (10mL)	Stock Solution (mL)	Deionised Water (mL)
800μMol	4	1
700μMol	3.5	1.5
600μMol	3	2
500μMol	2.5	2.5
400μMol	2	3

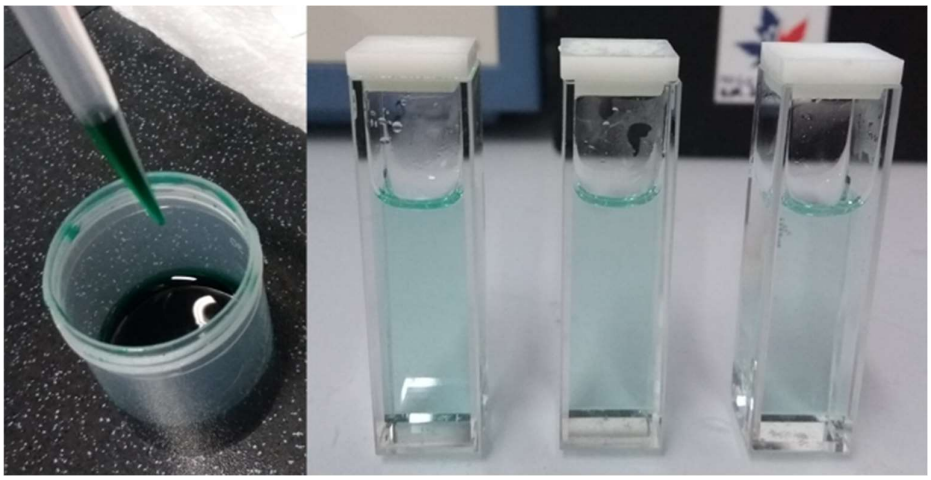

Figure 3.13: An Image showing the ICG stock solution (LHS) and diluted samples in cuvettes (RHS)

The scale used has a limit of 4 decimal places and so the smallest weight allowable is 0.0001g or 1000mg. The error involved in weighing and diluting samples is considered in the following section, it is important to acknowledge that the HSA is crystalline and becomes difficult to weigh accurately at the fourth decimal position. Likewise, the ICG is a very finely milled powder and so a tolerance of ± 2% or 0.0005 was allowed. The scale used, a Precisa XT220A, was within its calibration schedule and the technical documentation suggests that there is 0% tolerance if the calibration schedule is adhered to, good working practice was also employed to reduce the risk of error.

For the Gilson P1000 pipette with D1000 tip, the manufacturers document systematic error as ± 8.0μL for a volume of 1000μL, ± 4.0μL for a volume of 500μL and ± 3.0μL for a volume of 100μL. They also list random error as ≤1.5μL, ≤1.0μL and ≤0.6μL for volumes of 1000μL, 500μL and 100μL respectively. (Gilson S.A.S. 2019)

The Gardasoft CC320 trigger control unit has been selected to trigger the timed pulses for these experiments. The unit connects direct to a router via Ethernet and has 8 available inputs and outputs, all time delay information is manually input via the Gardasoft web interface. Under lab conditions, due to the university network protocol, a Local Area Network (LAN) was set up using a Sky router which allowed for direct communications between the Gardasoft controller and the laptop. Channels can be set to Active High or Active Low if they are to be constantly on or off respectively, the channels can also be configured to pulse at specified pulse width and delay. Input and output wires are secured direct to the controller via screw terminals. The accuracy of the CC320 module is typically 100μs when using this trigger in PTT mode (pulsed mode).

3.4 Experiment 1

This experiment is crucial to determine if the proposed experimental setup is viable and if fluorescence can be detected. This will verify that the camera is suitable and that the stock solution has been prepared correctly. The focus of this work is to investigate the effect of changing the excitation source and concentration of solution to determine if there is an optimal configuration to carry forward into the next experiments.

The samples varying in concentration will be prepared as above, following good working practice to reduce the risk of contamination. Each sample will be prepared by diluting a stock solution accordingly, a volume of 3.0mL will then be pipetted into a sealable cuvette for testing with the spectrometer. A second cuvette with equal concentration of HSA solution will also be prepared for comparison. A cuvette of deionised water will act as a reference. The cuvette position within the spectrometer setup will remain constant with the assistance of a mounting stage, Figure 3.14 shows the alignment jig whereby

cuvettes are pushed into the corner of the secured guide rails, double sided tape ensures that there is no movement of the guide rails or cuvette. The LASER source, spectrometer and cuvette type will be kept constant throughout the duration of this experiment. Ambient temperature will be recorded and noted with each repetition. Two excitation powers have been selected, 5mW and 10mW in order to obtain a complete data set. These limits have been chosen for their prevalence in literature, any excitation power higher than 10mW would be unlikely to hold any impact as it is irrelevant for the intended application.

The Ocean Optics USB4000 spectrometer is used with accompanying software. The auto feature is selected to select an appropriate integration time for fluorescent measurement, this is achieved by placing the ICG:HSA in front of the excitation and switching the LASER on, the peaks should reach around 80% of the window for the best results in accordance with the manufacturers guidelines. This integration time is recorded and maintained for the absorbance data collection for continuity. A boxcar width of 2 is applied to the spectrum to increase the signal to noise ratio without losing spatial resolution. A box car width of 2 essentially averages 5-pixel values, two to the left, the centre and two to the right therefore boosting the SNR by a factor of 2.2 as per the manufacturer's guidelines. A number of 5 scans to average was selected, again to increase the signal to noise ratio and to stabilise any fluctuations in the data. This will lengthen the time taken to acquire the scan but improves the SNR by a factor of 0.5.

Both the absorbance and fluorescence measurements will use the deionised water-filled cuvette as a reference to understand the optical properties of the HSA alone.

Absorbance Measurements

The absorbance application is selected from within the software, a light reference is taken whereby the deionised water-filled cuvette is in position and the LASER switched on. A dark reference is also stored whereby the above is repeated with the LASER

switched off. These references are stored and must be re-recorded once the excitation power is changed.

Fluorescence Measurements

The fluorescence application is selected from within the software, only a dark reference is taken here using the deionised water-filled cuvette with the LASER switched off. Once this reference has been stored, the excitation power can be changed without re-recording the dark reference.

The equipment arrangement is shown in Figure 3.15 and Figure 3.16 with the beam represented by a bold red line. The excitation and detector (spectrometer fibre) are adjacent to one another. The cuvette has been specifically chosen for its optical properties and is of a type commonly used in fluorescence analysis such as this one. The cuvettes are made from optical glass with a transparent window of 340-2500nm and pathlength of 10mm. The cuvettes are part of the brand Kromatek's standard fluorescence cell line with Teflon lid. It is important that the cuvettes are sealable so as to reduce the risk of contamination from the environment and to stop loss through evaporation.

The spectrometer experiment will also utilise the camera to detect the fluorescent decay with the camera and spectrometer opposite one another with each positioned adjacent to the light source. This part of experiment 2 will be fundamental to the success of experiment 3 as the LASER produces a small beam diameter which is easy to control and predict. The camera exposure time and focus can be assessed for suitability in experiment 3. There is also an opportunity to utilise the LabVIEW analysis programme designed for experiment 3 within experiment 2 to determine residual fluorescence.

Figure 3.14: A photograph showing the alignment jig for mounting cuvettes

The LASER will be used to illuminate the sample within the cuvette at both 5mW and 10mW while the single LED will illuminate the sample under at 7.2mW only. There are three illumination conditions to excite the ICG, 5mW LASER, 10mW LASER and 7.2mW LED. The cuvettes are positioned and data is collected before swapping the cuvette for another sample and repeating the process. Images are collected via the camera; fluorescence data is collected via the spectrometer and optical power is recorded via the power meter. In order to best describe the experimental setup and organisation of apparatus, the following schematics will be described.

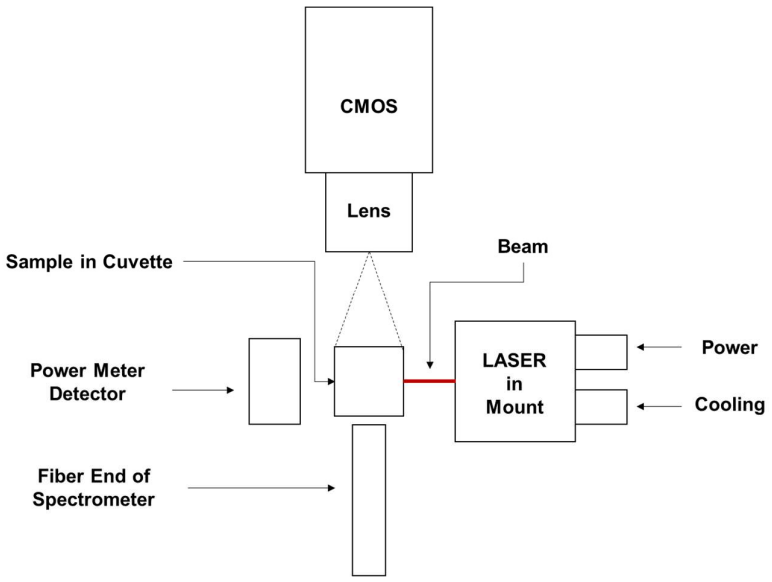

Figure 3.15: A schematic of the experimental setup with the LASER excitation source

In the above Figure 3.15 we see the apparatus arranged around the central sample. The power meter is in parallel to the excitation source while the camera and spectrometer are arranged perpendicular to the excitation source. During setup, the height of components is fine-tuned to align with the beam and the beam viewer card is used during this process. All mounts are secured to the optical bench so as to maintain component positioning between experiments.

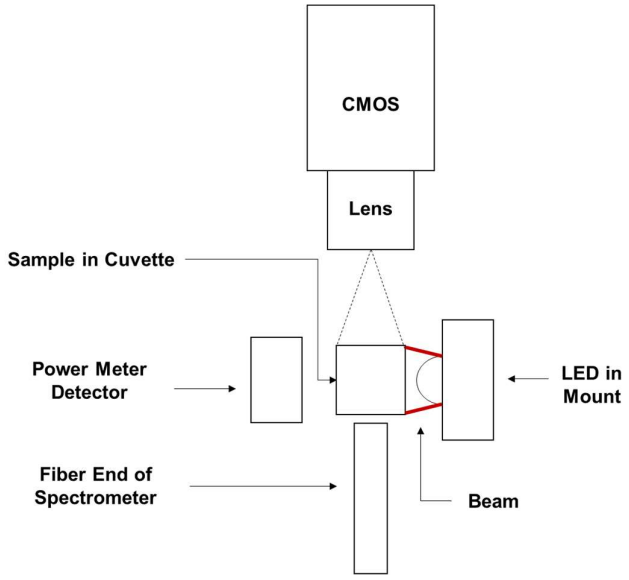

Figure 3.16: A schematic of the experimental setup with the LED excitation source

In the above Figure 3.16 we see again the apparatus arranged around the central sample. The power meter is in parallel to the excitation source while the camera and spectrometer are arranged perpendicular to the excitation source in agreement with the LASER configuration. During setup, the height of components is again fine-tuned to align with the source which in this instance, is visible by eye and significantly simpler to achieve. All mounts are secured to the optical bench in order to maintain component positioning between experiments.

Figure 3.17 shows the cuvette in position for excitation with the LED, the LED is mounted on to an aluminium plate and can be seen clearly through the contents of the cuvette. Ambient light is reflecting off the surfaces of the cuvette and the meniscus of the liquid contents within.

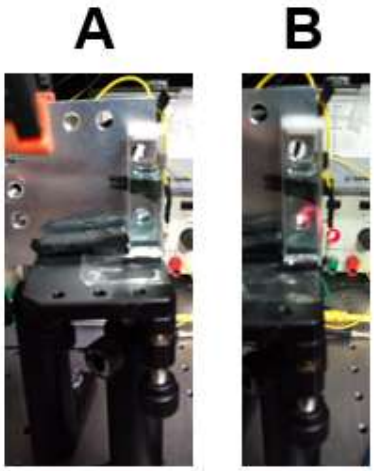

Figure 3.17: The cuvette in position for LED excitation seen with LED off (A) and LED on (B)

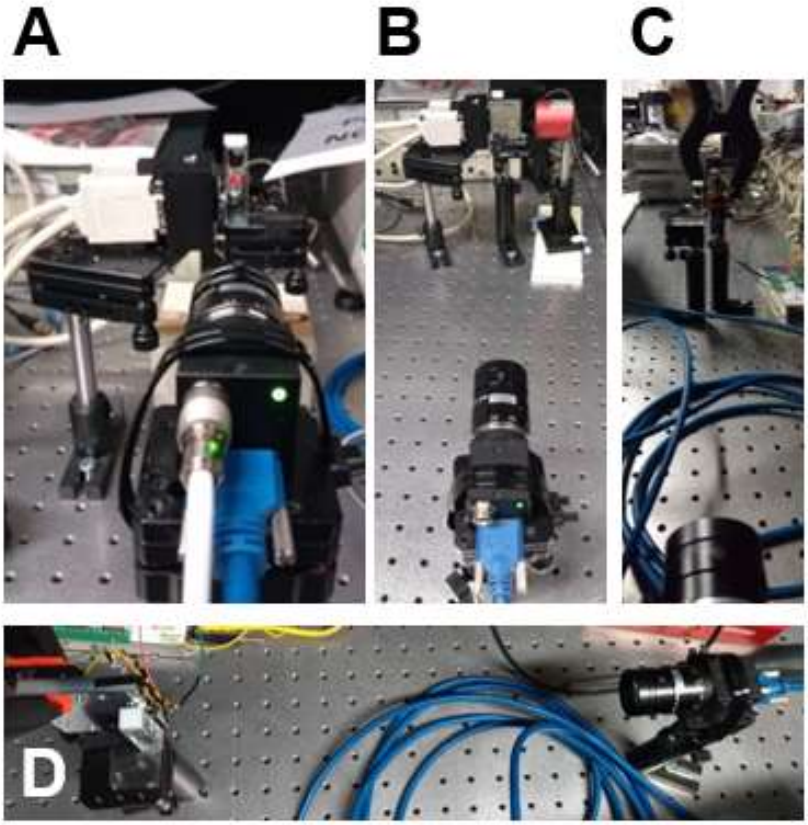

Figure 3.18: A collection of photographs to show the camera orientation with the LASER setup (A and B) and the LED setup (C and D)

To give a good indication of camera positioning with respect to the sample and the illumination source, Figure 3.18 presents a visual representation of arrangement for both the LED and LASER setups.

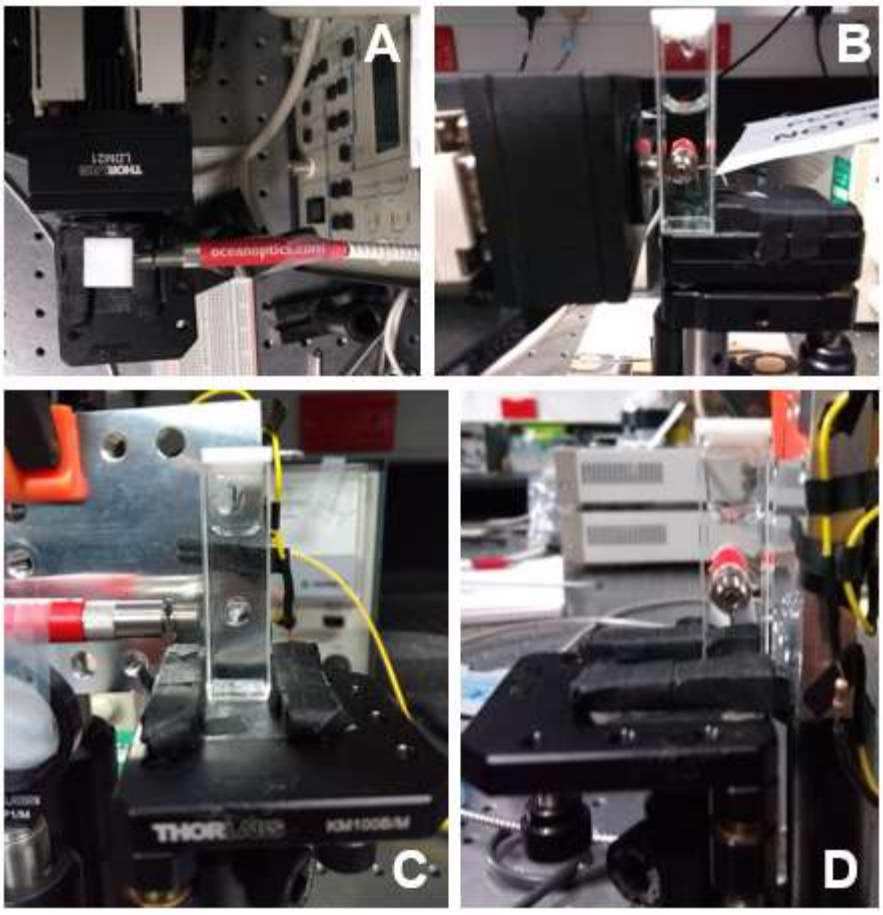

Figure 3.19: A collection of photographs to show the spectrometer orientation with the LASER setup (A and B) and the LED setup (C and D)

The spectrometer fibre is positioned perpendicular to the illumination source as seen in Figure 3.19 for both the LED and LASER setup. The fibre is placed as close as virtually possible to the wall of the cuvette and is height adjusted to detect maximum intensity. With the fibre positioned perpendicular to the LASER, there is no possibility of collecting any of the excitation source as the beam does not diverge significantly. The LED however produces a more divergent beam and so even at a perpendicular position, some of the excitation is detected.

Finally, the position of the power meter detector can be seen in Figure 3.20 for the LASER setup, the power meter detects light that has travelled from the source through the contents of the cuvette.

Figure 3.20: A photograph to show the power meter in parallel to the LASER source

3.5 Experiment 2

This experiment will focus on understanding the optical properties of ICG:HSA. Specifically, identifying the decay rate as there are many conflicting statements highlighted within the literature review with regards to this.

An analysis comparing the fluorescence intensity of the sample with varying concentration will also be conducted to determine if there is any relationship between fluorescence intensity and fluorescence lifetime with the concentration of ICG in solution.

The sample (ICG:HSA) is positioned in front of the camera and excitation source, a thermometer is placed close to the sample to record the local temperature, a second thermometer is used to record the ambient temperature as seen in Figure 3.22. Unfortunately, with the thermometer positioned within the liquid contents of the cuvette it is impossible to image without significant reflection from the external probe. This is true when using the fibre end of the spectrometer next to the cuvette, both the fibre and the temperature probe are metallic and cause unwanted reflection. Figure 3.21 shows a schematic of this concern and Figure 3.22 shows images collected with the thermometer probe in position. The fibre end of the spectrometer is moved out of the camera frame for imaging and the temperature probe is not imaged in position in order to remove the risk of unwanted reflection.

Temperature is recorded in experiment 2 to understand if there are any significant thermal effects on fluorescence decay and if a relationship exists between these two parameters.

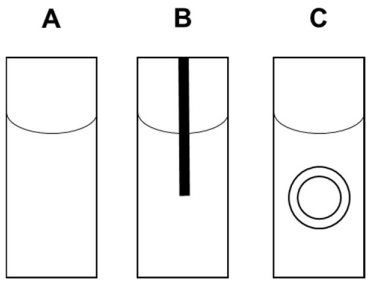

Figure 3.21: A schematic of a side-on view of the cuvette with liquid contents A, probe end of the thermometer B and fibre end of the spectrometer C

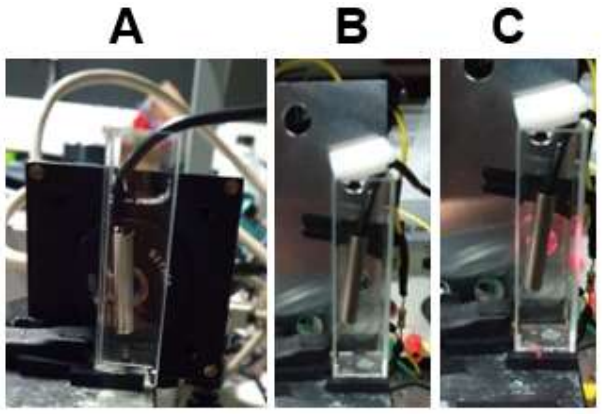

Figure 3.22: A photograph to show the external probe of the thermometer submerged in the liquid contents of the cuvette with LASER setup (A), LED setup (B) and LED illumination on (C)

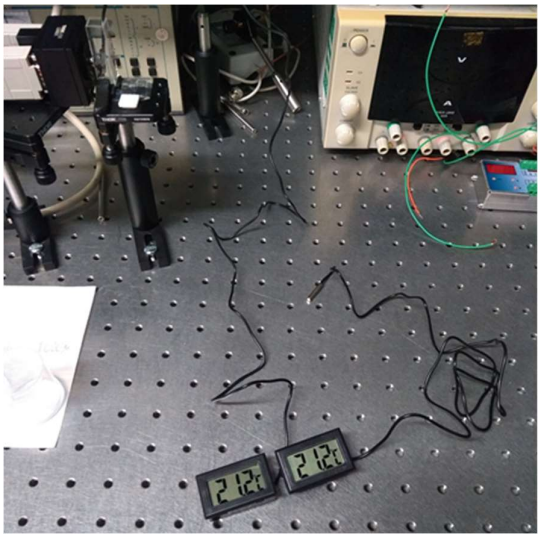

Figure 3.23: A photograph to show the LASER setup with external probe thermometer in position within the cuvette and another on the optical bench

3.6 Experiment 3

This experiment looks at the effect of making the following changes according to the schematic presented in Figure 3.24:

a. Exposure time/shutter speed (ΔS)

b. Excitation pulse length (ΔK)

c. Time delay between excitation pulse off and exposure open (ΔT)

The field visibility and fluorescence decay will be investigated during this experimental phase, whereby a single NIR LED and CMOS camera will be pulsed on and off sequentially. The aim of this experiment is to determine if it is possible to capture fluorescence without the need for filtering, relying on the decaying fluorescence signal while excitation is off. The ideal parameters will also be determined for future experiments wishing to exploit fluorescence decay rates and to document the outcomes of pulsing the excitation in this way. The trigger changes will be made via the Gardasoft controller, these delays and pulse widths are manually set via the web interface installed as per the manufacturer's recommendation. Each set of parameter changes is saved

with a unique alphanumeric code, the sequence of images collected is saved with a matching alphanumeric code in order to identify the pulsing properties.

Results from experiment 1 and 2 will provide a good understanding of parameters such as the optimum concentration of ICG:HSA solution and the ideal exposure time.

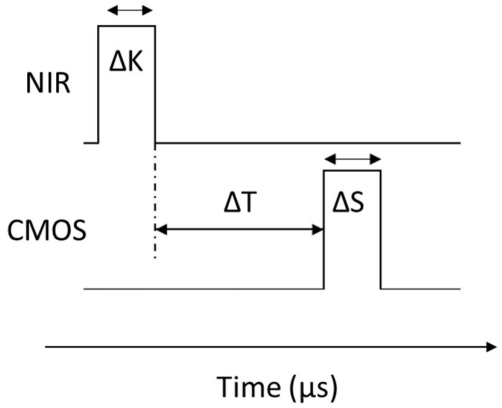

Figure 3.24: A schematic to show the trigger pattern and corresponding parameters

Ideally, the contrast between fluorescence and the background is strong enough to allow for some low-level bright field lighting across the entire FOV so that non-fluorescent structures may also be observed.

3.7 Data Analysis

Data from experiments 1 and 2 will be plotted by exporting data files from the spectrometer software, formatting them and using the data plotting programme Origin by OriginLab. For experiments 1 and 2, the software programme LabVIEW will also be used for a region of interest pixel analysis looking at the intensity values within the specified region of the image. Relevant information is extracted from the plots through a peak analysis. Temperature data and power meter data are manually recorded and input into a spreadsheet for processing and plotting. For data collection where time is a key parameter, the rate of change can be calculated by reading gradient information from the curves. Images analysed in LabVIEW will undergo a ROI analysis whereby only the relevant region of the image is analysed.

Noise present within the spectrometer traces will be smoothed using a Savitzky-Golay smoothing function to filter out the noise while preserving the shape of the peak. This applies to all data collected during experiment 1.

It is important to note data collection is repeated a number of times so that averaging, standard deviation and standard error can be calculated and presented.

3.8 Error Analysis

A combination of human error and equipment error will contribute to overall error. The error associated with ICG sample preparation, as the sample is diluted so heavily, will be influenced from the initial weighing as well as the pipette error in diluting. When weighing the dry samples, an accepted error range of 0.5% was allowed in order to increase efficiency.

See Table 3.3 and Table 3.4 for the error associated with weighing dry components for the ICG:HSA Solution (30ml, $1x10^{-4}$Mol solution) and HSA (30ml, $1x10^{-4}$Mol solution) respectively whereby the desired weight (DW) and actual weight (AW) are stated.

Table 3.3: Error associated with weighing of dry components

Batch Number	DW HSA (g)	AW HSA (g)	Error	Error (%)	DW ICG (g)	AW ICG (g)	Error	Error (%)
1	0.1117	0.1113	0.0004	0.36	0.0232	0.0230	0.0002	0.86
2	0.1117	0.1117	None	0.00	0.0232	0.0235	0.0003	1.29
3	0.1117	0.1121	0.0004	0.36	0.0232	0.0228	0.0006	2.59
4	0.1117	0.1119	0.0002	0.18	0.0232	0.0233	0.0001	0.43
5	0.1117	0.1122	0.0005	0.45	0.0232	0.0233	0.0001	0.43
6	0.1117	0.1120	0.0003	0.27	0.0232	0.0228	0.0004	1.72
7	0.1117	0.1119	0.0002	0.18	0.0232	0.0230	0.0002	0.86
8	0.1117	0.1116	0.0001	0.09	0.0232	0.0234	0.0002	0.86
9	0.1117	0.1117	None	0.00	0.0232	0.0234	0.0002	0.86
10	0.1117	0.1115	0.0002	0.18	0.0232	0.0231	0.0001	0.43
11	0.1117	0.1119	0.0002	0.18	0.0232	0.0231	0.0001	0.43
12	0.1117	0.1117	None	0.00	0.0232	0.0230	0.0002	0.86
13	0.1117	0.1116	0.0001	0.09	0.0232	0.0233	0.0001	0.43
14	0.1117	0.1114	0.0003	0.27	0.0232	0.0234	0.0002	0.86
15	0.1117	0.1114	0.0003	0.27	0.0232	0.0233	0.0001	0.43
16	0.1117	0.1121	0.0004	0.36	0.0232	0.0234	0.0002	0.86
17	0.1117	0.1119	0.0002	0.18	0.0232	0.0232	None	0.00
18	0.1117	0.1121	0.0004	0.36	0.0232	0.0230	0.0002	0.86
19	0.1117	0.1120	0.0003	0.27	0.0232	0.0230	0.0002	0.86
20	0.1117	0.1118	0.0001	0.09	0.0232	0.0233	None	0.00
21	0.1117	0.1115	0.0002	0.18	0.0232	0.0233	0.0001	0.43
22	0.1117	0.1119	0.0002	0.18	0.0232	0.0235	0.0003	1.29
23	0.1117	0.1117	None	0.00	0.0232	0.0233	0.0001	0.43
24	0.1117	0.1117	None	0.00	0.0232	0.0233	0.0002	0.86

Table 3.4: Error associated with weighing of dry components

Batch Number	DW HSA (g)	AW HSA (g)	Error	Error (%)
1	0.1117	0.1123	+0.0006	0.54%
2	0.1117	0.1112	-0.0005	0.45%
3	0.1117	0.1120	+0.0003	0.27%
4	0.1117	0.1116	-0.0001	0.09%
5	0.1117	0.1114	-0.0003	0.27%

Table 3.5: Maximum error associated with dilution

Desired Concentration	Maximum Uncertainty ICG (ICG:HSA)	Maximum Uncertainty HSA (ICG:HSA)	Maximum Uncertainty HSA (HSA reference)
1000μMol (stock)	±8.0μL	±8.0μL	±8.0μL
800μMol	±8.0μL	±8.0μL	±8.0μL
700μMol	±8.0μL	±8.0μL	±8.0μL
600μMol	±8.0μL	±8.0μL	±8.0μL
500μMol	±8.0μL	±8.0μL	±8.0μL
400μMol	±8.0μL	±8.0μL	±8.0μL

3.9 Conclusion

Three experiments are conducted using a variation of the same setup to fulfil three separate investigations. Success of experiment 2 and 3 depends on experiment 1 and changes to experiment design may be made following completion of experiment 1. As the solutions containing ICG are prepared daily and disposed of each evening, the experiments are repeated according to the time available to do so with the general understanding that the more repetitions, the better and more confident the results.

The methodology chapter describes all of the background processes and preparation required before any data is collected as this is all relevant and important to the project. Literature specific to parameters is included in order to provide findings that are relevant to existing knowledge and studies.

Component selection, soldering, calibrations, using unfamiliar equipment, using unfamiliar software, liaising with suppliers and communicating with experts was all completed during setup of experiments. Significant time was invested into research, development and testing of designs before the final methodology was confirmed so as to maximise efficiency within the lab. This project required the use of several pieces of lab equipment each with their respective accompanying software which required time to explore all features and determine suitability for use.

4 Results and Discussion

Processed results are presented in this chapter alongside statistical values where required. The majority of data collected during this project are JPEG images from the camera that have been analysed in LabVIEW post data acquisition. This chapter will not contain raw images as these will not necessarily be clear in print however, an example of an image collected is presented in Figure 4.1. Where timed experiments have been completed, experimental rates will be calculated and presented within this chapter.

This chapter will also interpret the data for each experiment detailed within the methodology. The importance and significance of each experiment will also be commented on.

Experiments 1, 2 and 3 were all conducted as planned however this required significantly more preparation than first assumed. Samples were prepared daily and so these were finite in supply, as soon as verification that HSA alone does not hold any fluorescent properties when excited at 780nm as expected, no reference cuvette containing HSA solution only was required thus reducing the preparation time. Efficiency and confidence in mixing and diluting solutions improved throughout the testing period. Good working practice was followed for cleaning and handling optical components. A LASER safety course was attended early on at the National Physical Laboratory to ensure LASER experiments are conducted safely. Fortunately, the 780nm LED and LASER diode produced a visible beam.

The main research objective includes imaging aqueous solutions of ICG with a single camera which, if successful, would follow with an analysis of the importance of filters in imaging frames containing fluorescing material. Research questions surrounding the optical properties of ICG and the ideal setup for imaging are also raised. In brief, the viability of a single detector imaging system, without the use of filters, is investigated specifically for use in the removal of cancerous tissue in the breast via fluorescence

endoscopy. See Figure 4.1, Figure 4.2, Figure 4.3 and Figure 4.4 for a visual representation of what is visible through the camera and handheld beam viewer.

4.1 General Observations

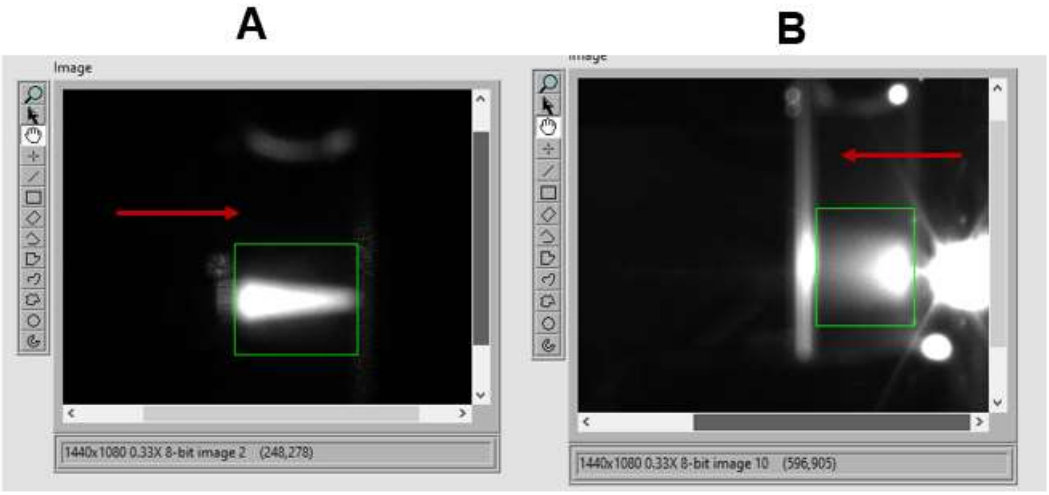

Figure 4.1: Images loaded into the LabVIEW programme showing fluorescence of a 1000µMol sample of ICG:HSA at an exposure time of 249998µs under 10mW LASER illumination (A) and a 1000µMol sample of ICG:HSA at an exposure time of 124998µs under LED illumination (B), Arrows added to show the direction of light.

The following Figure 4.2 shows a picture taken through the handheld beam viewer which helps to visualise light at invisible IR wavelengths. When practicing using this apparatus, it was shocking to see how much IR pollution exists from security cameras in a suburban environment. The image labelled “A” shows fluorescence within the cuvette only and there is no fluorescence observed direct at the source. The image labelled “B” shows the single LED with a cluster of unused LEDs behind the aluminium mount. The dome shape of the LED is well preserved in these images, both have been zoomed in for clarity as the beam viewer is designed for use with the eye and not a camera.

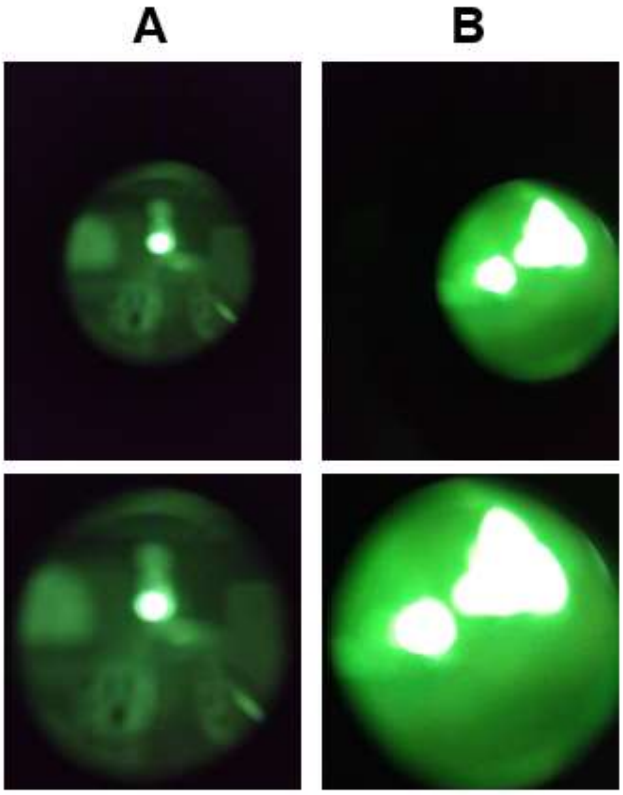

Figure 4.2: The view through the handheld beamviewer for illumination with LASER (A) and LED (B)

Both Figure 4.3 and Figure 4.4 present images acquired during data collection whereby excitation power of the LED is changed as well as the contents of the cuvette. It is evident that fluorescence is detectable using the existing setup and it is important to note that the fluorescence is not detectable by eye while the excitation is. This is a significant finding which will be discussed accordingly.

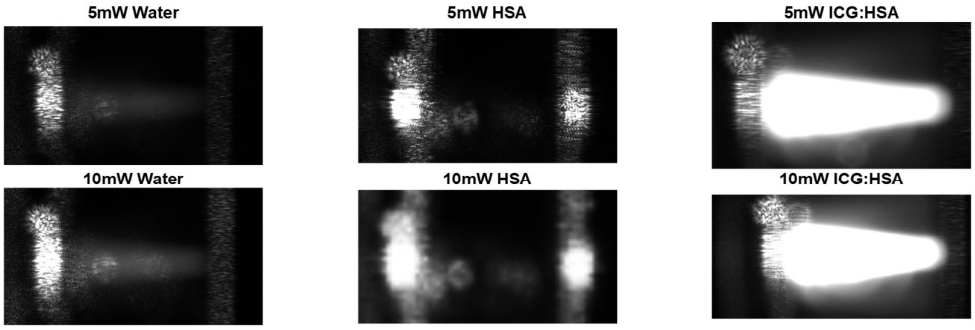

Figure 4.3: Images of Cuvette contents taken with varying LASER excitation under a 1 second exposure

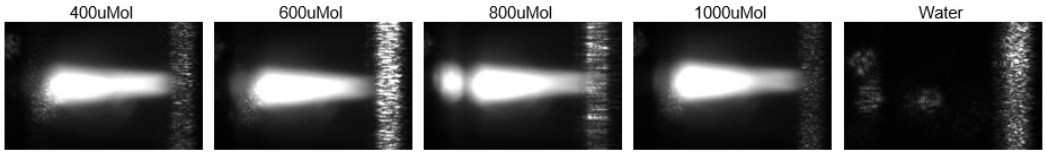

Figure 4.4: Images of ICG:HSA samples at varying concentrations with 10mW LASER excitation captured under an exposure of 249998µs, deionised water is used as a reference.

The following Table 4.1 presents the power observed at the surface of the sample for each illumination condition.

Table 4.1: Power conversion for each illumination condition

Illumination Source	Power (mW)	Intensity at the sample surface (mW/cm^2)
LED	7.2	36.67
LASER	5.0	70.74
LASER	10.0	141.47

4.2 Spectrometry Results

The following figures, Figure 4.5, Figure 4.6, Figure 4.7, Figure 4.8, Figure 4.9, Figure 4.10, Figure 4.11 and Figure 4.12 present averaged and smoothed fluorescence data. The x-axis represents wavelength in nm while the y-axis represents fluorescence intensity in spectrometer counts.

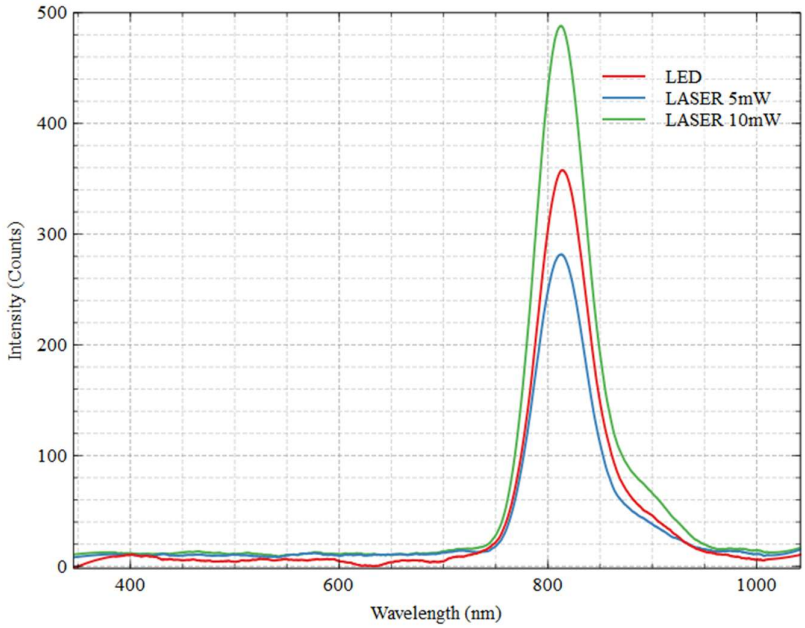

Figure 4.5: Averaged and smoothed spectrometer data for ICG:HSA 400μMol

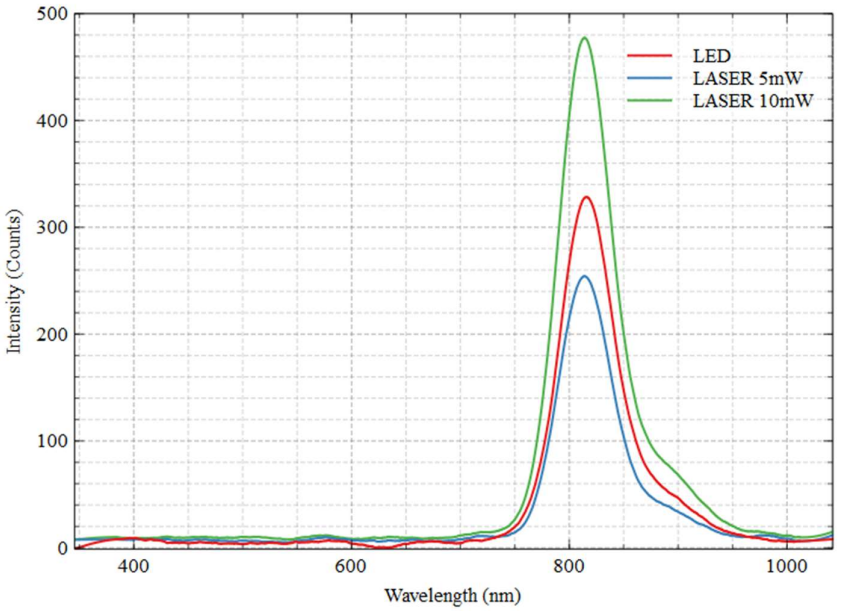

Figure 4.6: Averaged and smoothed spectrometer data for ICG:HSA 600µMol

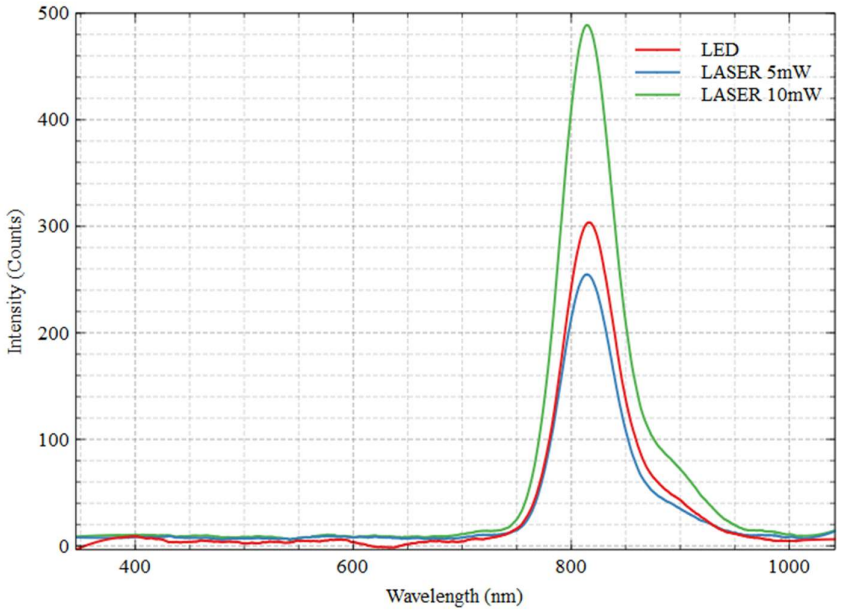

Figure 4.7: Averaged and smoothed spectrometer data for ICG:HSA 800µMol

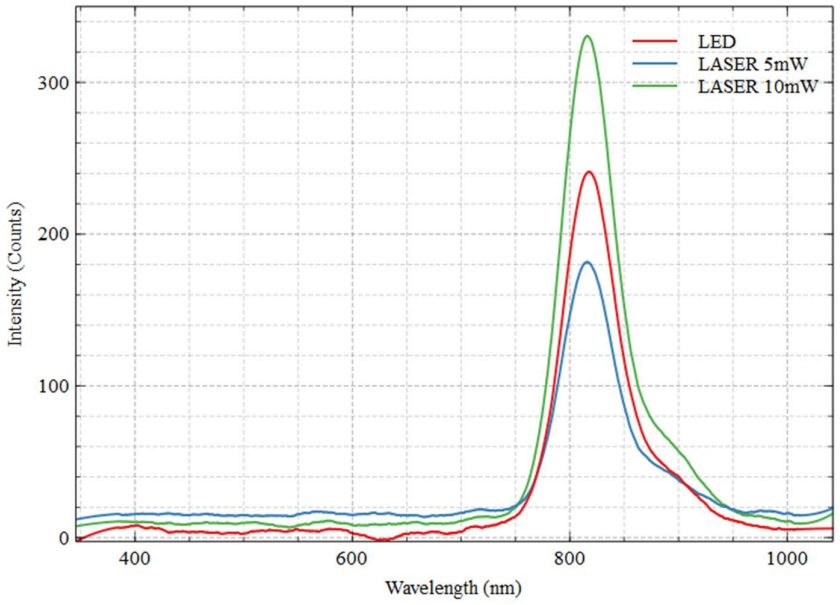

Figure 4.8: Averaged and smoothed spectrometer data for ICG:HSA 1000µMol

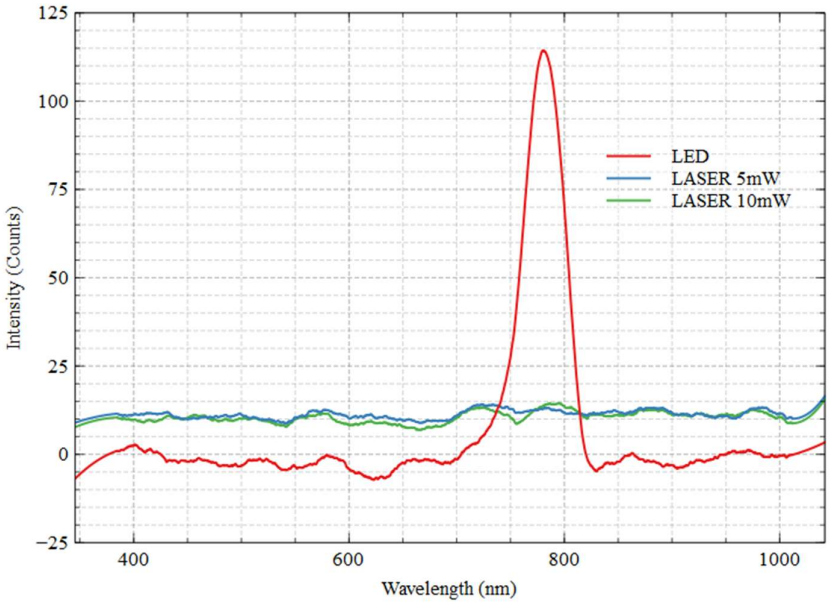

Figure 4.9: Averaged and smoothed spectrometer data for Water

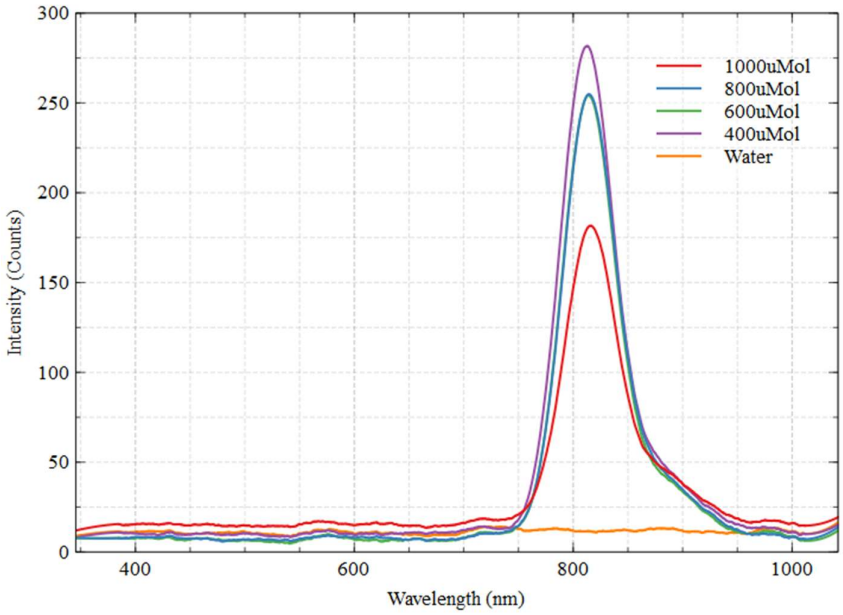

Figure 4.10: Averaged and smoothed spectrometer data with 5mW LASER excitation

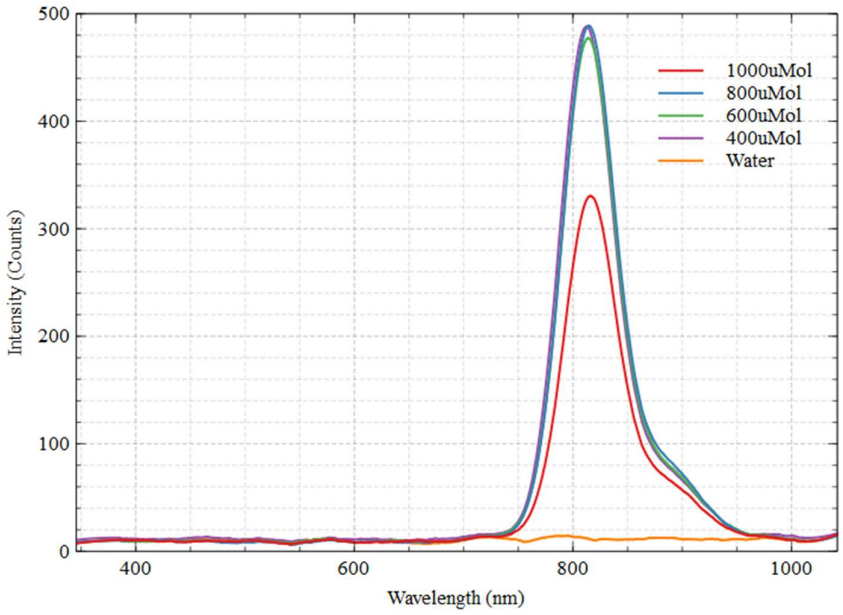

Figure 4.11: Averaged and smoothed spectrometer data with 10mW LASER excitation

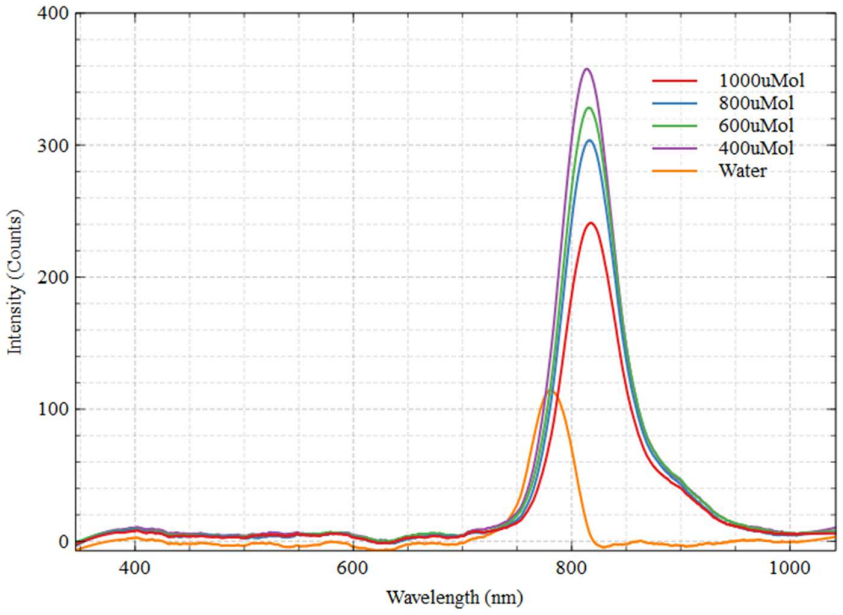

Figure 4.12: Averaged and smoothed spectrometer data with LED Excitation

From the following tabulated information, we see that the two LASER power settings yield almost identical results with power significantly impacting on the intensity value. Note the peak wavelength value for water in Table 4.2 and Table 4.3, representing data collected from the 5mW and 10mW LASER illumination conditions respectively. This value for water is not consistent with any of the other tabulated data, it represents the highest intensity value which happens to exist at the very end of the wavelength range of the spectrometer. The relatively low intensity value can be considered as noise and not a true peak as observed in Figure 4.10 and Figure 4.11.

Table 4.2: Peak Analysis with 5mW LASER Excitation

Solution	Peak Wavelength (nm)	Intensity Value (Counts)
400µMol	812.980	281.765
600µMol	814.088	254.386
800µMol	814.088	254.864
1000µMol	815.934	181.673
Water	1041.939	16.458

Table 4.3: Peak Analysis with 10mW LASER Excitation

Solution	Peak Wavelength (nm)	Intensity Value (Counts)
400µMol	812.610	488.143
600µMol	814.088	477.518
800µMol	814.457	488.869
1000µMol	815.934	330.663
Water	1041.939	15.573

Table 4.4: Peak Analysis with LED Excitation

Solution	Peak Wavelength (nm)	Intensity Value (Counts)
400µMol	813.904	357.757
600µMol	815.565	328.373
800µMol	817.041	303.514
1000µMol	817.778	241.144
Water	780.034	114.309

See Figure 4.5, Figure 4.6, Figure 4.7, Figure 4.8, Figure 4.9, Figure 4.10, Figure 4.11 and Figure 4.12 with a peak analysis presented in Table 4.2, Table 4.3 and Table 4.4 for reference to fluorescence data collected with the spectrometer.

Fluorescence data is collected under each excitation condition and the results are presented accordingly. Here we can see that the fluorescence wavelength is centred around 815nm, 35nm longer than the excitation. Each figure corresponding to fluorescence spectrometry shows the wavelength range of the spectrometer along the x-axis with the y-axis representing the relative intensity of fluorescence in spectrometer units. The spectra are firstly arranged by concentration as well as the three excitation conditions for clarity. The relationship between the concentration of ICG in solution, the

excitation source and detected fluorescence can be identified clearly. Fluorescence intensity is highest under 10mW LASER excitation with the LED producing a more intense fluorescence than the 5mW LASER condition. Consistent with literature, the lowest concentration on test provides the highest fluorescence intensity under each excitation condition. The data presented is a representation of multiple days of repeat testing as to avoid errors due to rogue mixing or dilution calculations. The spectrometer collects fluorescence data at intervals of 0.2nm and has a range of 200-1100nm.

The reference cuvette containing deionized water shows no fluorescence as expected when excited with the 5mW and 10mW LASER source. The separate LED spectra however, show a central peak at 780nm. The reason for this is due to the divergence of the LED beam, the light travels through the cuvette containing water (at the excitation wavelength) and is detected by the spectrometer. No fluorescence is detected due to the lack of ICG in the sample. As the results presented represent the excitation wavelength of the LED only, we have a better understanding of the “intensity” which accounts for the y-axis of the spectra in the remaining figures related to this spectrometer data. The spectrometer and accompanying software define fluorescence as a measurement of the relative irradiance which is not a quantified numerical value. The LED provides just over 7mW of forward optical power and so the peak represented by the cuvette containing water only represents a fraction of the source which has travelled through two cuvette walls (optical glass) and a volume of water to reach the detector positioned perpendicular to the source. For reference, the cuvettes have a pathlength of 10mm and the glass thickness is 1.25mm.

4.3 Pixel Analysis

The following figures, Figure 4.13, Figure 4.14 and Figure 4.15 present data taken from images collected and analysed in the LabVIEW ROI programme. The x-axis represents the concentration of ICG:HSA whereby a value of zero indicates the reference, water while the y-axis represents the intensity of pixels within the set ROI in grayscale values.

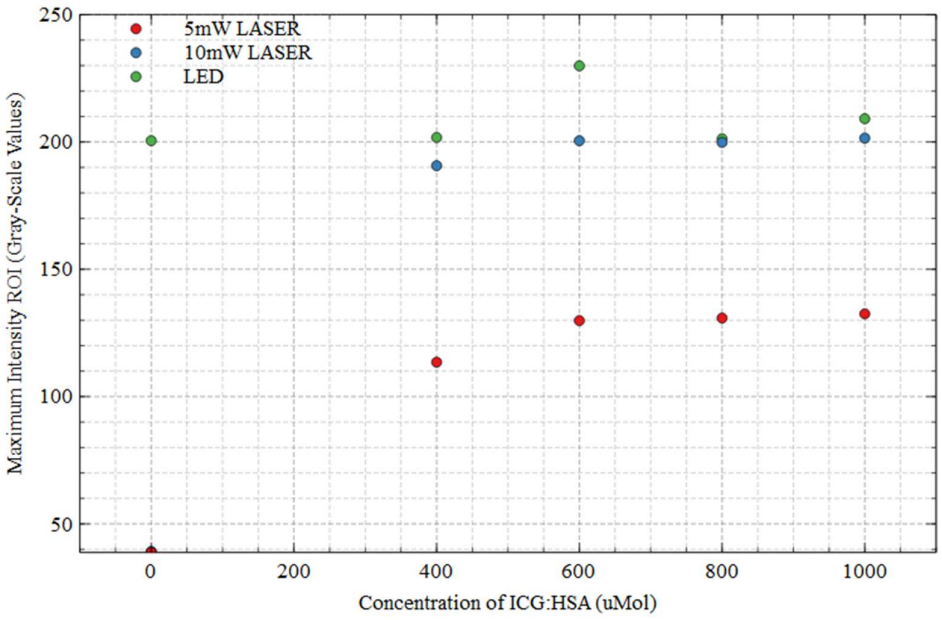

Figure 4.13: A plot to show the maximum intensity of pixels within the selected region for each concentration of ICG:HSA under each excitation condition. Image captured at an exposure of 78124µs and the region of interest represents an average area of 107618 pixels

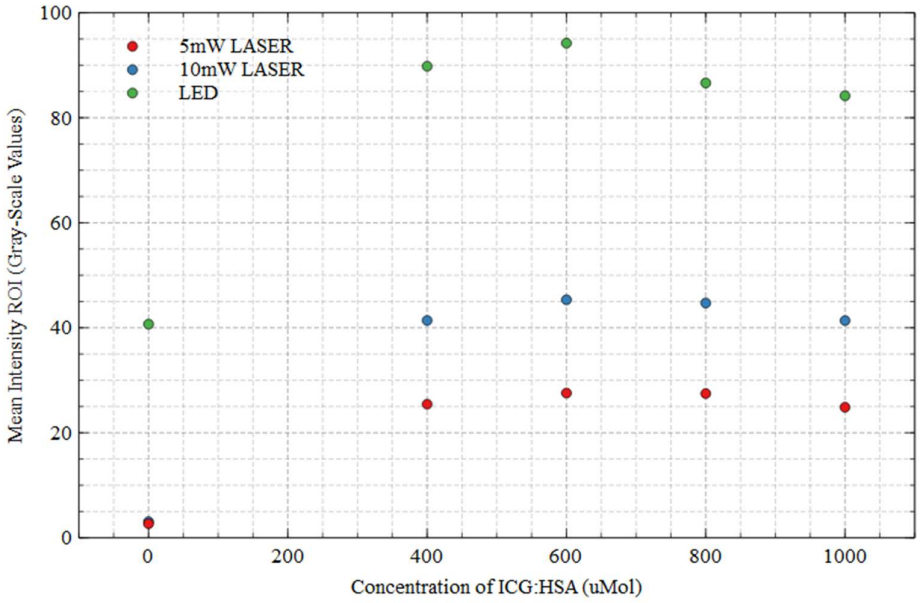

Figure 4.14: A plot to show the mean intensity of pixels within the selected region for each concentration of ICG:HSA under each excitation condition. Image captured at an exposure of 78124µs and the region of interest represents an average area of 107618 pixels

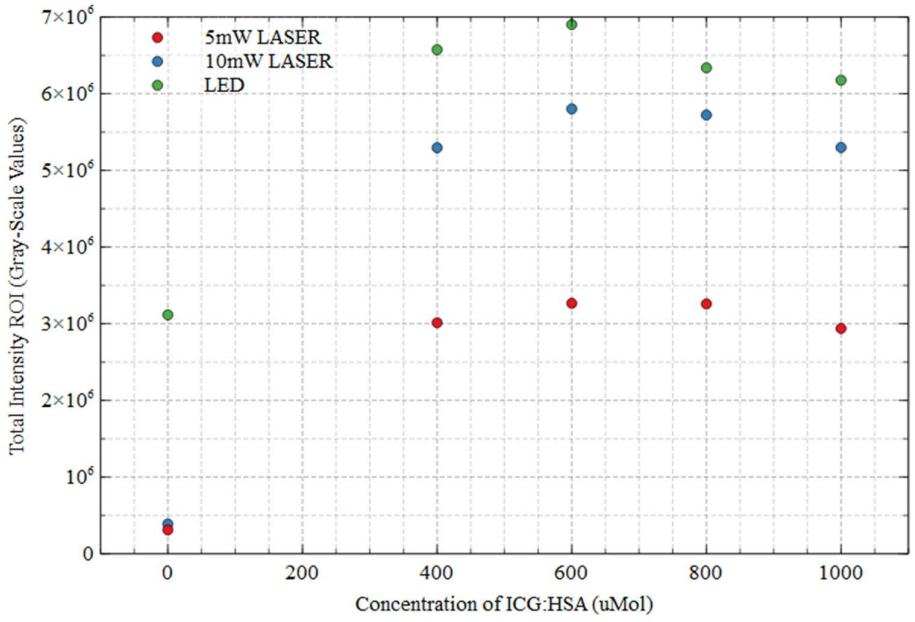

Figure 4.15: A plot to show the intensity of all pixels within the selected region for each concentration of ICG:HSA under each excitation condition. Image captured at an exposure of 78124µs and the region of interest represents an average area of 107618 pixels

Table 4.5: Maximum Pixel Intensity within the Region of Interest, in Grayscale Units

Solution	5mW LASER	10mW LASER	LED
400µMol	113.50	190.67	201.75
600µMol	129.83	200.50	229.88
800µMol	130.83	199.83	201.25
1000µMol	132.50	201.50	209.13
Water	38.80	39.20	200.50

Table 4.6: Mean Pixel Intensity within the Region of Interest, in Grayscale Units

Solution	5mW LASER	10mW LASER	LED
400µMol	25.44	41.39	89.81
600µMol	27.56	45.33	94.20
800µMol	27.47	44.71	86.62
1000µMol	24.86	41.37	84.18
Water	2.67	3.06	40.69

Table 4.7: Total Intensity of Pixels within the Region of Interest, in Grayscale Units

Solution	5mW LASER	10mW LASER	LED
400µMol	3012810.00	5295325.00	6573716.25
600µMol	3266543.33	5801596.67	6902006.25
800µMol	3258541.67	5721840.00	6337798.75
1000µMol	2938073.33	5298403.33	6176162.50
Water	310678.40	388289.20	3115578.75

To quantify the intensity of the fluorescence, the spectrometer data is combined with images captured with a single CMOS camera. The maximum, mean and total intensity

of the ROI respectively for each concentration and excitation source on test are presented to accompany the spectrometer results, see Figure 4.13, Figure 4.14 and Figure 4.15 with tabulated values presented in Table 4.5, Table 4.6 and Table 4.7. Images collected are opened in LabVIEW and a region of interest is drawn manually encompassing the contents of the cuvette and excluding the light source. An analysis was conducted in order to obtain the intensity values for pixels within the selected region. These values are plotted and presented to compliment the spectrometry data. The CMOS camera images are unfiltered hence the reason for a higher intensity under LED excitation, not observed in the spectrometer results. The upper intensity limit is 256 grayscale units which would saturate the image, consideration of exposure time, excitation power and ICG concentration will yield the most useful images whereby all fluorescent regions are clearly visible without any areas of saturation.

No filtering was applied to the camera setup as confirmed by the spectrometer results. With the exception of water under LED excitation, there is no source wavelength within the results. The camera is in an equivalent position to the spectrometer, in parallel to the source so that the cuvette and its contents are imaged.

The results obtained from experiment 1 are better than expected, firstly the fluorescence is detectable on camera without need for filters, considering the relatively low QE at this wavelength range it is very clear to see the fluorescence as well as background detail within the frame. All solutions containing ICG show fluorescence and the control samples containing water only and HSA only show no fluorescence as expected.

Note that water (0µMol ICG:HSA) under LED illumination shows as an anomaly in results presented in Figure 4.13, Figure 4.14 and Figure 4.15. This is due to the beam characteristics of the LED as discussed previously.

Results obtained from experiment 1 show that LED and LASER are comparable in regards to their ability to illuminate the sample and excite the fluorophore. As the ICG is in aqueous solution, LASER light is preferable as there is virtually no possibility of

excitation light directly hitting the detector. Importantly, no filtering is required for results collected from experiment 1 and it is evident that the emission wavelength is not visible to the human eye without the use of the camera. The camera selected offers a low-cost component for the overall system and its specifications are comparable to those taken from literature. The difference in visibility between the emission and excitation wavelengths offers a significant advantage to the argument against using filters. It is reasonable to say that if saturation is visible through the camera but not by eye then ICG is present. The results cannot tell us if this is applicable under real-world conditions as this was a lab simulation but they can tell us that both LASER and LED at 780nm at power less than 10mW is adequate for illumination and excitation of ICG samples. We can confidently identify the presence of ICG in solution and the concentration presenting the highest fluorescence intensity peak was in agreeance with values reported in literature.

Following the success of experiment 1 with detectable fluorescence and a better understanding of the relationship between concentration and fluorescence intensity, experiment 2 can go ahead without any substantial changes.

4.4 Timed Data

The following figures, Figure 4.16, Figure 4.17 and Figure 4.18 present data to show the rate of change in optical power using the power meter. The x-axis represents time in seconds and the y-axis represents detected optical power in mW.

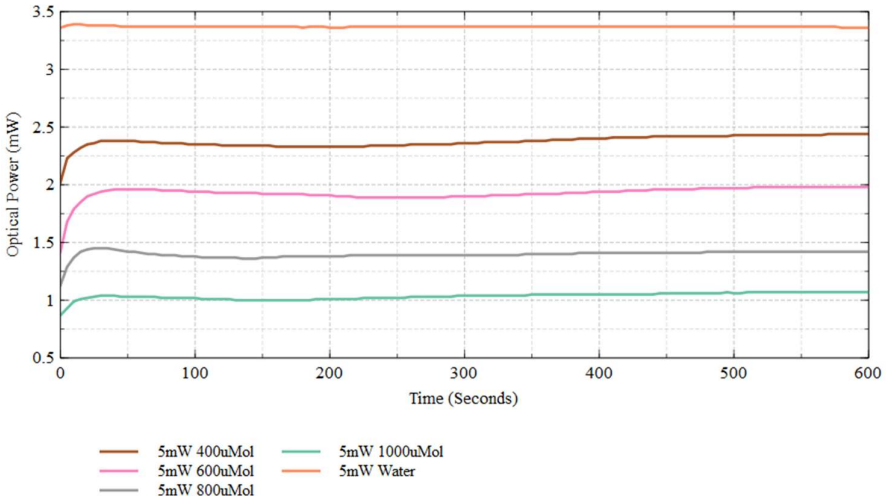

Figure 4.16: A plot to show the change in optical power with time with the power meter in parallel to the source with 5mW LASER Excitation

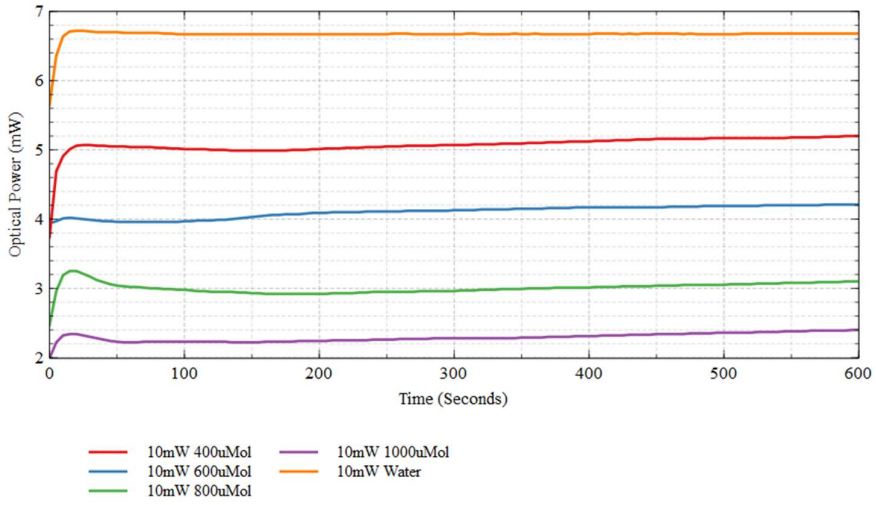

Figure 4.17: A plot to show the change in optical power with time with the power meter in parallel to the source with 10mW LASER Excitation

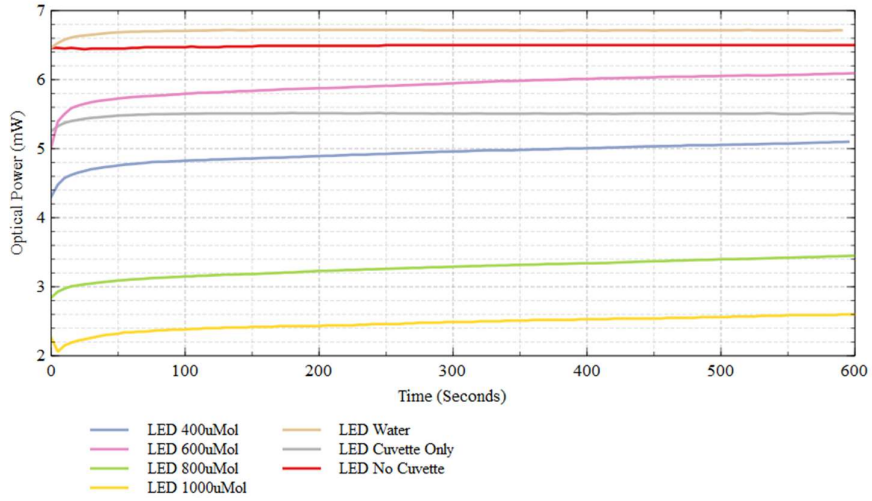

Figure 4.18: A plot to show the change in optical power with time with the power meter in parallel to the source with LED Excitation

Table 4.8: Power changes at 5mW LASER Excitation in mW

Solution	Power at T=0s	Power at T=300s	Power at T=600s	Rate in Period 1 mW/min	Rate in Period 2 mW/min
400µMol	2.02	2.36	2.44	0.068	0.016
600µMol	1.42	1.90	1.98	0.096	0.016
800µMol	1.13	1.39	1.42	0.052	0.006
1000µMol	0.87	1.04	1.07	0.034	0.006
Water	3.36	3.37	3.36	0.002	-0.002

Table 4.9: Power changes at 10mW Excitation in mW

Solution	Power at T=0s	Power at T=300s	Power at T=600s	Rate in Period 1 mW/min	Rate in Period 2 mW/min
400µMol	3.74	5.07	5.20	0.266	0.026
600µMol	3.94	4.13	4.21	0.038	0.016
800µMol	2.47	2.96	3.10	0.098	0.028
1000µMol	1.99	2.28	2.40	0.058	0.024
Water	5.65	6.67	6.68	0.204	0.002

Table 4.10: Power changes with LED Excitation in mW

Solution	Power at T=0s	Power at T=300s	Power at T=600s	Rate in Period 1 mW/min	Rate in Period 2 mW/min
400µMol	4.30	4.96	5.10	0.132	0.028
600µMol	5.02	5.95	6.10	0.186	0.030
800µMol	2.84	3.29	3.45	0.090	0.032
1000µMol	2.26	2.49	2.60	0.046	0.022
Water	6.46	6.72	6.72	0.052	0.000
Empty Cuvette	2.25	5.51	5.50	0.652	-0.002
No Cuvette	6.46	6.50	6.50	0.008	0.000

Images are collected every 60 seconds for 10 minutes at an exposure time of 124998µs, a power meter reading is recorded manually at 5 second intervals to compliment the camera data and confirm the presence of photobleaching or decay in fluorescence over

time, see Figure 4.16, Figure 4.17 and Figure 4.18 with tabulated values presented in Table 4.8, Table 4.9 and Table 4.10.

When looking at Table 4.8 and Table 4.9, we see the effect that changing the excitation power has on the rate of change in fluorescence intensity according to the power meter. When looking at the second half of the time period, to allow for any initial fluctuations to settle, the rate of change is mildly influenced by a change in illumination power, this is likely due to the relatively short time period analysed but again, the rate is recorded per minute and all are relatively small values. We see that an increase in power generally increase the rate of degradation which is to be expected.

The results indicate slight degradation of the fluorescence at a varying rate. It is important to note the apparatus orientation as this can provide explanation as to why the power meter values are increasing with time. The power meter is arranged opposite the source which would not necessarily indicate the rate of fluorescence decay. The optical power present at the beginning of the experiment is greater than the that after an observation period of 10 minutes according to the data. It is reasonable to assume that over time the fluorescent material within the cuvette is absorbing energy and possibly photobleaching therefore more source energy is detected. Source energy passing through the cuvette without absorption will be detected as there is no filter applied to remove light at the excitation wavelength. Without using a filter this cannot be verified but is an observation from experimental work. No filter was used so as to simplify the system and to verify that a filter is not essential when using a single camera detection technique. If photobleaching is present, in this instance the rate is very low and would likely be barely detectable. As the LASER is operated in continuous mode, the observed difference in power may be due to fluctuations of the LASER itself.

The following Figure 4.19 presents temperature data collected from inside of the cuvette over a period of time in set intervals. The x-axis represents time in seconds and the y-axis represents the temperature in ºC.

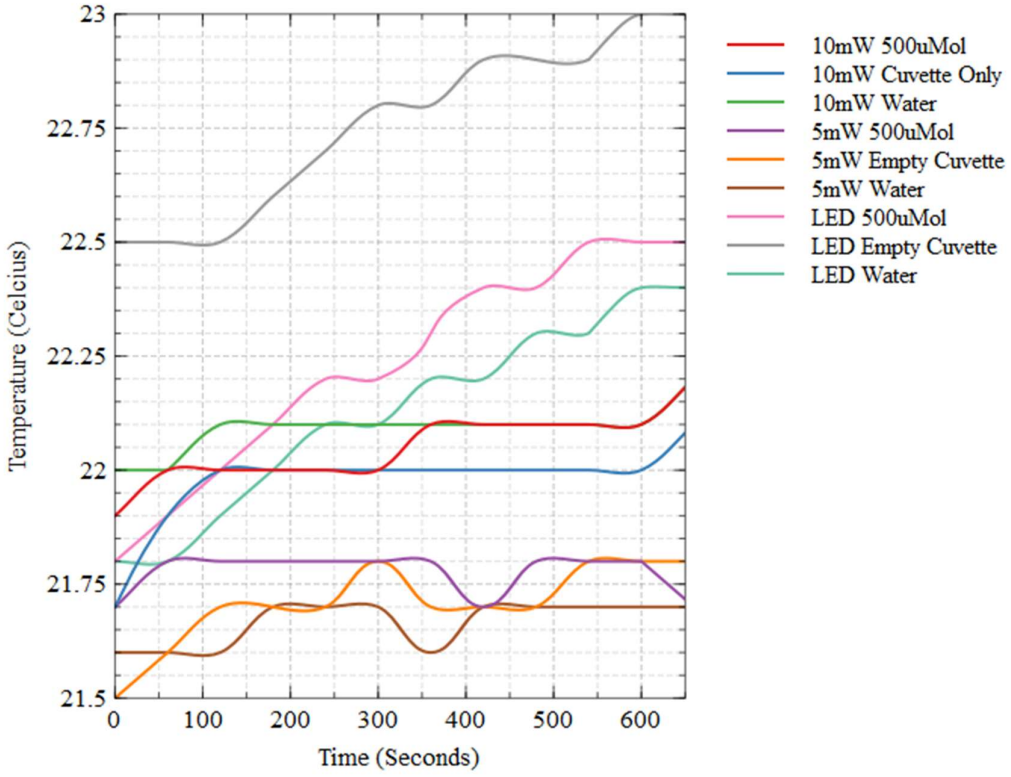

Figure 4.19: A plot to show how temperature changes with time from inside the cuvette with differing contents and source of excitation

Table 4.11: Temperature changes with 5mW excitation in degrees Celsius

Solution	Temp at T=0s	Temp at T=300s	Temp at T=600s	Rate in Period 1 ºC/min	Rate in Period 2 ºC/min
Water	21.6	21.7	21.7	0.02	0.00
500µMol	21.7	21.8	21.8	0.02	0.00
Empty/Air	21.5	21.8	21.8	0.06	0.00

Table 4.12: Temperature changes with 10mW excitation in degrees Celsius

Solution	Temp at T=0s	Temp at T=300s	Temp at T=600s	Rate in Period 1 ºC/min	Rate in Period 2 ºC/min
Water	22.0	22.1	22.1	0.02	0.00
500µMol	21.9	22.0	22.1	0.02	0.02
Empty/Air	21.7	22.0	22.0	0.06	0.00

Table 4.13: Temperature changes with LED excitation in degrees Celsius

Solution	Temp at T=0s	Temp at T=300s	Temp at T=600s	Rate in Period 1 ºC/min	Rate in Period 2 ºC/min
Water	21.8	22.1	22.4	0.06	0.06
500µMol	21.8	22.2	22.5	0.08	0.06
Empty/Air	22.5	22.8	23.0	0.06	0.04

Temperature within the cuvette was recorded and the average temperature increase over a period of 11 minutes is presented in the results, see Figure 4.19 and Table 4.11, Table 4.12 and Table 4.13. The LASER is connected to a thermoelectric cooler so as to maintain the operating temperature for output stability, the LED is not connected to an active thermal management system during experiment as it is mounted in a custom aluminium holder. The difference in thermal management is likely to have a significant effect on temperature within the cuvette.

The following figures, Figure 4.20, Figure 4.21 and Figure 4.22 present another pixel analysis whereby images are collected over a period of time in set intervals in order to understand the rate of change. The x-axis represents time in seconds and the y-axis represents intensity of pixels within the set ROI in grayscale values.

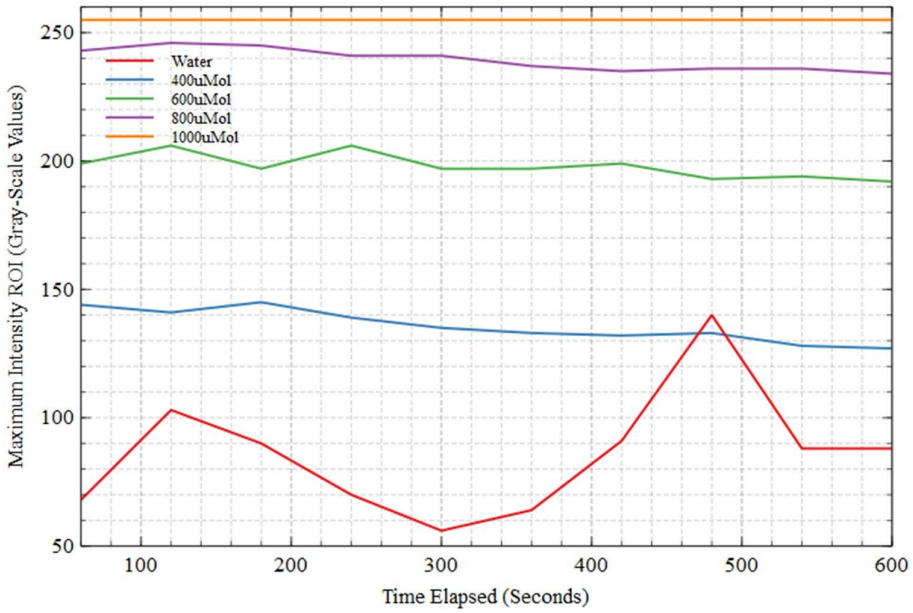

Figure 4.20: A plot to show the maximum intensity of pixels within the selected region for each concentration of ICG:HSA under 10mW LASER excitation over a time period of 10 minutes. Image captured at an exposure of 124998µs and the region of interest represents an area of 53578 pixels

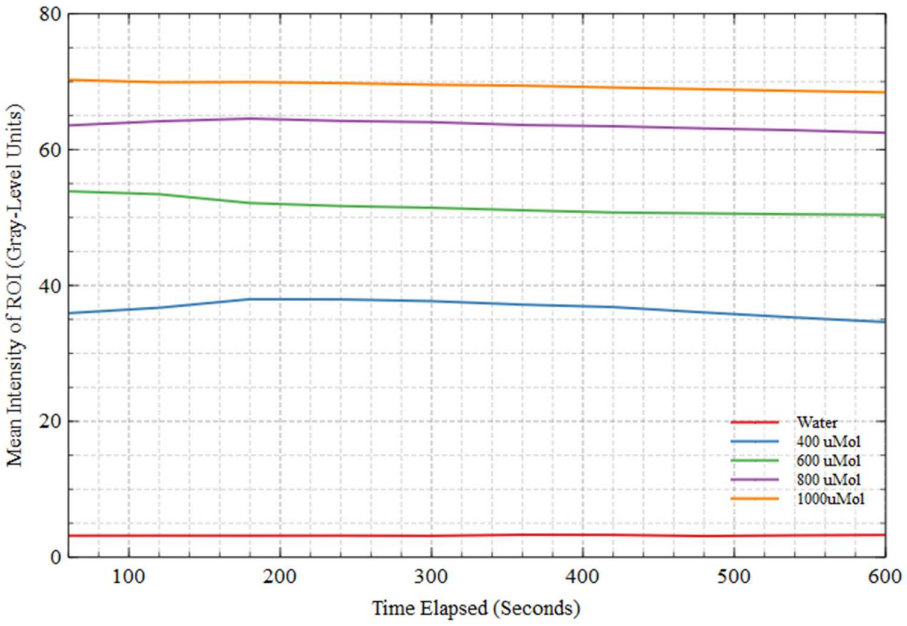

Figure 4.21: A plot to show the mean intensity of pixels within the selected region for each concentration of ICG:HSA under 10mW LASER excitation over a time period of 10 minutes. Image captured at an exposure of 124998µs and the region of interest represents an area of 53578 pixels

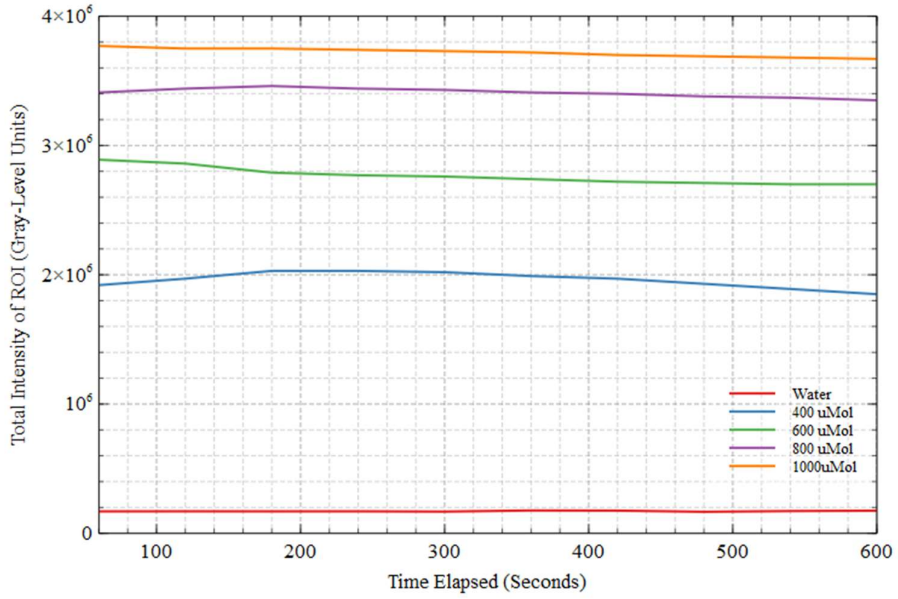

Figure 4.22: A plot to show the intensity of all pixels within the selected region for each concentration of ICG:HSA under 10mW LASER excitation over a time period of 10 minutes. Image captured at an exposure of 124998µs and the region of interest represents an area of 53578 pixels

Tabulated data includes the rate calculated in grayscale units (GSU) per minute in line with the previous rate calculations.

Table 4.14: Maximum pixel intensity within the region of interest with 10mW excitation, in Grayscale Units

Solution	Intensity at T=60s	Intensity at T=300s	Intensity at T=600s	Rate in Period 1 GSU/min	Rate in Period 2 GSU/min
400µMol	144	135	127	-1.8	-1.6
600µMol	199	197	192	-0.4	-1.0
800µMol	243	241	234	-0.4	-1.4
1000µMol	255	255	255	0.0	0.0
Water	68	56	88	-2.4	6.4

Table 4.15: Mean pixel intensity within the region of interest with 10mW excitation, in Grayscale Units

Solution	Intensity at T=60s	Intensity at T=300s	Intensity at T=600s	Rate in Period 1 GSU/min	Rate in Period 2 GSU/min
400µMol	35.92	37.69	34.61	0.354	-0.616
600µMol	53.86	51.44	50.39	-0.484	-0.210
800µMol	63.56	64.04	62.48	0.096	-0.312
1000µMol	70.27	69.55	68.43	-0.144	-0.224
Water	3.17	3.14	3.27	-0.006	0.026

Table 4.16: Total pixel intensity within the region of interest with 10mW excitation, in Grayscale Units

Solution	Intensity at T=60s	Intensity at T=300s	Intensity at T=600s
400μMol	1.92E+06	2.02E+06	1.85E+06
600μMol	2.89E+06	2.76E+06	2.70E+06
800μMol	3.41E+06	3.43E+06	3.35E+06
1000μMol	3.77E+06	3.73E+06	3.67E+06
Water	169851	168107	175117

Results obtained from experiment 2 are not as expected, a decay in fluorescence is observed over time however, one parameter did not identify as being more significant than any other and in general, the decay was not substantial. Literature indicates a mix of statistics regarding fluorescence decay rate however the time on test was perhaps not enough to produce any significant results. It is important to note that typically, minimally invasive fluorescence endoscopy procedures will last however long a surgeon needs to complete their task but as the patient is fully sedated, the shorter this time the better. As experiments were repeated, a maximum of 11 minutes was dedicated to each concentration for each repetition and this yielded results which require extrapolation.

Results obtained from experiment 2 indicate that a decline in fluorescence intensity is detectable with the power meter and from a pixel analysis of images collected, see Figure 4.20, Figure 4.21 and Figure 4.22. This is important as we see that a decline in fluorescence intensity is observed at every concentration on test. When looking at the mean pixel intensity, Table 4.15 and the power values, Table 4.9, for the second half of the time period to allow for any fluctuations to settle, it appears that concentration of ICG in solution does not have a significant impact on the rate of fluorescence intensity degradation. Both data sets are recorded from excitation with the 10mW LASER

illumination for a fair comparison however the differences in values are insignificant considering that the rate is calculated per minute.

The results cannot tell us what significance any or all of the parameters on test have on the rate of fluorescence decay and we cannot confidently say that we have observed photobleaching. The relationship between concentration of ICG in solution, illumination power and rate of fluorescence degradation cannot be quantified from the results collected. In order to assess the impact that fluorophore concentration and illumination power has on the degradation rate, a longer time period should be assessed. It is reasonable to assume that photobleaching is complex and its rate controlled by a number of mechanisms which is consistent with literature.

The Effect of Adjusting Camera Exposure with respect to Signal Intensity

The following Figure 4.23, Figure 4.24 and Figure 4.25 present another pixel analysis whereby images are collected with a variable exposure time in order to understand the relationship between exposure time, illumination source and saturation. The x-axis represents exposure time in micro seconds and the y-axis represents intensity of pixels within the set ROI in grayscale values. Figure 4.26 shows images representing data analysed in this section to show the relationship between intensity and exposure time.

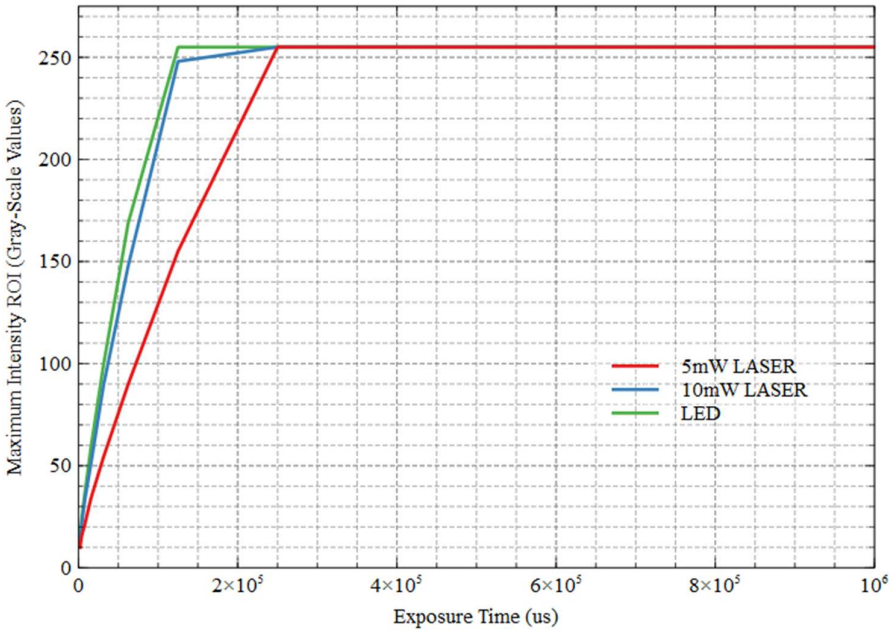

Figure 4.23: A plot to show the maximum intensity of pixels within the selected region for a 500µmol solution of ICG:HSA under all excitation conditions with varying exposure time. The region of interest represents an area of 260804 pixels under the 5mW and 10mW LASER excitation conditions and 287650 pixels for LED excitation

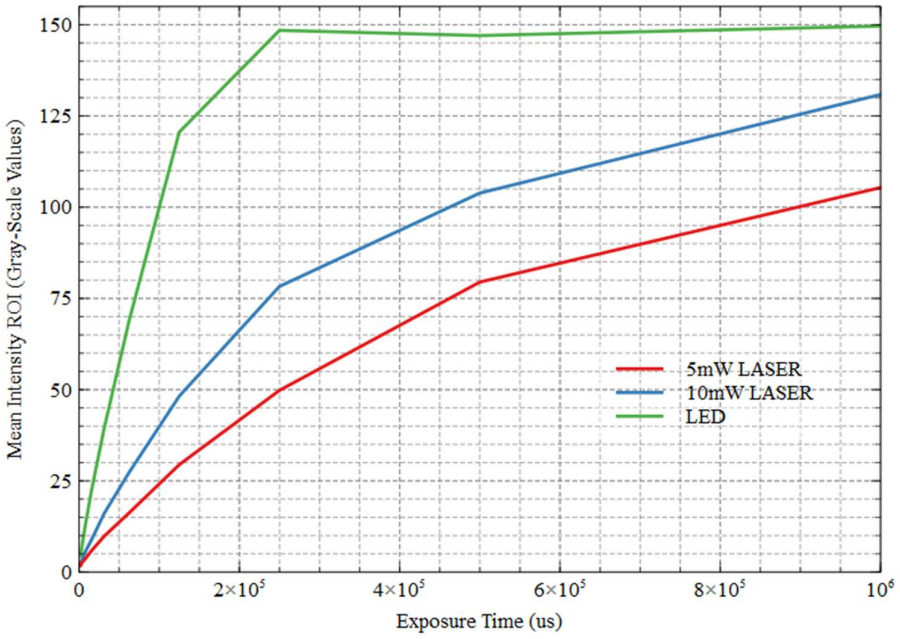

Figure 4.24: A plot to show the mean intensity of pixels within the selected region for a 500µmol solution of ICG:HSA under all excitation conditions with varying exposure time. The region of interest represents an area of 260804 pixels under the 5mW and 10mW LASER excitation conditions and 287650 pixels for LED excitation

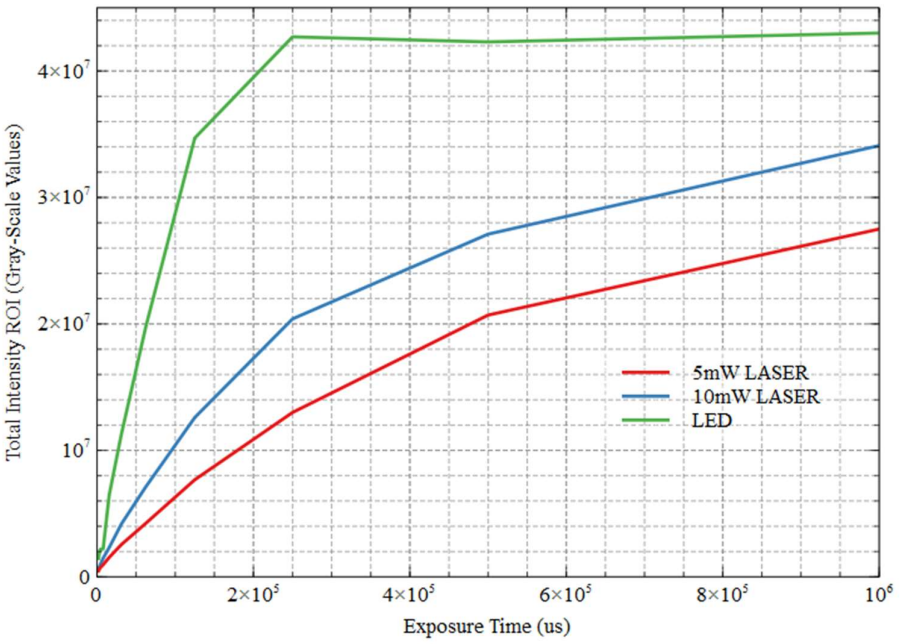

Figure 4.25: A plot to show the total intensity of all pixels within the selected region for a 500µmol solution of ICG:HSA under all excitation conditions with varying exposure time. The region of interest represents an area of 260804 pixels under the 5mW and 10mW LASER excitation conditions and 287650 pixels for LED excitation

Table 4.17: Maximum pixel intensity of a 500µMol solution within the region of interest with varying exposure time, in Grayscale Units

Exposure Time (µs)	5mW LASER	10mW LASER	LED
1953	10.0	13.0	15.0
3906	15.5	21.0	24.0
7812	21.0	33.0	36.0
15625	34.0	51.0	59.0
31250	54.0	89.0	99.0
62500	90.0	148.0	169.0
125000	155.0	248.0	255.0
250000	255.0	255.0	255.0
1000000	255.0	255.0	255.0

Table 4.18: Mean pixel intensity of a 500µMol solution within the region of interest with varying exposure time, in Grayscale Units

Exposure Time (µs)	5mW LASER	10mW LASER	LED
1953	1.80	2.40	4.50
3906	2.70	3.56	7.61
7812	3.67	5.63	12.94
15625	5.90	8.91	22.52
31250	9.82	16.06	39.38
62500	16.25	27.35	69.00
125000	29.44	48.22	120.59
250000	49.80	78.29	148.45
1000000	79.48	103.87	147.03

Table 4.19: Total pixel intensity of a 500µMol solution within the region of interest with varying exposure time, in Grayscale Units

Exposure Time (µs)	5mW LASER	10mW LASER	LED
1953	1.80	2.40	4.50
3906	2.70	3.56	7.61
7812	3.67	5.63	12.94
15625	5.90	8.91	22.52
31250	9.82	16.06	39.38
62500	16.25	27.35	69.00
125000	29.44	48.22	120.59
250000	49.80	78.29	148.45
1000000	79.48	103.87	147.03

Results obtained from experiment 3 were disappointing as the limitation on frame rate was not considered initially. The relationship between exposure time and image quality is analysed to indicate if it will be possible to capture any background landmarks within the frame which account for frame constituents which are not fluorescing, the illumination source and/or direct reflections. See Figure 4.23, Figure 4.24 and Figure 4.25 with tabulated values presented in Table 4.17,

Table 4.18 and Table 4.19. Figure 4.26 provide a visual representation of changes made to the exposure time. As expected, the shorter the exposure time, the lower the mean and total intensity of pixels within the ROI. It is interesting to see that as the exposure time is shortened; the gap shortens between the maximum pixel intensities across the three illumination powers. Overall, the LED offers more ideal imaging conditions at shorter exposure times. The optical power of the LED is set between the two LASER illumination powers, yet the pixel intensity values indicate that the LED provides more illumination generally. This is as expected due to the divergence of the beam produced

by the LED. In reality this would have no impact as light regardless of its original properties would be manipulated for use with an LLG.

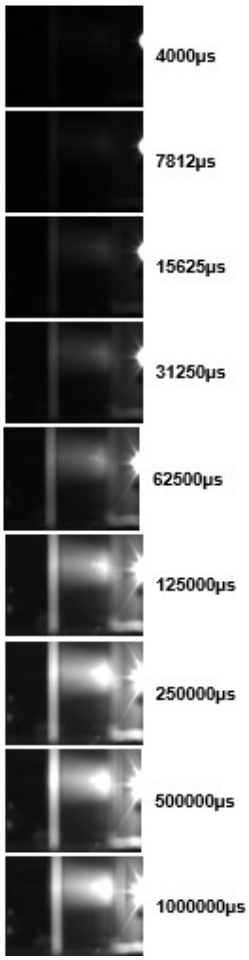

Figure 4.26: Images of a 500µMol solution of ICG:HSA illuminated with a single LED under varying exposure times

4.5 Time Controlled Pulsing

The pulsing procedure is documented in a spreadsheet with the accompanying sequence of images saved to file. Table 4.20 shows that changing the exposure time to shorter than 4855μs has no effect on the resulting frame rate which means that the frame rate is limited to 199.87 which is equivalent to around 200Hz.

Table 4.20: The relationship between exposure time and frame rate

Exposure Time (μs)	Resulting Frame Rate	Acquisition Frame Rate
4866	199.40	199.87
4862	199.55	199.87
4859	199.71	199.87
4855	199.87	199.87
4851	199.87	199.87
4847	199.87	199.87
4843	199.87	199.87

Variable parameters such as pulse width and pulse delay can be verified within the data sequence by reviewing the number of frames with the LED on and number of dark frames. While the speed of data collection was inadequate for detecting residual fluorescence or the decaying fluorescence, sequences show that in certain frames the LED was imaged during a phase change. The images sequences presented below will be accompanied by a brief description in case the contrast of the image is lost in print. A cuvette containing a solution of 500μMol ICG:HSA is imaged under LED illumination whereby the LED and camera are trigger controlled and camera exposure time is software controlled. Figure 4.27, Figure 4.28, Figure 4.29, Figure 4.30, Figure 4.31 and Figure 4.32 represent a portion of images selected from very large data sets. Images are sequential and dark frames, LED off, are not included amongst these figures other than to acknowledge the beginning or end of the LED pulse.

Figure 4.27: Images in sequence captured in buffered mode at an exposure time of 4855µs

Figure 4.27 shows three consecutive frames whereby the LED is the only distinguishable feature. No fluorescence is observed within these three frames. The middle frame represents a time duration of 4855µs where at some point within this frame, the LED pulse ended causing a significant decrease in intensity.

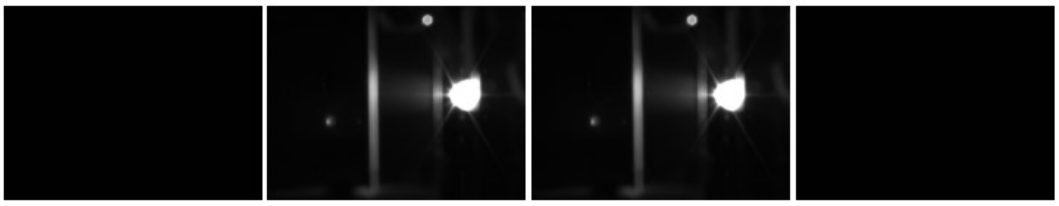

Figure 4.28: Images in sequence captured in streaming mode at an exposure time of 16666µs

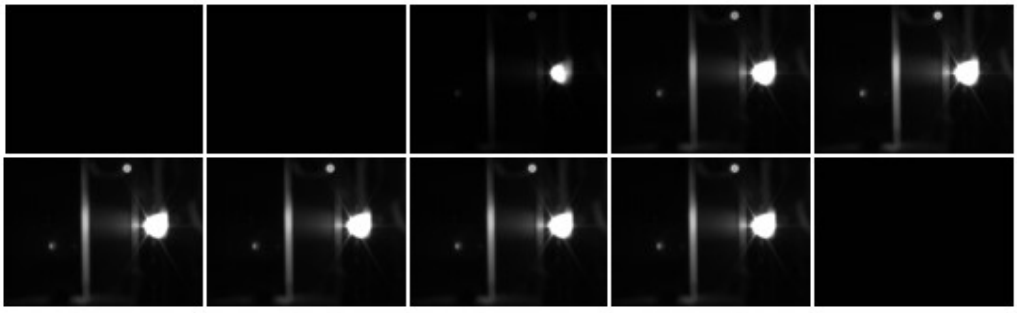

Figure 4.29: Images in sequence captured in buffered mode at an exposure time of 16666µs

Figure 4.28 and Figure 4.29 present a good example of the balance needed between mode and image quality. The camera offers two modes, buffered and streaming.

Buffered mode essentially results in less dropped frames as images are buffered into system memory during recording. Streaming mode results in a high risk of dropped frames as images are not buffered during recording and are saved according to the hard drive speed. The difference in number of frames is significant in this research, from the above figures we can see that the number of frames with LED on is different and the only parameter change between the two datasets is the buffer mode. Both figures show fluorescence within the cuvette at a lower intensity when compared to the LED which is saturating. Figure 4.29 shows that the LED pulse begins at some point within the frame as a reduced intensity is observed in the third image along the top row, this event is completely missed during data collection seen in Figure 4.28.

While the figures presented in this section show mostly buffered images, data was collected under both conditions during testing as dropped frames became a noticeable issue when reducing the exposure time.

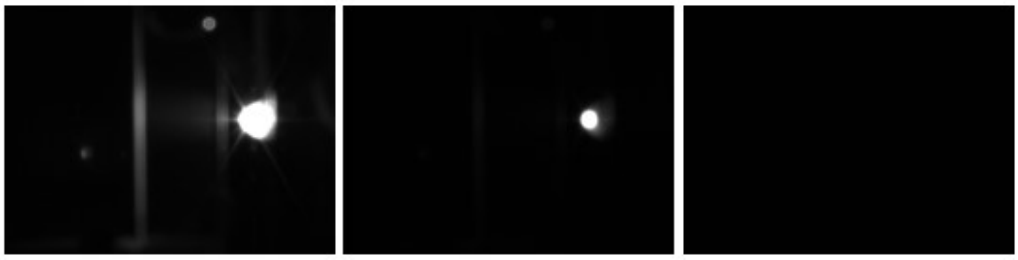

Figure 4.30: Images in sequence captured in buffered mode at an exposure time of 8331µs

Figure 4.30 again shows the LED and fluorescence within the cuvette however, by the next frame the LED pulse has ended and the fluorescence is no longer detectable. The final frame shows the LED off and is a dark frame. Figure 4.31 shows two sequences selected from the same dataset to demonstrate the difference in intensity within the frame capturing the start of a new pulse. The top sequence shows that the LED was off for more of the 4855µs than seen in the second sequence as the intensity of the LED is significantly reduced. The third frame in both sequences shows the LED on and fluorescence within the cuvette.

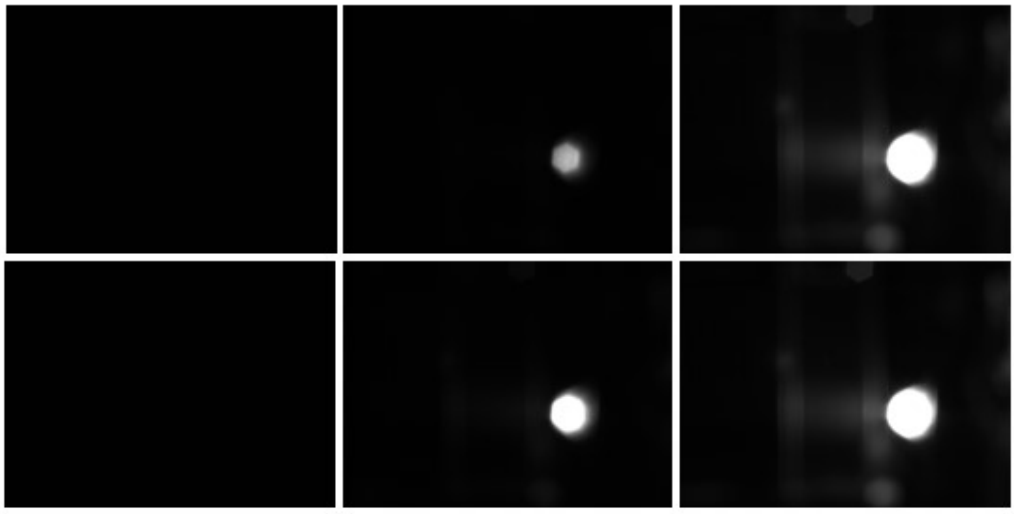

Figure 4.31: Images in sequence captured in buffered mode at an exposure time of 4855µs

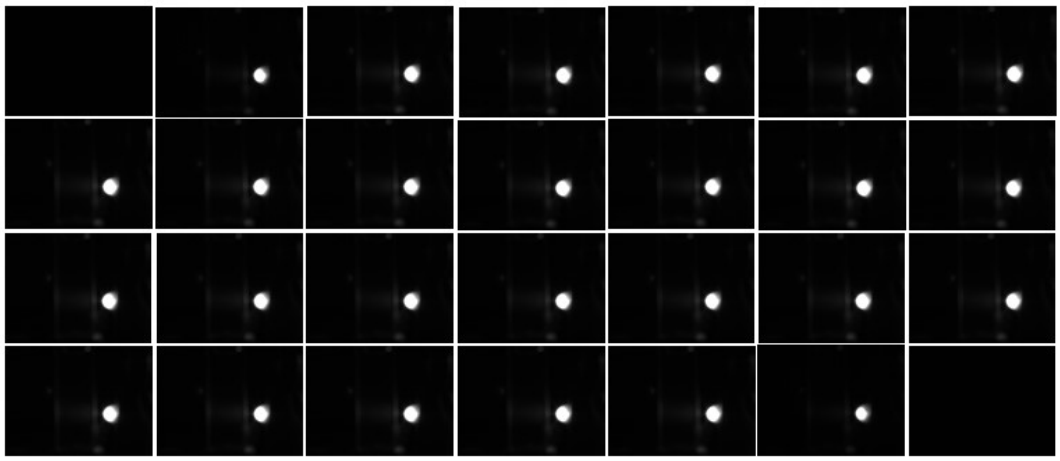

Figure 4.32: Images in sequence captured in buffered mode at an exposure time of 4855µs

The above Figure 4.32 presents a complete pulse width of 100ms, fluorescence within the cuvette is visible across all frames with LED on. In the second frame we see that the LED pulse begins during capture as the intensity of the LED in this frame is less than it is in the subsequent frames.

With regards to time-controlled pulsing, see Table 4.20, Figure 4.27, Figure 4.28, Figure 4.29, Figure 4.30, Figure 4.31 and Figure 4.32. This experiment yielded thousands of image sequences however not one was quick enough to capture any residual

fluorescence with LED off. Images presented related to this experiment show images captured in sequence whereby the LED is on, in a phase between on and off and then fully off in frame three of three. This accounts for the length of exposure time, frame two of three covers a time period whereby the LED is on for a fraction of the frame and off for a fraction of the frame. The combined effect shows the dome of the LED with a “halfway” illumination.

A GPIO trigger was connected between the LED controller and the camera in order to synchronise data collection. The lowest framerate possible at 4855µs was selected so that once the LED channel is set low, the camera channel is set high and an image is captured. No combination of testing conditions has resulted in any detectable fluorescence in the frame captured as soon as the excitation is switched off. This confirms that the ICG:HSA solutions on test do not have a lasting fluorescence decay that is detectable at frame rates of 199.98Hz or lower. There is no present residual “glow effect” following excitation and therefore the fluorescent marker cannot be exploited by imaging it using a pulsed source and a corresponding negatively pulsed detector at a rate of 200Hz or lower. This could have had a significant impact on patient safety during endoscopic diagnostics and therapy if viable. Literature indicates that femtosecond and picosecond pulse rates are appropriate for capturing ICG decay however, this system is limited by the human eye in regards to visible residual fluorescence. The cost of a high-speed camera system for fluorescence endoscopy would be exponentially higher than the proposed design and would not hold any value in real-world applications. If the fluorescence decay could have been detected via a camera capturing at millisecond speeds, then this would allow surgeons to visualize fluorescent material (diseased tissue) during endoscopic procedures in real-time.

Results obtained from experiment 3 tell us that it is not possible to collect residual fluorescence with the current detection method and pulsing protocol, this is in agreeance with values found in literature. The results cannot tell us that this is transferable to real-word applications as we know that a femtosecond or picosecond decay rate will not be

useful to the real-world application. A quicker pulsing procedure should be tested to confirm if there is any chance to observe residual fluorescence at the frame rate limit of the human eye or not. If the residual fluorescence or decaying signal cannot be observed at millisecond pulse rates then the properties of the fluorophore cannot be exploited as proposed. This research confirms that at an exposure time equivalent to 200Hz, there is no detectable residual fluorescence when a sample containing ICG in solution is excited at 780nm. If any residual fluorescence existed, then this could have a significant impact on medical imaging techniques such as minimally invasive fluorescence endoscopy as it would allow for a pulsed excitation. Pulsing the excitation would reduce the total time whereby the source is emitting, thus reducing the energy that the patient is exposed to during the procedure. Currently at least one NIR channel is mixed with a white light channel with both remaining on throughout the surgery. The risk of damage through excess heat is significantly higher when the channels remain on. Should there be any residual fluorescence in the moments following the excitation off, $\Delta K=0$ then a faster exposure time should be used to detect its presence, $\Delta T=0$ and $\Delta S<4855\mu s$.

4.6 Conclusion

Results presented in this research indicate that it is possible to image fluorescence and non-fluorescing landmarks within the field using the proposed setup without the need for filters. The experiments verify that fluorescence, generated from excitation of ICG in a solution, degrades with time during exposure to light at the excitation wavelength. The changes in fluorescence intensity observed during this study do not indicate a proportional relationship between concentration of ICG in solution and degradation of fluorescence. Data collected indicates that there are most likely secondary mechanisms occurring at a molecular level within the solution that has an effect on absorption and consequently on fluorescence.

The results show that there is a relationship between the rate of degradation of fluorescence and the optical power of the excitation source but again, this is not proportional. In general, as expected, the higher the optical power of the excitation, the quicker the rate of degradation of fluorescence. It is important to note that fluorescence degradation observed in this research was very small and likely undetectable to the human eye. Temperature inside the cuvette was recorded for each excitation source. The LED recorded a temperature increase 50% higher than the 10mW LASER and 80% higher than the 5mW LASER however, this data does not suggest any proportional relationship with fluorescence decay. The thermal differences observed are likely to impact on changes in the solution at a molecular level which contributes to the overall effect of photodegradation. According to the experimental findings, after a period of 10 minutes there will a detectable difference in fluorescence intensity however, this difference is not significant and may not even be detectable to the naked eye.

Results from this experimental work verify that exposing a solution containing ICG to a 780nm excitation source generates detectable fluorescence that cannot be seen by the naked eye. Over time, a reduction in fluorescence intensity is observed and this can be detected using either a power meter or an off-the-shelf CMOS camera. The camera used recorded a quantum efficiency of less than 30% at NIR wavelengths however, both fluorescent and non-fluorescent regions could be detected with good contrast. This refers to the ICG sample within the cuvette and the non-fluorescing background within the frame respectively. For liquid samples, the experimental setup is able to confirm the presence of ICG without the need for filters.

LASER excitation delivered to the sample is coherent and wavelength specific so there is little need to use filters, this is especially relevant given that excitation is within the visible range yet the fluorescence is not. Additionally, there is also little need for focusing optics which can result in costly design, manufacturing and maintenance of equipment. Furthermore, cost of the LASER diode used for this research was significantly less than the LEDs of comparable wavelength and power.

Results and Discussion

The most important finding of this experimental research is that light at 780nm can be used to image ICG stained samples without the need for a secondary, designated white light channel. At 780nm, the ICG samples emit fluorescence that was detectable by camera at around 815nm. The 780nm excitation was detectable by both the human eye and camera therefore, if there is a region of intensity visible within the camera frame that cannot be seen with the naked eye, we can confidently say that this is fluorescence. If a region of the camera frame shows pixels with high intensity values where a bright region can also be seen with the naked eye, for example, reflection from the source – then we can confidently say that this is not fluorescence.

Using only the 780nm channel, it is possible to view the fluorescent and non-fluorescent content within the frame. While the frame would not be viewed in optimal conditions, using a setup similar to this experimental analysis, the patient would be subject to just one excitation source therefore reducing the risk of thermal damage by 50% by eliminating a secondary source.

The camera used during this data collection was a monochrome camera and this was selected in preference to the colour alternative due to the quantum efficiency curve at NIR wavelengths. Almost all of the example images presented show the grayscale image of the setup whereby the fluorescence and rest of frame are visible, the fluorescence is saturating the frame however, a higher frame rate would reduce this saturation and allow a more precise boundary of fluorescence. A frame rate of 120Hz was acceptable in terms of contrast and detection of non-fluorescent landmarks within the frame.

With regards to experimental parameters, the 400µMol solution provided the highest fluorescence intensity and comprised the lowest quantity of fluorophore therefore making it cheaper when compared to the remaining concentrations, this is supported in literature and was expected. The differences between illumination source were inconclusive, when considering optical power, beam properties, thermal effects, lack of fair testing conditions with respect to cooled mounts, cost and ease of use, it is difficult to determine if LED was

superior to LASER or vice versa. The LASER was far easier to control and resulted in better images as we can be sure that no source wavelengths are present in the images, the same does not hold true for the LED which would require filtering to verify.

The findings presented within this work do not provide adequate explanation as to why there are a very few endoscopy illumination systems utilising LASER. A LASER based system would yield a higher efficiency and due to the properties of the beam, would be a suitable alternative to LED however, the LED circuit is simple and was easy to adapt for pulsing. Overall, it is fair to conclude that during this project, there was no profound differences between the two sources.

4.7 Future Work

A small study was conducted to include within this section. In the real-world application, the sample would not be translucent and contained within a glass cuvette. It is important to understand the effect of replicating real-world conditions in order to determine how transferable these results are. In the real-world application, the presence of ICG would indicate diseased tissue. We have seen in literature that the surfaces of tissue are highly reflective and it is likely that without the use of a filter, the scatter direct from the NIR illumination would be saturating and could result in false positives.

To best replicate the real-world application, a solution of 500μMol ICG:HSA will be pipetted onto a cotton swab until the swab is visibly saturated. A small plastic plate will be used to protect the equipment from any leakage underneath the swab. As the cuvettes from experiments 1 and 2 are highly polished, the proposed swab setup will avoid excessive reflection and should result in a more realistic approach to imaging. Figure 4.33 shows the LASER setup whereby the cuvette is swapped for a cotton swab which has been saturated with ICG:HSA solution. A swab soaked in water is used as a control.

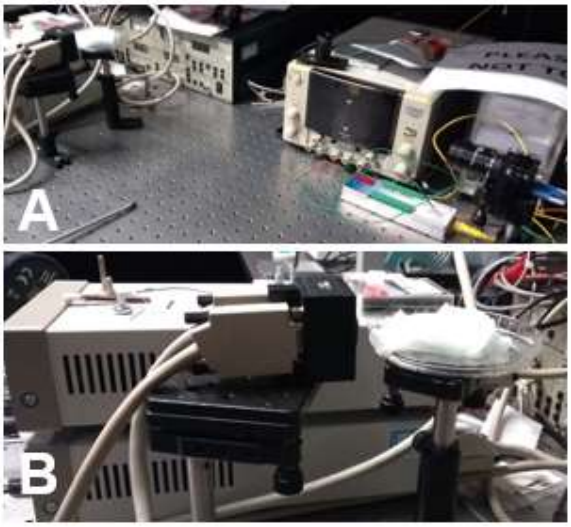

Figure 4.33: A photograph to show the setup for imaging an ICG:HSA saturated swab with LASER illumination showing the complete setup (A) and detail of the LASER mount and sample (B)

From images collected using soaked swabs there was no distinguishable difference in intensity between ICG:HSA swabs and water swabs. Only the use of a filter would be able to confirm the presence of fluorescence. The reason for this is due to the scattering effect of the cotton material. The swabs are imaged under two conditions, ambient lighting on and excitation off, ambient lighting off and excitation on so as to compare the shape and complexity of the swabs. Figure 4.34 and Figure 4.35 show images collected whereby fluorescence cannot be verified. In Figure 4.34 we can see that there is significant scatter which is more intense nearest to the source, without filters we cannot verify that this is fluorescence although we could assume that the intensity is a combination of excitation (majority) and fluorescence (minority). Figure 4.35 shows two repetitions of an experiment whereby the cuvettes are swapped out and imaged, again without a filter in position we cannot assume that there is significant fluorescence imaged. When looking at this experiment during testing, red illumination is observed due to scattering at the surface. We know that the emission wavelength is not visible with the naked eye and so we cannot assume that there is no fluorescence present. It is interesting to note that the water-soaked swab appears to show a significantly higher

intensity than the ICG:HSA which verifies that the main component of this intensity is scatter from the source, this could result in false positives without verification via filter.

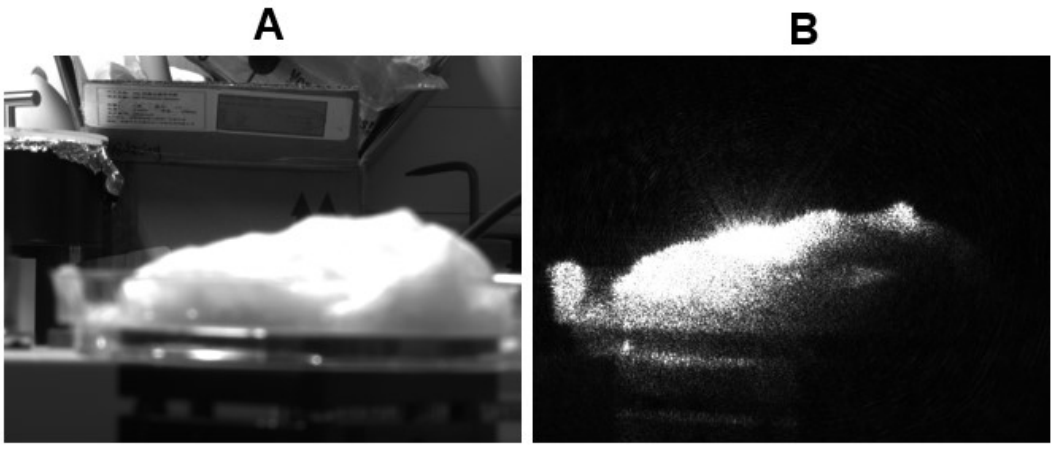

Figure 4.34: Images of an ICG:HSA soaked swab under ambient (A) and NIR (B) illumination. Exposure time is 1 second.

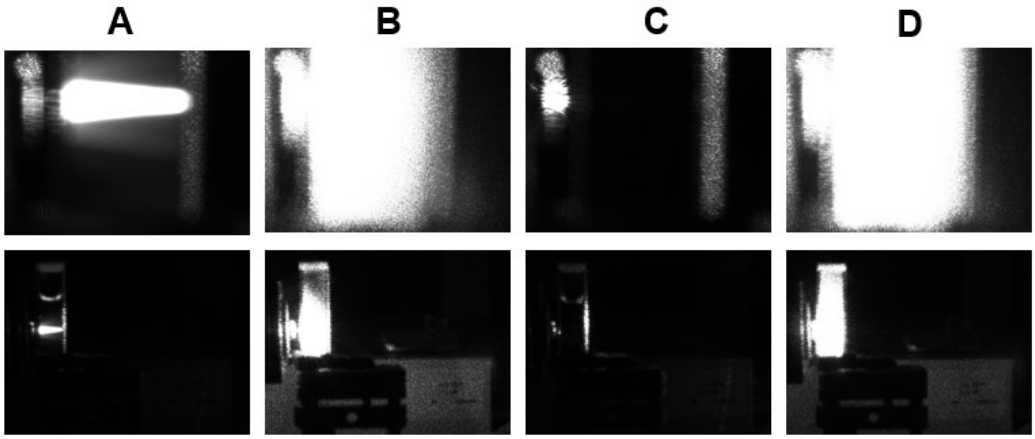

Figure 4.35: Images of cuvettes filled with ICG:HSA solution (A), ICG:HSA soaked swab (B), water (C) and a water soaked swab (D) under 10mW LASER excitation. Exposure time is 1 second and the experiment is repeated along the second row.

Future work should consider the use of the colour camera to see if this can improve on clarity and enable better distinguishing between fluorescing material and reflecting (815nm and 780nm). A filter should be used to verify results presented in this project in order to confirm if the use of filters within final equipment design is essential. Use of the LED and LASER illumination options should be tested with connection to an LLG to assess the differences in output and efficiency of the two systems.

5 Conclusion and Future Prospects

This chapter will conclude the thesis by confirming the contributions to the field and how the research aims and objectives have been fulfilled. Findings will be related back to relevant studies where appropriate.

This thesis showcases a future work component of a prototyped endoscopy illumination source, for a novel cancer detection method established at Imperial College London. A brief introduction of all relevant topics is introduced together with a literature review highlighting the advantages and disadvantages of modern endoscopic imaging systems. With three separate experiments, the viability of a single camera, single channel, simplified illumination system is investigated. Gaps in knowledge identified in the earlier thesis chapters are incorporated into the scope of experimental design in order to contribute information which is both useful and relevant to the field. The results are discussed to assess if research objectives have been satisfied and if there are any contributions to knowledge. A summary of the contributions to knowledge can be found in Table 5.1 which will conclude the chapter.

- A test unit comprising an NIR LED and NIR LASER was designed and produced within the lab.
- Images were collected without filters to show a sample containing aqueous ICG and frame background under NIR illumination. The illumination wavelength is visible and so the ICG in solution fluoresces while non-fluorescing background landmarks remain visible. The contrast observed between the fluorescence and background is very high with the fluorescence often saturating the detector however, contrast between objects in the background remains high enough to clearly identify items comprising the non-fluorescing regions of the frame. For example, fluorescence within the cuvette appears as a very bright region of the frame as does the illumination source and any direct reflections however, the

equipment in the background including mounts, power supply etc. are also distinguished in the frame.

- A contribution is made regarding the importance of filtering when imaging solutions containing ICG. As the solutions tested were aqueous, the fact that filters were not utilised did not compromise on image quality due to the detection differences between the camera and human eye. All existing, commercially available systems use filtering and filters are an important verification tool, this research has proven that filters enhance image quality especially when considering the application and the high reflectivity of surfaces in vivo.
- The NIR illumination and detector are sequenced with the aim of detecting the decaying signal, the quickest possible frame rate was 200Hz which is confirmed to be too slow to detect any fluorescence decay. Literature values are found to offer conflicting statements with regards to fluorescence decay and it is important to acknowledge that the research stating decay rates in the region of picosecond and femtosecond do not specify if ICG is bound to HSA in a 1:1 molar ratio which is known to enhance fluorescence intensity and stability. The femtosecond research suspended ICG in solutions of water, milk and 1% intralipid (Gerega et al., 2011) and the picosecond research suspended ICG in solution of water, milk and blood but did not indicate the molar ratio (Homulle et al., 2016) in fact this study reported that the most stable lifetimes occurred in the water-based solutions which the relevant literature generally disagrees with. In general, a significantly quicker frame rate is unlikely to capture the decaying signal or make any substantial difference in image quality due to the limitations of the human eye response.
- A decay in fluorescence is observed over time and presented as a contribution to existing knowledge. The results show that a combination of ICG concentration, temperature and illumination power impact on fluorescence intensity over time. The combined effect of these three parameters appears to cause a significant

impact and a longer time on test is proposed to determine if one parameter is more effective than another. Photobleaching could not be confirmed in the allocated time on test.

- Images are analysed in a custom LabVIEW programme. The camera specifications are comparable to that used at ICL during their testing with the Cymtec light source and so quality of images collected is comparable. A pulsed system hypothetically would enhance patient safety and would not compromise on image quality however, due to a pulse limit of 200Hz, this could not be verified in practice.
- There was no significant difference between using LED or LASER, each had its own advantages and disadvantages during experimental procedures however, there appears to be no reason for the very limited number of systems using LASER only and it is proposed that LASER be considered as an alternative to LEDs and Xenon bulb technology. Images collected using the LASER illumination were preferable to LED as there was virtually no source detectable in images either direct or from reflection thus enhancing image quality.
- It is confirmed that a simplified setup is sufficient for imaging aqueous ICG samples under lab conditions.

The aims and objectives were addressed through experimental findings. Experiment parameters were set in accordance with literature and two systems were created, one comprising an LED and the other, a LASER diode. Data obtained from the experiments was analysed and compiled to answer the research questions. The three experiments were designed to each investigate one principal question.

From this experimental work, the optical properties of ICG in solution are investigated using an excitation wavelength of 780nm. Apparatus, including a single monochrome CMOS camera and LED controller, are assembled for synchronised data collection whereby aqueous solutions of ICG:HSA are exposed to controlled pulses of excitation

wavelength. The main objective is to understand more about the optical properties of ICG in solution with the aim to exploit these properties and enhance its usage.

With the safety surrounding fluorescence endoscopy as the motivation for this work, significantly reducing energy exposure through pulsing of the NIR channel would result in an improvement in patient wellbeing. This experiment has confirmed that there is no detectable fluorescence post-excitation-pulse at frame rates of 200Hz and lower with a slight delay in signal generation (0.1ms). This indicates that in order to detect fluorescence at a frame rate of 200Hz, the source must always be present and subsequently filtered out of the frame. This research shows that at 780nm, both fluorescent and non-fluorescent regions of the frame can be detected using a single CMOS camera. This may be of benefit in future work as the excitation wavelength is visible to the naked eye but the fluorescence is not. If a region of high intensity is visible through the camera lens but not by eye then we can assume that this is fluorescence. This is a very simple and effective way to determine if there is ICG present within a sample.

With regards to photostability of ICG in solution, a variety of parameters and conditions have been investigated to demonstrate that there is no one parameter that proportionally affects the very small decrease in fluorescence intensity observed. Instead, it is likely that a combination of parameters influence the rate of fluorescence decay and some of which, should be considered for their impact at a molecular level.

From this experimental work, LASER as an excitation source performed better than LED when used to excite the fluorescent marker ICG at 780nm however, this was only circumstantial due to the mount of the LASER removing any direct imaging of the diode and the reduction in reflection when compared to the LED. A single monochrome camera as the sole detector is a viable option and could be used for sub-optimal imaging allowing for a significant reduction in patient exposure to energy that can be harmful. The monochrome camera was selected for its higher quantum efficiency at the wavelength

range of interest when compared to the colour alternative however, a colour camera would offer higher quality imaging of background non-fluorescing regions of the frame.

As patient safety is a priority, the benefits of reducing energy exposure should be considered along with the harm that removing a white light channel would cause with the proposed system as future work. If the objective is to detect the presence of diseased (ICG stained) tissue and give a good indication of its size and location then a simpler single channel system may be sufficient and significantly reduce the risk of thermal damage to healthy surrounding tissue.

A variety of parameters and conditions have been investigated and the findings presented to demonstrate the similarities and differences between the current illumination techniques and how these are detected using a single monochromatic camera. The main objective is to enhance patient safety during minimally invasive procedures while maintaining high quality, real-time images with clear contrast between fluorescence and background without compromising on contrast amongst the background of the frame which is typically much darker.

This research is valuable to manufacturers of endoscopy illumination systems. The potential that using an NIR LASER with a single high pass filter and single camera could significantly disrupt the existing market. With a focus on patient safety as a priority for medical device manufacturers, this proposed design could not only reduce the risk of thermal damage to healthy tissue but could also significantly reduce the cost and complexity of the overall design. For example, the custom optics comprised within the Cymtec light source are expensive and require coatings and additional processing, use of a LASER in place of the LEDs would result in a lower cost, higher efficiency system. The results imply that a high pass filer would be required for use in-vivo. This would filter the excitation wavelengths leaving only the emission wavelengths, to confirm the presence of fluorescence within the frame. Although a monochrome camera was used, this research has verified that landmarks within the frame are visible at this wavelength

range. Emission wavelengths were not visible with the naked eye but were detected on camera with excellent contrast. A single camera such as that used within this study was sufficient to capture the entirety of the frame. The frame rate was limited due to hardware limitations however this camera has a specification similar to that used in the study at Imperial College London. When compared to existing, commercially available systems, use of a single camera could significantly impact on the final cost as many reviewed required 2 or 3 individual cameras each with their own filter set. This study has verified that a single camera setup does not significantly impact on image quality and removes the requirement for image merging which we have observed to negatively impact on image quality.

This study contributes to the field of fluorophore imaging as well as the endoscopy manufacturing sector. Suggestions proposed for a change in illumination system and single camera imaging would not have been relevant without imaging the fluorophore under lab conditions. The setup allowed for an optical analysis of the fluorophore ICG, to determine whether any of its optical properties could be exploited in order to enhance its usage for this application. The research presents a simplified system which is capable of producing images that match the quality of existing systems. The overall output is significantly reduced as a single 780nm channel can be used alone and this illumination source can be LASER. The pulsed experiments confirm that at an acquisition rate of 200Hz, there is no detectable fluorescence decay. This indicates that a filter is required to remove the excitation wavelengths so as to isolate fluorescent regions of the frame. Many transferable skills have been acquired during this project from sourcing components and building the setup from scratch, to designing the image analysis programme and applying knowledge acquired throughout the process regarding very large datasets including, how to extract the specific information of interest and how best to present this.

This study did not include testing on any biological tissue and so there are exisiting limitations as the application is minimally invasive removal of cancerous tissue in the

breast. The use of filters would be essential in the real application however, to image fluorescence with an aqueous solution of ICG:HSA under LASER illumination does not require filtering. Due to the reflection and scatter from biological surfaces, there is an understanding that a filter would be required to remove this unwanted signal. The framerate limited by hardware was another restriction of this study, both the LED controller and computer processor contributed to this limitation. The future work component found in the results and discussion chapter highlights the impact that a change in the physical state of the sample holds. The aqueous solutions are swapped for cotton swabs, images collected represent a high percentage of scattered excitation combined with a small percent of fluorescence which without a filter is indistinguishable. The filter selected should be precise in order to retain as much intensity from fluorescence wavelengths as possible and reduce the risk of false positives and false negatives.

Further research should be conducted on biological tissue to better simulate the application. The team at ICL imaged cancerous tissue which had been bathed in ICG solution as the Cymtec system had not been granted approval for human clinical trials (Qi et al., 2017). Use of the low power LASER should be used in comparison to LED to determine if there is any localised temperature change within the tissue following a long exposure. Use of a filter should be used to determine the success ratio of visualising fluorescence in samples with high scatter and reflection. Further programming to the LabVIEW ROI intensity programme could determine the parameters of the fluorescence through a boundary analysis to indicate the size of tissue removal to surgeons at the earliest convenience.

As a single camera setup has proven successful, filtered and unfiltered signal could be combined in real-time to enhance image quality. With a single camera there will be no risk of error applying the merged images or pseudocolor as we have seen in the literature. A colour camera could be tested in future, the quantum efficiency of the colour version of this camera at the NIR wavelength range was significantly lower hence the

reason for selecting the monochrome. A colour camera would improve image quality and help surgeons better identify landmarks within the frame. Project budget allowed for the purchase of only one camera therefore this was not tested however, the ICL camera was also monochrome for the detection of fluorescence only. In general, further research should focus on recreating an environment similar to the real world application to enhance relevance and to determine feasibility for commercialising a system such as that proposed here. A commitment to enhancing the functionality of the LabVIEW to accompany the system would also be very valuable moving forward and could have potential to incorporate artificial intelligence into endoscopic procedures such as this.

The work presented in this thesis has contributed to knowledge of the fluorophore ICG and fluorescence imaging. It holds value for any medical device manufacturer who is willing to collaborate with a team such as ICL to improve on patient outcomes, accessibility and affordability of systems and ultimately, to disrupt the market. Through commitment to improving patient safety we have potentially revealed a more efficient and cost-effective system design, which could have a significant impact on the future of endoscopy and fluorescence endoscopy.

Table 5.1: Summary of contributions to knowledge

Theoretical Contributions
The sample preparation techniques taken from literature are transferable and accurate in preparing ICG:HSA samples for imaging studies.
Results presented regarding optimal concentration of ICG in solution enhances and supports existing literature. The lowest concentration of ICG on test yielded the highest fluorescence intensity, this could result in minimising waste of solution which would reduce the overall cost of usage.

A frame rate of 200Hz is not sufficient to capture the decaying fluorescent signal in aqueous solutions. Due to the limited response of the human eye, the fluorescent decay cannot be imaged in real-time. For this application, the concept of imaging the decaying signal is not viable.
A decrease in fluorophore intensity is detectable over a short period of time. A relationship exists between the rate of change in intensity and the combination of fluorophore concentration, temperature and illumination power.
When imaging aqueous solutions, with the intention of confirming the presence of ICG, LASER is the preferred illumination source due to its beam properties. The beam is not detected on camera, with the camera positioned perpendicular to the source, therefore virtually no excitation is present in images.
When imaging aqueous solutions, with the intention of confirming the presence of ICG, a high pass filter is required if using an LED illumination source. Excitation light is present in images due to the divergence of the beam and will need to be removed to confirm presence of fluorescence.
The LabVIEW programme was adequate to analyse the intensity of pixels within the prescribed region and proved to be a simple and effective tool for processing data sequences.
The risk of excessive heat exposure during endoscopic procedures is investigated in this research. Over a 10-minute period, the local temperature increase at the sample was not significant and the discrepancies in temperatures measured for each illumination condition have been accounted for. For investigative procedures lasting 10 minutes or less, this risk of thermal damage is virtually zero.

Practical Contributions
A single monochrome camera is sufficient to capture all landmarks within the field of view including bright (fluorescing) regions and dim (non-fluorescing) regions of the frame. If contrast could be enhanced through selection of a colour camera, there is no reason to incorporate multiple cameras into system design. The literature shows that the multi-image combination protocols are risky and can alter the complexity of the bright regions of the image, which are arguably the most important regions. A single camera maintains positioning and complexity of all landmarks within the frame and offers a significant reduction in system cost and complexity.
A simplified system comprising a single monochrome camera and LASER is sufficient to determine the presence of ICG in aqueous solutions when the excitation wavelength is 780nm. This is due to the visibility differences between the excitation and fluorescence when looking at the sample with the naked eye. The camera detects both the excitation and fluorescence therefore, if a bright region is visible on screen but not by eye, we can confirm the presence of ICG within the solution. This makes for a very inexpensive and simple detection system and could be suitable for applications such as lab screening of human tissue samples.
A filter is not an essential component when confirming the presence of ICG in aqueous samples excited with 780nm LASER illumination.
Both LED and LASER are suitable components for an illumination system used in fluorescence endoscopy. A comparison between the two sources confirms no significant differences for this application. There appears to be no reason for the very small number of LASER based systems in the current market for endoscopy products.
A high pass filter is required to image ICG in vivo, this will remove scattered excitation light and confirm the precise location and size of the fluorescing region. An illumination system for endoscopy should incorporate a filter to remove the excitation wavelength.

780nm is suitable to illuminate a field of view and is visible to the naked eye. If imaging ICG during lab-based experiments, a second white light channel is not essential to illuminate the remainder of the field.
As aqueous samples are not comparable to ICG stained tissue, the experimental setup as a concept requires modification for solid samples with the addition of a filter to remove excitation wavelengths. The solid samples imaged are illuminated successfully however, the detector cannot distinguish between excitation and emission wavelengths. This small and simple lab setup could be suitable for lab screening of human tissue samples (biopsy) with the addition of a filter component.
The methodology described, contributes to research and development for any manufacturers aiming to setup a simple and inexpensive testing protocol for prototype endoscopy systems. The combination of measuring instruments gives a thorough analysis of fluorescence intensity and optimal illumination conditions.

6 List of Publications

Qi, J., Nabavi, E., Hu, Y., Rees-Whippey, D., Curtis, A., Price, C., Copner, N., Sanassy, C., Leiloglou, M., Leff, D., Hanna, G. and Elson, D. (2017) A light-weight near infrared fluorescence endoscope based on a single color camera: a proof-of-concept study. 2017 Conference on Lasers and Electro-Optics Pacific Rim (CLEO-PR) 31 July-4 Aug. 2017 DOI: 10.1109/CLEOPR.2017.8119082

Curtis, A., Li, K., Roula, M.A. and Copner, N. Combined Fluorescence and Bright Field Imaging via a Single CMOS Detector Without Filters to Improve on Patient Safety during Endoscopic Procedures – An Experimental Study Analysing the Output of both LASER and LED Near Infrared Sources on In Vitro Samples. Journal of Biomedical Photonics & Engineering, [S.l.], v. 6, n. 4, p. 040303, Dec. 2020. ISSN 2411-2844. doi:10.18287/JBPE20.06.040303.

Curtis, A., Li, K., Roula, M.A. and Copner, N. The Optical Properties of Indocyanine Green suspended in Solution as Observed under Near Infrared LED and LASER Light Conditions. International Journal of Science and Engineering Applications Volume 10-Issue 05, 80 - 89, 2021, ISSN:- 2319 – 7560. doi:10.7753/IJSEA1005.1005

7 References

Abo, T., Nanashima, A., Tobinaga, S., Hidaka, S., Taura, N., Takagi, K., Arai, J., Miyaaki, H., Shibata, H. and Nagayasu, T. (2015) Usefulness of intraoperative diagnosis of hepatic tumours located at the liver surface and hepatic segmental visualization using indocyanine green-photodynamic eye imaging. European Journal of Surgical Oncology. Volume 41, Issue 2, February 2015, Pages 257-264

Ai, F., Ju, Q., Chen, X., Wang, F. and Zhu, G. (2015) A core-shell-shell nanoplatform upconverting near-infrared light at 808nm for luminescence imaging and photodynamic therapy of cancer. Nature Scientific Reports 2015;5: 10785

Ai, Z., Ho, C.J.H., Aw, J., Attia, A.B.E.A., Mu, J., Wang, Y., Wang, X., Wang, Y., Liu, X., Chen, H., Gao, M., Chen, X., Yeow, E.K.L., Liu, G., Olivio, M. and Xing, B. (2016) In vivo covalent cross-linking of photon-converted rare-earth nanostructures for tumour localization and theranostics. Nature Communications 2016 Jan 20;7:10432

Akorn Inc. (2009) See what you're missing with IC.Green (Indocyanine Green for injection, USP) P259 Rev10/09.

Alander, J.T., Kaartinen, I., Laakso, A., Pätilä, T., Spillmann, T., Tuchin, V.V., Venermo, M. and Välisuo, P. (2012) A Review of Indocyanine Green Fluorescent Imaging in Surgery. International Journal of Biomedical Imaging Volume 2012;2012:940585.

Alander, J.T. (2013) ClinICGA = Finnish Indocyanine Green Imaging Development Group - A consortium to promote and develop indocyanine green imaging for clinical applications. Presentation slides available at lipas.uwasa.fi/~TAU/memos/ClinICGA/Slides/slides.php?Page=-1

Allied Vision Manta G-158 Data Sheet GigE "Vision camera featuring the Sony IMX273 CMOS sensor" version 1.3.3

Andersen BB, Gundersen HJ, Pakkenberg B. Aging of the human cerebellum: a stereological study. J Comp Neurol. 2003 Nov 17 466(3):356-65

References

Asche, F (2017) Modern CMOS Sensors and Their Use in Fluorescence-Based Applications. White Paper published by BASLER AG. November 2017

Benson, R.C. and Kues, H.A. (1979) Fluorescence Properties of Indocyanine Green as Related to Angiography. Physics in Medicine & Biology 1978 Jan;23(1):159-63

Binns, C (2009) Cut-by-Color Surgery. Popular Science article iD: 2009-06

Boddington, S., Sutton, E., Jones, E., Purcell, D., Henning, T., Tavri, S., Meier, R., Sista, A., Fu, Y. and Daldrup-Link, H. (2008) Improved fluorescence of indocyanine green in vitro and in vivo after simple cooling procedures. Contrast Media & Molecular Imaging 2008, 3, 191-197

Bohil AB, Robertson BW, Cheney RE. Myosin-X is a molecular motor that functions in filopodia formation. PNAS 2006. 103(33): pp. 12411-12416

Bozkurt, A. and Onaral, B. (2004) Safety assessment of near infrared light emitting diodes for diffuse optical measurements. Biomedical Engineering Online 2004, 3:9

Bragg, W. (1921) Electrons and Ether Waves. The Twenty-Third Robert Boyle Lecture. May 11th, 1921. Oxford University Junior Scientific Club

Crane, L.M.A., Themelis, G., Pleijhuis, R.G., Harlaar, N.J., Sarantopoulos, A., Arts, H.J.G., van der Zee, A.G.J., Ntziachristos, V. and van Dam, G.M. (2011) Intraoperative Multispectral Fluorescence Imaging for the Detection of the Sentinel Lymph Node in Cervical Cancer: A Novel Concept. Molecular Imaging Biology 2011 October 13(5) 1043-1049

Crull, J.W. and Schafer, S.A. (1996) Indocyanine Green Degradation During High-Intensity Laser Irradiation. SPIE 2671, Lasers in surgery: Advanced Characterization, Therapeutics, and Systems VI, (17 May 1996)

Ellison, Sarah (2015) “The Historical Evolution of Endoscopy” Honors Theses Paper 2571 Lee Honors College at Scholar Works at WMU

References

Envemeka, Chukuka. S (2001) Attenuation and penetration of visible 632.8 nm and invisible infra-red 904nm light in soft tissues. LASER Therapy Volume 13, 95-101

Frangioni, J. (2008) New Technologies for Human Cancer Imaging. American Society of Clinical Oncology. August 2008 Volume 26 Number 24

Frank AO, Chuong CJ, Johnson RL. A finite-element model of oxygen diffusion in the pulmonary capillaries. J Appl Physiol. 1997 Jun82(6):2036-44. p.2037

Fujiwara, M., Mizukami, T., Suzuki, A. and Fukamizu, H. (2009) Sentinel lymph node detection in skin cancer patients using real-time fluorescence navigation with indocyanine green: preliminary experience. Journal of Plastic, Reconstructive & Aesthetic Surgery Volume 62 Issue 10 pp373-378

Furukawa, N., Oi, H. Yoshida, S., Shigetomi, S., Kanayama, S. and Kobayashi, H. (2010) The Usefulness of the Photodynamic Eye for Sentinel Lymph Node Identification in Patients with Cervical Cancer. Tumori Journal Vol. 96, Issue 6, 2010 pp936-940

Geddes, C., Parfenov, A., Roll, D., Uddin, J. and Lakowicz, J. (2003) Fluorescence Spectral Properties of Indocyanine Green on a Roughened Platinum Electrode: Metal Enhanced Fluorescence. Journal of Fluorescence 2003 November; 13(6): 453-457

Gerega, A., Zolek, N., Soltysinski, T., Milej, D., Sawosz, P., Toczylowska, B. and Liebert, A. (2011) Wavelength-resolved measurements of fluorescence lifetime of indocyanine green," J. Biomed. Opt. 16(6), 067,010 (2011)

Gibbs S.L. (2012) Near infrared fluorescence for image-guided surgery. Quantitative Imaging in Medical Surgery 2012 Sep; 2(3): 177–187

Gilson S.A.S (2019) PIPETMAN Classic Specifications LT801627_A

Gioux, S., Choi, H. and Frangioni, J. (2010) Image-Guided Surgery using Invisible Near-Infrared Light: Fundamentals of Clinical Translation. Molecular Imaging 2010 October; 9(5): 237-255

References

Hachey, K., Gilmore, D., Armstrong, K., Harris, S., Hornick, J., Colson, Y. and Wee, J. (2016) Safety and Feasability of Near Infrared Image-Guided Lymphatic Mapping of Regional Lymph Nodes in ESophogeal Cancer. Journal of Thoracic Cardiovascular Surgery. 2016 August; 152(2): 546-554

Haj-Hosseini, N., Behm, P., Shabo, I. and Wårdell, K. (2014) Fluorescence spectroscopy using indocyanine green for lymph node mapping. Proceedings of SPIE, the international Society for Optical Engineering, (8935), 893504, 1-6

Hamamatsu.com

Handa, T., Katare, R.G., Nishimori, H., Wariishi, S., Fukutomi, T., Yamamoto, M., Sasaguri, S. and Sato, T. (2010) New device for intraoperative graft assessment: HyperEye charge-coupled device camera system. General Thoracic Cardiovascular surgery 2010 Feb 58(2) 68-77

Hirano, A., Kamimura, M., Ogura, K., Kim, N., Hattori, A., Setoguchi, Y., Okubo, F., Inoue, H., Miyamoto, R., Kinoshita, J., Fujibayashi, M. and Shimzu, T. (2012) A Comparison of Indocyanine Green Fluorescence Imaging Plus Blue Dye and Blue Dye Alone For Sentinel Node Navigation Surgery in Breast Cancer Patients. Annals of Surgical Oncology. 19, pages4112–4116(2012)

Homulle, H. A. R., Powolny, F., Stegehuis, P. L., Dijkstra, J., Li, D.U-., Homicsko, K., Rimoldi, D., Muehlethaler, K., Prior, J. O., Sinisi, R., Dubikovskaya, E., Charbon , E. and Bruschini, C. (2016) Compact solid-state CMOS single-photon detector array for in vivo NIR fluorescence lifetime oncology measurements. Biomedical Optics Express, 7(5), 1797-1814, 2016

Hutteman, M., Mieog, J., van der Voost, J., Liefers, G., Putter, H., Löwik, C., Frangioni, J., van de Velde, C. and Vahrmeijer, A. (2011). Randomized, double-blind comparison of indocyanine green with or without albumin premixing for near-infrared fluorescence imaging of sentinel lymph nodes in breast cancer patients. Breast Cancer Research and Treatment. 2011 May; 127(1): 163-170

References

ICNIRP Guidelines (2013) Guidelines on Limits of Exposure to Incoherent Visible and Infrared Radiation. Published in Health Physics 105(1):74-96;2013

Ito, S., Muguruma, N., Kimura, T., Yano, H., Imoto, Y., Okamoto, K., Kaji, M., Sano, S. and Nagao, Y. (2006). Principle and clinical usefulness of the infrared fluorescence endoscopy. The Journal of Medical Investigation. Vol. 53 2006

Jain, A., Bansal, R., Kumar, A, and Singh, K.D. (2015) A comparative study of visual and auditory reaction times on the basis of gender and physical activity levels of medical first year students. International Journal of Applied and Basic Medical Research 2015 May-Aug; 5(2): 124–127

Jonak, C., Skvara, H., Kunstfeld, R., Trautinger, F. and Schmid, J. A. (2011) Intradermal Indocyanine Green for In Vivo Fluorescence Laser Scanning Microscopy of Human Skin: A Pilot Study. PLoS ONE. 2011;6(8):e23972

KARL STORZ Endoscopy-America Inc. (2018) KARL STORZ Launches New 4 mm Endoscopic NIR/ICG Fluorescence Imaging System to Enhance Minimally Invasive Neurosurgery. KARL STORZ, Our Company, Press, Human Medicine 06.12.2018

Klein, M (1964) Einstein and the wave-particle duality. The Natural Philosopher, 1964. Bobs-Merrill

Kozin, E.D., Lehmann, A., Carter, M., Hight, E., Cohen, M., Nakajima, H.H. and Lee, D.J. (2014) Thermal effects of endoscopy in human temporal bone model: implications for endoscopic ear surgery. Laryngoscope 2014 Aug: 124(8): E332-E339

Krombach F, Münzing S, Allmeling AM, Gerlach JT, Behr J, Dörger M. (1997) Cell size of alveolar macrophages: an interspecies comparison. Environ Health Perspect. 1997 Sep105 Suppl 5:1261-3

References

Lee, B.T., Matsui, A., Hutteman, M., Lin, S.J., Winer, J.H., Laurence, R.G. and Frangioni, J.V. (2010) Intraoperative Near-Infrared Fluorescence Imaging in Perforator Flap Reconstruction: Current Research and Early Clinical Experience. Journal of Reconstructive Microsurgery 2010; 26(1): 059-065

Lee, E.S., Kim, T.S. and Kim, SK. (2015) Current status of optical imaging for evaluating lymph nodes and lymphatic system. The Korean Journal of Radiology 2015 Jan-Feb;16(1):21-31

MarketsandMarkets (Feb 2019) Near Infrared Imaging Market by Product Type (NIR Fluorescence Imaging, Reagents), Application (Cancer surgery, Plastic surgery, Gastrointestinal surgery) End Users (Hospitals & Clinics, Research laboratory, Pharmaceutical companies) - Global Forecast to 2023. Market Research Report, Feb 2019, Code: MD4138

MarketsandMarkets (Aug 2019) Endoscopy Equipment Market by Product (Endoscope (Flexible, Rigid, Capsule) Visualization Systems, Endoscopic Ultrasound, Insufflator)), Application (GI Endoscopy, Laparoscopy, Cystoscopy, Bronchoscopy, Colonoscopy, Arthroscopy) - Global Forecast to 2024. Market Research Report, Aug 2019, Code: MD2212

Mellor, R.H., Stanton, A.W., Azarbod, P., Sherman, M.D., Levick, J.R. and Mortimer, P.S. (2000) Enhanced Cutaneous Lymphatic Network in the Forearms of Women with Postmastectomy Oedema. Journal of Vascular Research 2000 37:501-512

Mieog, JSD., Troyan, SL., Hutteman, M., Donohue, KJ., van der Worst, JR., Stockdale, A., Liefers, GJ., Choi, HS., Gibbs-Strauss, SL., Putter, H., Gioux, S., Kuppen, PJK., Ashitate, Y., Löwik, CWGM., Smit, VTHBM., Oketokoun, R., Ngo, LH., van de Velde, CJH., Frangioni, JV. and Vahrmeijer, AL. (2011) Toward optimization of imaging system and lymphatic tracer for near-infrared fluorescent sentinel lymph node mapping in breast cancer. Annals of Surgical Oncology 2011; 18-2483-91

References

Modlin IM, Begos DG, Ballantyne GH. (2010) Laparoscopic Gastrointestinal Surgery: Current State of the Art. Edr. Spiro HM. Clinical Gastroenterology

Nagaya, T., Nakamura, Y.A., Choyke, P.L. and Kobayashi, H. (2017) Fluorescence-Guided Surgery. Frontiers in Oncology. 22 December 2017

Nairat, M., Konar, A., Kaniecki, M., Lozovoy, V and Dantus, M. (2014) Investigating the role of human serum albumin protein pocket on the excited state dynamics of indocyanine green using shaped femtosecond laser pulses. Royal Society of Chemistry PCCP 2015, 17, 5872

National Center for Biotechnology Information. PubChem Database. Cardio-Green, CID=11967809

National Center for Biotechnology Information. PubChem Database. Human serum albumin, CID=72941834

National Institute for Occupational Safety and Health Division of Biomedical and Behavioural Science, (1982) Biological Effects of Infrared Radiation – Technical Report. U.S. Department of Health and Human Service

Ohnishi, S., Lomnes, S., Laurence, R., Gogbashian, A., Mariani, G. and Frangioni, J. (2005) Organic Alternatives to Wuantum Dots for Intraoperative Near-Infrared Fluorescent Sentinel Lymph Node Mapping. Molecular Imaging Vo 4. No. 3 July 2005 pp 172-181

Olympus.co.uk

Philip, R., Penzkofer, A., Bäumler, W., Szeimes, R.M. and Abels, C. (1995) Absorption and fluorescence spectroscopic investigation of indocyanine green. Journal of Photochemistry and Photobiology A: Chemistry 96 1996 137-148

Photon Focus (2008) User Manual MV-D752E-40 CMOS Area Scan Cameras V1.2

References

Potter, M.C., Wyble, B., Hagmann, C.E. and McCourt, E.S. (2014) Detecting meaning in RSVP at 13ms per picture. Attention, Perception & Psychophysics 76, pages 270–279 (2014)

Prahl, S. (2019). Optical Absorption of Indocyanine Green (ICG) 2019 Online Spectra available at omlc.org/spectra/icg

Qi, J., Nabavi, E., Hu, Y., Rees-Whippey, D., Curtis, A., Price, C., Copner, N., Sanassy, C., Leiloglou, M., Leff, D., Hanna, G. and Elson, D. (2017) A light-weight near infrared fluorescence endoscope based on a single color camera: a proof-of-concept study. 2017 Conference on Lasers and Electro-Optics Pacific Rim (CLEO-PR) 31 July-4 Aug. 2017 DOI: 10.1109/CLEOPR.2017.8119082

Rosenthal E L, Warram J M, Bland K L and Zinn K R (2015) The Status of Contemporary Image-Guided Modalities in Oncologic Surgery. Ann. Surg. 2015 Jan:261(1): 46-55

Schaafsma, B.E., Mieog, J.S.D., Hutteman, M., van der Voost, J.R., Kuppen, P.J.K., Löwik, C.W.G.M., Frangioni, J.V., van de Velde, C.J.H. and Vahrmeijer, A.L. (2011) The clinical use of indocyanine green as a near-infrared fluorescent contrast agent for image-guided oncologic surgery. The Journal of Surgical Oncology 2011 Sep 1; 104(3) 323-332

Shingnapurkar, S.H., Mitra, D.K., Kadav, M.S., Shah, R.A., Rodrigues, S.V. and Prithyani, S.S. (2016) The effect of indocyanine green-mediated photodynamic therapy as an adjunct to scaling and root planing in the treatment of chronic periodontitis: A comparative split-mouth randomized clinical trial. Indian Journal of Dental Research 2016, Vol. 27, Iss. 6, pp 609-617

Stryker.com

Surat, P. (2021) Photobleaching in Fluorescence Microscopy. AZO Lifesciences Online.

References

Tedford, C., Delapp, S., Jacques, S. and Anders, J. (2015) Quantitative analysis of transcranial and intraparenchymal light penetration in human cadaver brain tissue. LASERs in Surgery and Medicine. Volume 47, Issue 4, April 2015, 312-322.

Thorlabs LED780E Specsheet January 4, 2014 16385-S01, Rev D.

Troyan, S.L., Kianzad, V., Gibbs-Strauss, S.L., Gioux, S., Matsui, A., Oketokoun, R., Ngo, L., Khamene, A., Azar, F. and Frangioni, J. (2009) The FLARETM Intraoperative Near-Infrared Fluorescence Imaging System: A First-in-Human Clinical Trial in Breast Cancer Sentinel Lymph Node Mapping. Annals of Surgical Oncology 2009 Oct 16(10) 2943-2952

Wang, T.D and Van Dam, J (2004) Optical Biopsy: A New Fronteir in Endoscopic Detection and Diagnosis. Clinical Gastroenterology and Hepatology. Volume 2 Issue 9 September 2004, pp 744-753

Watson, S (2009) Twenty Years Later, LASIK Has Its Pros and Cons. WebMD, Eye Health, News. WebMD Health News December 20, 2019

WHO (2017) World Health Organisation, Breast cancer: prevention and control [Online]

Wood, M (2012) Etendue. Out of the Wood by Mike Wood. Winter 2012 pp18-20

Yaqoob, Z., McDowell, E., Wu, J., Heng, X., Fingler, J. and Yang, C. (2006) Molecular contrast optical coherence tomography: A pump-probe scheme using indocyanine green as a contrast agent. Journal of Biomedical Optics 2006 Sept-Oct; 11(5):054017

Yuan, B., Chen, N. and Zhu, Q. 2004. Emission and absorption properties of indocyanine green in Intralipid solution. Journal of Biomedical Optics 2004; 9(3): 497-503

Zhu, H. and Blackborow, P. (2011) Etendue and Optical Throughput Calculations. Energetiq Technologies Inc. Application Note ref: 002-2-14-2011

8 Appendix A – Continuous Development

Initial Spectrometry Results

Unfortunately, with no previous experience of using ICG I quickly learned that my calculations did not represent realistic values. This became apparent as soon as the samples were mixed as the following figures show. The ICG:HSA solution appears very dense and ink like and once placed into the jig for testing it was evident that no light was able to penetrate through the solution and so all spectrometer readings from this day of testing cannot contribute to this research. The high optical density was confirmed using the beam viewer card and moving the cuvette in and out of the light path.

The ICG:HSA solution comprised of 5.0mL deionised water, 0.06g ICG and 0.28g HSA to give a concentration of 15,480µM which was exponentially higher than desired.

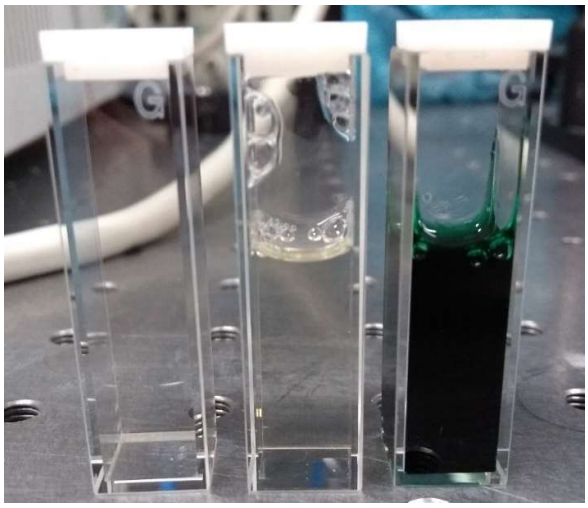

Figure 8.1: A photograph showing an empty reference cuvette, HSA sample and ICG:HSA (L-R)

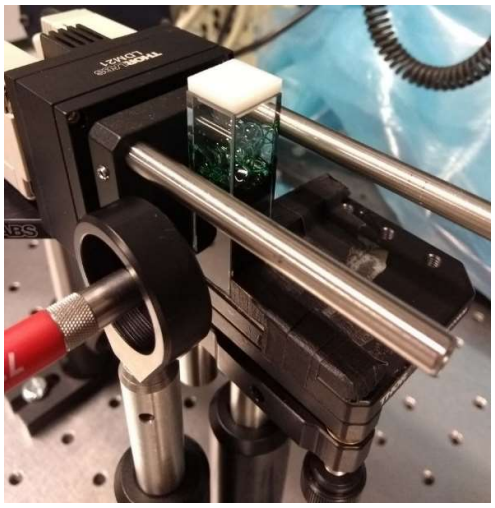

Figure 8.2: A photograph showing a mounted ICG:HSA sample

Following this setback, a literature review yielded an insight into identifying the error and how best to rectify. A study published in the Korean Journal of Radiology (Lee et al., 2015) includes Figure 8.3 in the findings. Here a commercial ICG kit is diluted to 0.25% and 0.002% (Right to Left) shown in white light imaging and under NIR conditions, it is evident that the lower the concentration the stronger the fluorescent signal. The solution on the left is 125 times weaker than on the right however the stronger solution shows no florescence and appears to be the same as my original attempt at mixing an ICG solution. The image presented in Figure 8.4 shows another similar looking ICG solution however, this is again pre-dilution and to be used for a photodynamic therapy (PDT) dental application whereby the final concentration is 1mg/mL of ICG in sterile water (Shingnapurkar et al., 2016). Figure 8.5 shows samples diluted starting from 5mg/mol and ending with 0.005mg/mol (Alander, 2013)

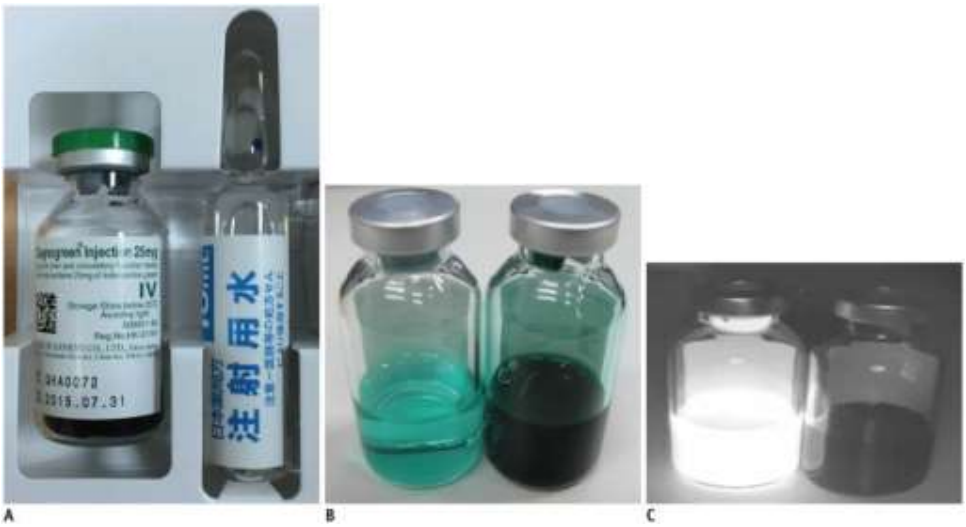

Figure 8.3: An Image showing a commercial ICG kit and the subsequent dilutions (Lee, et al., 2015)

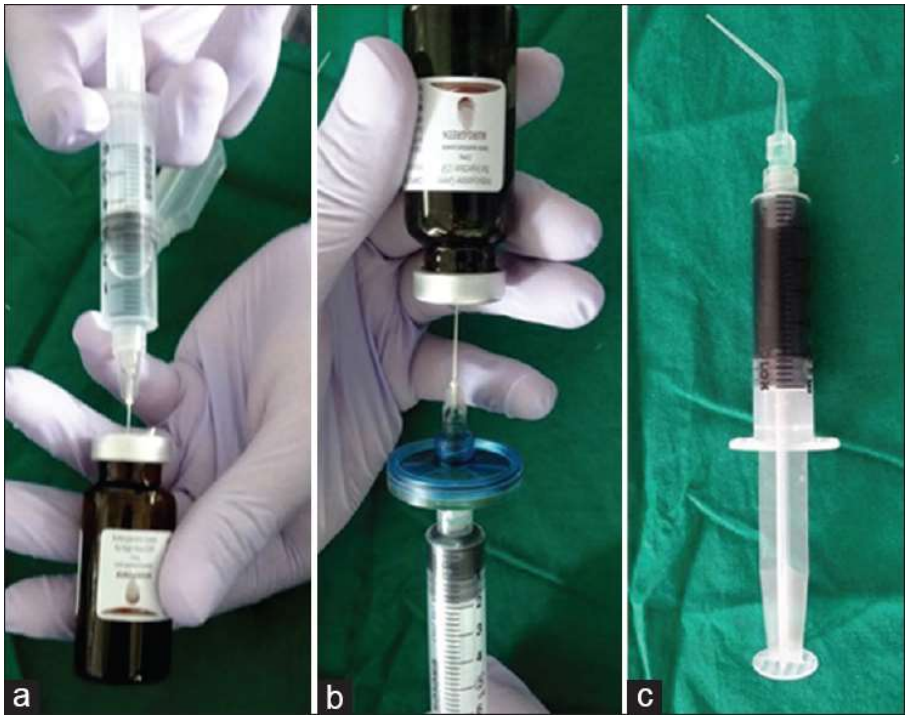

Figure 8.4: An image showing an ICG preparation (Shingnapurkar et al., 2016)

Figure 8.5: Dilutions of ICG starting with 5mg/mol and reducing in concentration L-R (Alander, 2013)

9 Appendix B – Component Selection

Camera Selection

In total, 9 CMOS cameras were shortlisted all with USB 3 connectivity and Windows compatibility. Each option has its own unique qualities however, the most important feature for this research is the capability to record photons at 800nm wavelength and so the Quantum Efficiency at this range was what distinguished the camera selected from the available choice.

	04S2M	**16S2M**	**23S3M**	**31S4M**	**32S4M**	**50S5M**	**63S4M**	**120S4M**	**200S6M**
Frame Rate	522	226	163	55	118	35	59.6	31	18
Pixel Size (µM)	6.9	3.45	3.45	3.45	3.45	3.45	2.4	1.85	2.4
QE (530nm)	61.82	64.81	65.78	73	73	62.51	73.05	73.27	79
QE (800nm)	26.5	27	24	26.5	25	25	20	25	21
Resolution	720 x 540	1440 x 1080	1920 x 1200	2048 x 1536	2048 x 1536	2248 x 2048	3072 x 2048	4000 x 3000	5472 x 3648
Sensor Format	1/2.9"	1/2.9"	1/2.3"	1/1.8"	1/1.8"	2/3"	1/1.8"	1/1.7"	1"
ADC (bit)	8 10 12	10 12	10 12	10 12	10 12	12	10 14	10 12	10 12
Megapixels (MP)	0.4	1.6	2.3	3.2	3.2	5	6.3	12	20
CMOS	yes	Yes	Yes	Yes	Yes	Yes	yes	yes	Yes
Chroma	Mono	Mono	Mono	Mono	Mono	Mono	Mono	Mono	Mono
Sensor (Sony)	IMX287	IMX273	IMX392	IMX265	IMX252	IMX264	IMX178	IMX226	IMX183
Exposure Range (seconds)	4 µs to 30	4 µs to 30	5 µs to 30	-	-	-	-	-	-
Gain Range (dB)	0 to 47	0 to 47	0 to 47	-	-	-	-	-	

Absolute Sensitivity Threshold (y)	6.81	4.55	4.39	4.43	4.29	4.43	4.03	5.09	4.97
Saturation Capacity (e-)	22187	11179	11088	10791	10858	10824	14204	11323	14794
Temporal Dark Noise (e-)	3.71	2.45	2.39	2.26	2.35	2.27	2.42	3.23	3.26
Dynamic Range dB	74.43	71.58	71.68	71.83	71.62	71.83	73.73	69.64	71.89
Config Port	USB 3	USB 3	GigE	GigE	USB 3	GigE	GigE	GigE	USB 3
Price (£)	346.8	318	486	498	726	790.8	426	546	694.8
Readout (Shutter)	Global	Global	Global	Global	Global	Global	Rolling w/ global reset	Rolling w/ global reset	Rolling w/ global reset
Lens Mount	CS	CS	C	C	C	C	C	CS	C

10 Appendix C – Software Function Definitions

Ocean Optics OceanView Software version 1.6.3 Lite Actions

Fluorescence

A type of relative irradiance measurement in which the energy given off by materials excited by light at shorter wavelengths is measured. Advantages of fluorescence include high sensitivity, high speed (intensity changes in the order of picoseconds) and safety (non-destructive to sample and no hazardous by-products).

Absorbance

Absorbance spectra are a measure of how much light a sample absorbs. For most samples, absorbance relates linearly to the concentration of the substance. OceanView uses an equation to determine the concentration of a species in solution. The software uses this equation to evaluate each pixel on the detector and produce the absorbance spectrum.

$$A_\lambda = -log_{10}\left(\frac{S_\lambda - D_\lambda}{R_\lambda - D_\lambda}\right)$$

Whereby, S represents the sample intensity at a given wavelength (λ), D represents the background intensity at λ and R is the reference intensity at λ.

The concentration of a species in a solution directly affects the absorbance of a solution, this relationship is known as Beer's Law:

$$A_\lambda = \varepsilon_\lambda cl$$

Whereby A represents absorbance at a given wavelength (λ), Ɛ represents the extinction coefficient of the absorbing species at a given wavelength and c, represents the concentration of the absorbing species given l, the optical path length of the absorption.

Reflection

Reflection is the return of radiation by a surface, without a change in wavelength. Reflection mode is also the spectral processing mode used for transmission spectroscopy, as the math necessary to complete transmission is identical to that required for reflection.

OceanView calculates the reflection of a solution using the following equation:

$$\%T_\lambda = \left(\frac{S_\lambda - D_\lambda}{R_\lambda - D_\lambda}\right) x\ 100\%$$

Whereby S represents the sample intensity at a given wavelength (λ), D represents the background intensity at a given wavelength and R represents the reference intensity at a given wavelength.

Transmission is the percentage of energy passing through a sample relative to the original reference amount. This is also the spectral processing mode used for reflection spectroscopy and the equation is identical to that above.

Terminology from the OceanView library:

Scans to Average

The more scans to average used, the greater the signal to noise ratio. Total acquisition time will be the number of scans to average multiplied by the integration time.

Boxcars

Using a small number of boxcars will increase the signal to noise ratio however, it will also flatten the peaks. It is good to use between 1 and 5 boxcars.

Integration Time

As you increase the integration time, the percentage of noise in the signal will increase. We define the maximum integration time of our spectrometers as that integration time

whereby the noise comprises 50% of the total signal/ if you can use a larger diameter fibre you can use a shorter integration time.

Optical density

1OD allows 10% of light to be transmitted through the sample

2OD allows 1% of light to be transmitted through the sample

3OD allows 0.1% of light to be transmitted through the sample

4OD allows 0.01% of light to be transmitted through the sample

Image Analysis Methodology

Browse through the file directory built in to the LabVIEW programme and select the file for analysis. The fluorescence appears across the path length of the beam within the cuvette, more often than not the cuvette walls can be detected easily due to the light scattering and reflection seen.

In order to standardise the method for analysing the data, a region of interest should be drawn between the walls of the cuvette containing the cone shaped fluorescence.

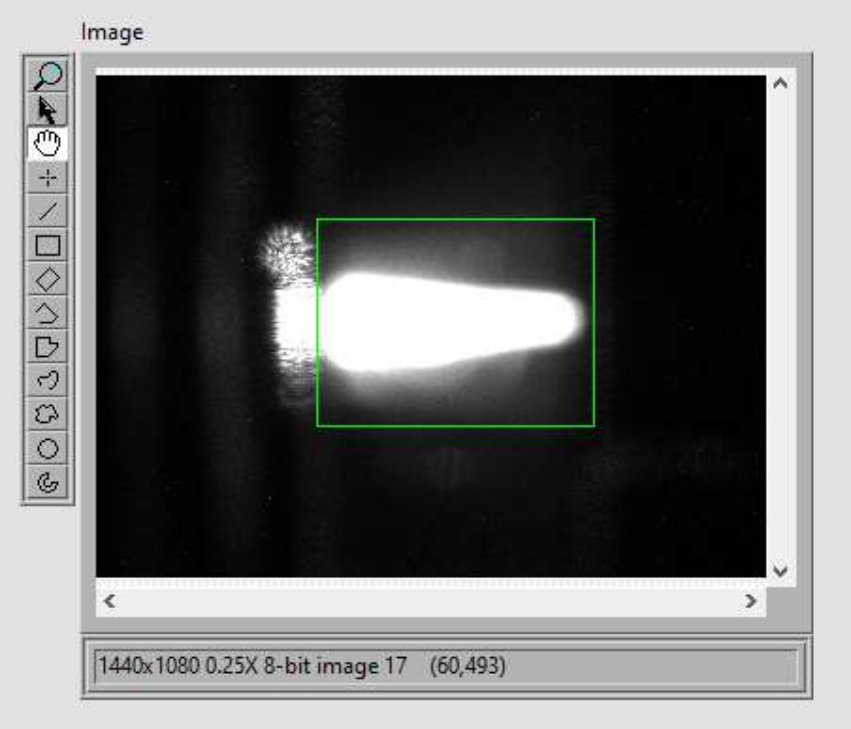

Figure 10.1: An image loaded in LabVIEW showing a 500µMol solution of ICG:HSA illuminated with 10mW LASER at an exposure time of 1 second

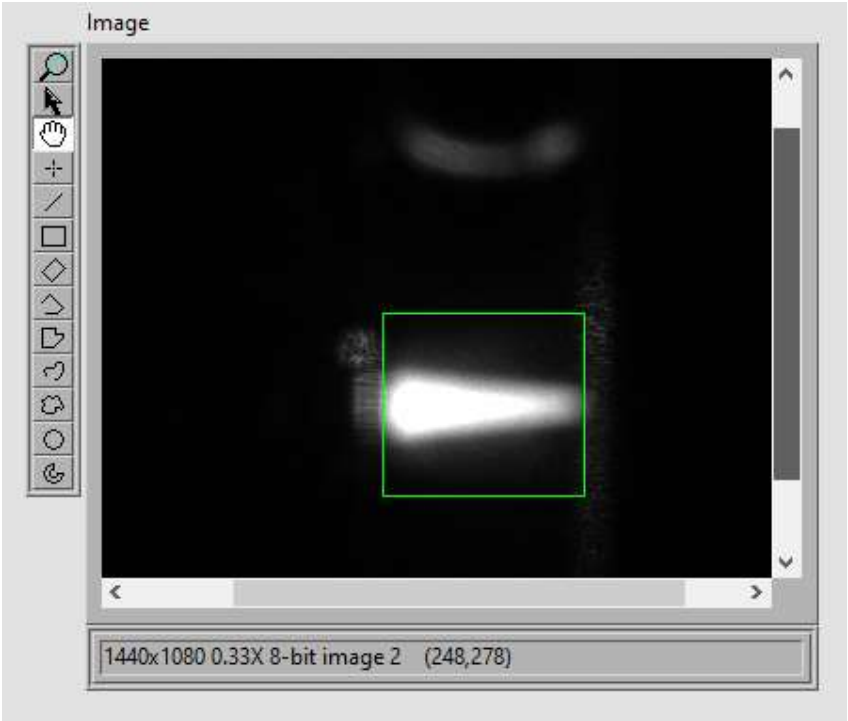

Figure 10.2: An image loaded in LabVIEW showing a 500µMol solution of ICG:HSA illuminated with 10mW LASER at an exposure time of 249998µs

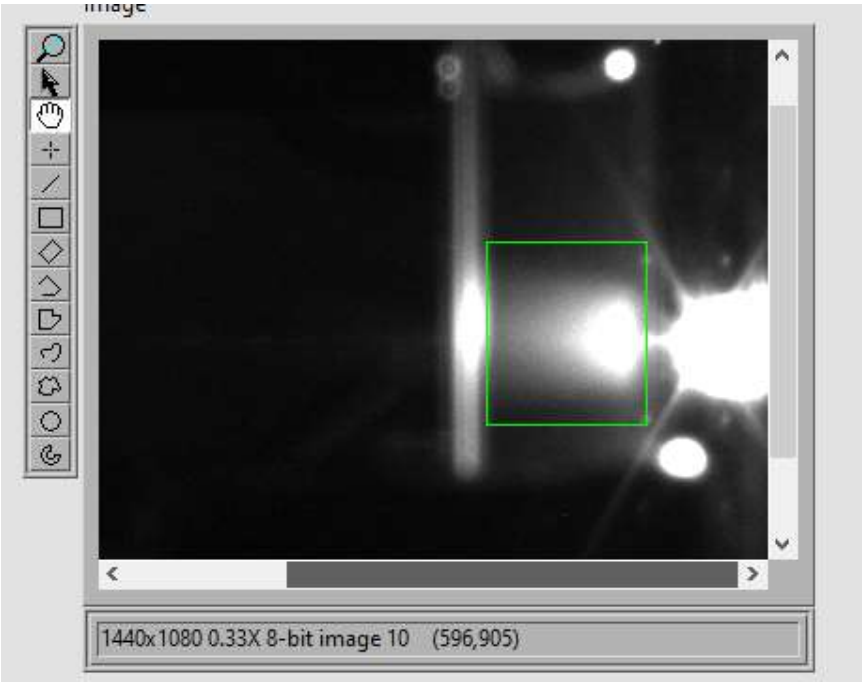

Figure 10.3: An image loaded in LabVIEW showing a 500µMol solution of ICG:HSA illuminated with 7.2mW LED at an exposure time of 124998µs